**2D Thin-Film Flow of a Non-Newtonian Fluid Between Elastic Boundaries**

By

Copyright 2011

**Sunil Karri**

Submitted to the graduate degree program in Mechanical Engineering and the Graduate Faculty of the University of Kansas in partial fulfillment of the requirements for the degree of Master of Science.

_____

Chairperson, Dr. Sarah L. Kieweg

_____

Dr. Sara E. Wilson

_____

Dr. Kenneth J. Fischer

Date Defended: August 19, 2011

The Thesis Committee for Sunil Karri

certifies that this is the approved version of the following thesis:

2D Thin-Film Flow of a Non-Newtonian Fluid Between Elastic Boundaries

_____

Chairperson, Dr. Sarah L. Kieweg

Date approved: August 19, 2011

# Abstract

This thesis presents a numerical technique to optimize the efficacy of anti-HIV vaginal drug delivery systems known as microbicides. A microbicide is a topical, prophylactic agent that acts as a barrier from transmission of HIV and other sexually transmitted infections (STIs). A microbicidal formulation consists of an anti-HIV active ingredient within a drug delivery vehicle such as a polymeric gel. For a microbicide to be effective it must be able to perform its function by adhering to the epithelial surface. The effectiveness of the gel depends on the gel's rheological properties as well as the vaginal tissue properties, vaginal geometry, external forces like gravity and other factors like dilution, etc.

As a next step in the design of a microbicidal delivery vehicle, this thesis primarily focuses on the combined effect of gravity, tissue elasticity, and rheological properties and their influence on the gel distribution. A 2D numerical model for the flow a non-Newtonian fluid between elastic boundaries is presented. The following models are considered:

- Power-law fluid model with linear elastic boundary condition,
- Ellis fluid model with linear elastic boundary condition,
- Power-law fluid model with non-linear elastic boundary condition.

The equations describing the evolution of the gel shape were solved numerically using implicit finite difference method along with Newton's search method for the non-

linear system of equations. A parametric and sensitivity analysis of coating behavior to changes in non-Newtonian fluid properties for different elasticities combined with gravity was presented.

The results of the parametric study showed that the combined effect of tissue elasticity and gravitational forces greatly influenced the gel coating. A higher tissue elasticity resulted in greater spreading length, faster spreading rates and dominance over gravitational force. The gel consistency had greater impact on gel coating compared to shear-thinning index; a higher consistency resulted in slower spreading rates. The shear-thinning index is relatively of less importance; however, it may be important for long spreading times.

Sensitivity analysis for 10% changes in consistency and shear-thinning index showed high sensitivity for synergistic change in both parameters. The sensitivity of spreading length for changes in consistency were greater compared to changes in shear-thinning index.

In conclusion, the relative importance of each parameter has been determined. These results will ultimately help in determining optimal gel properties for microbicidal gel in groups of women with different tissue elasticities. Thus, this work will help in designing better microbicides.

# Acknowledgement

I thank my advisor Dr. Sarah L. Kieweg, for all her time, support, guidance and constant encouragement during my masters. I would like to thank my committee Dr. Kenneth J. Fischer and Dr. Sara E. Wilson for all their valuable time and suggestions.

I thank my parents, Bhagavati and Ramam Karri, and sister, Sujana for all the love, support and advice. I thank my girl friend Manjari, for always being there and encouraging me.

I thank my lab group: Bin Hu, Vitaly Kheyfets, Amber Markey, Todd McDonald, Mark Pacey, Thora Whitmore, Taylor Wilson, for all their help, suggestions, exchange of ideas and all the fun times in the lab.

This work was supported by NIH R21 AI082697 and NIH KI2 HD052027. The high performance computing resources were funded by NSF MRI 0821625.

# Table of Contents

Abstract ..... iii

Acknowledgement ..... v

Table of Contents ..... vi

Table of figures ..... xi

List of Tables ..... xiv

List of variables ..... xv

Important Abbreviations ..... xvii

Chapter 1 Introduction ..... 1

1.1 Introduction ..... 1

1.2 What are microbicides? ..... 3

1.3 Non-Newtonian fluids ..... 5

1.3.1 Power-law or Ostwald de Waele model ..... 8

1.3.2 Ellis model ..... 9

1.3.3 Carreau-Yasuda model ..... 9

1.3.4 Herschel-Bulkley model ..... 10

1.4 Vaginal anatomy ..... 11

1.5 Review of relevant literature for thin-film flows in microbicides ..... 17

1.6 Research objectives ..... 19

1.7 Guide to thesis document ..... 20

Chapter 2 Governing Equations and Numerical Methods ..... 22

2.1 Evolution equation for power-law model with linear elastic boundary ..... 23

2.1.1 Conservation of linear momentum ..... 23

2.1.2 Lubrication approximation ..... 23

2.1.3 Boundary conditions ..... 25

2.1.4 Power-law constitutive model ..... 27

2.1.5 Evolution equation using law of conservation of mass ..... 28

2.2 Evolution equation for Ellis model with linear elastic boundary condition ..... 29

2.2.1 Ellis fluid constitutive model ..... 29

2.2.2 Evolution equation from law of conservation of mass ..... 31

2.3 Evolution equation for power-law model with non-linear elastic boundary condition ..... 31

2.3.1 Boundary conditions ..... 32

2.3.2 Evolution equation from law of conservation of mass ..... 35

2.4 Evolution equation for power-law model with linear viscoelastic boundary condition ..... 36

2.4.1 Viscoelastic boundary condition ..... 36

2.4.2 Evolution equation applying law of conservation of mass ..... 38

2.5 Numerical methods and solution ..... 39

2.5.1 Discretization ..... 39

2.6 Convergence study ..... 43

Chapter 3 Results and Discussion: Parametric Study ..... 46

3.1 Parametric study for power-law fluid model with linear elastic boundary condition ..... 46

3.1.1 Effect of elastic and gravitational forces ..... 47

3.1.2 Effect of shear-thinning index *n* ..... 52

3.1.3 Effect of consistency, *m* ..... 57

3.1.4 Summary of results for parametric study of power-law model with linear elastic boundary condition ..... 60

3.2 Parametric study for an Ellis model with linear elastic boundary condition ..... 60

3.2.1 Effect of elastic and gravitational forces ..... 61

3.2.1 Effect of shear-thinning, number, $\alpha$ ..... 63

3.2.2 Effect of zero shear stress viscosity, $\eta_o$ ..... 69

3.2.3 Effect of shear stress at half value of viscosity $\tau_{1/2}$ ..... 71

3.2.4 Summary of results for parametric study of an Ellis fluid model with linear elastic boundary condition. ..... 72

3.3 Parametric study for a power-law fluid model with non-linear elastic boundary condition ..... 73

3.3.1 Effect of elastic and gravitational forces ..... 73

3.3.2 Effect of shear-thinning index, *n* ..... 75

3.3.3 Effect of consistency, *m.* ..... 79

3.3.4 Summary of results for parametric study of power-law model with non-linear elastic boundary condition ..... 80

3.4 Summary of parametric study ..... 81

Chapter 4 Results and Discussion: Sensivity Analysis ..... 83

4.1 Sensitivity analysis for the power-law model with linear elastic boundary condition ..... 84

4.1.1 Percent sensitivity of spreading length, *L* for 10% decrease in consistency, *m*. ..... 85

4.1.2 Percent sensitivity of spreading length for 10% increase in shear-thinning index, *n*. ..... 87

4.1.3 Percent sensitivity of spreading length for 10% decrease in consistency, m and 10% increase in shear-thinning index, *n* ..... 90

4.2 Sensitivity analysis for the power-law model with non- linear elastic boundary condition ..... 92

4.2.1 Percent sensitivity of spreading length for 10% decrease in consistency, *m*…… ..... 93

4.2.2 Percent sensitivity of spreading length for 10% increase in shear-thinning index, *n*…… ..... 95

4.2.3 Percent sensitivity of spreading length for both 10% decrease in consistency, *m*, and 10% increase in shear-thinning index, *n* ..... 97

4.3 Summary of sensitivity analysis..... 98

Chapter 5 Conclusions and Future work..... 100

5.1 Summary of major findings..... 100

5.2 Application of results obtained from the parametric study of a power-law fluid with linear elastic model ..... 102

5.3 Limitations and Future work ..... 104

5.4 Conclusion..... 105

Appendix I……..……106

Bibliography: ..... 108

# Table of figures

Figure 1.1 Illustration of a microbicide gel being inserted using an applicator and the impact of elasticity and gravity on the gel distribution over the epithelium. ..... 4

Figure 1.2 Constitutive relationship for different kinds of fluids ..... 6

Figure 1.3 A log-log plot showing the rheological data obtained using a plate and cone rheometer, for a 3% Hydroxyethyl cellulose sample. ..... 8

Figure 1.4 Sketch shows the deformation $h(x,t)$ in the vaginal wall..... 14

Figure 2.1 Sketch showing the initial shape of the bolus. ..... 24

Figure 2.2 Plot showing how the parameters for non-linear elastic model were chosen based on stress-strain relationship. ..... 33

Figure 2.3 Sketch of aVoigt viscoelastic model ..... 37

Figure 2.4 Convergence study of spatial discretization for tissue elasticity, $E$ = 10 kPa, consistency, $m$ = 400 Psec$^{n-1}$ and shear-thinning index, $n$ = 0.8. ..... 44

Figure 2.5 Convergence study of spatial discretization for tissue elasticity, $E$ = 100 kPa, consistency, $m$ = 400 Psec$^{n-1}$ and shear-thinning index, $n$ = 0.8. ..... 45

Figure 3.1 Flow profiles of power-law fluid with different elasticities (linear elasticity), illustrating the effect of tissue elasticity, $E$ on coating of the gel. ..... 49

Figure 3.2 Plot illustrates the gel coating behavior for different tissue elasticities. ..... 51

Figure 3.3 Effect of shear-thinning index, $n$ on spreading length, $L$ for low tissue elasticity, $E$ = 1 kPa and low gel consistency, $m$ = 100 Psec$^{n-1}$. ..... 53

Figure 3.4 Effect of shear-thinning index, *n* on spreading length, *L* for low tissue elasticity, *E* = 1 kPa and high gel consistency, *m* = 400 $Psec^{n-1}$. ..... 54

Figure 3.5 Effect of shear-thinning index, *n*, on spreading length, *L* for high elasticity, *E* = 50 kPa and high consistency, *m* = 400 $Psec^{n-1}$..... 55

Figure 3.6 Effect of gel consistency, *m* on spreading length, *L* for tissue elasticity, *E* = 1kpa and shear-thinning index, *n* = 0.5..... 58

Figure 3.7 Spreading profile for flow time of t=2 seconds, tissue elasticity, *E* = 1kPa, consistency, *m* = 600 $Psec^{n-1}$ and shear-thinning index, *n* = 0.5. ..... 59

Figure 3.8 Flow profiles of Ellis fluid with different tissue elasticities (linear elasticity), illustrating the effect of tissue elasticity on coating of the gel. ..... 62

Figure 3.9 Effect of shear-thinning, number $\alpha$ of an Ellis fluid on spreading length, *L*. . 65

Figure 3.10 Effect of shear-thinning number, $\alpha$ of an Ellis fluid on spreading length, *L* for change in shear stress at half value of viscosity, $\tau_{1/2}$. ..... 66

Figure 3.11 Effect of shear-thinning number, $\alpha$ of Ellis fluid on spreading length L for change in zero shear rate viscosity..... 67

Figure 3.12 Effect of shear-thinning number, $\alpha$ of Ellis fluid on spreading length, *L*, for change in tissue elasticity, *E*. ..... 68

Figure 3.13 Effect of zero shear rate viscosity $\eta_o$ of an Ellis fluid on spreading length, *L*. ..... 70

Figure 3.14 Effect of shear stress for half viscosity, $\tau_{1/2}$ of an Ellis fluid model on spreading length, *L*..... 72

Figure 3.15 Flow profiles of power-law fluid with different elasticities (non-linear elasticity), illustrating the effect of tissue elasticity on coating of the gel..... 74

Figure 3.16 Effect of shear-thinning index, *n*, on spreading length, *L*, for tissue elasticity, $E_o$ = 0.994 kPa and λ = 8.66 and consistency, *m* = 100 $Psec^{n-1}$. ..... 76

Figure 3.17 Effect of shear-thinning index, *n*, on spreading length, *L*, for elastic parameters, $E_o$ = 0.994 kPa and λ = 8.66 and consistency, *m* = 400 $Psec^{n-1}$..... 77

Figure 3.18 Effect of shear-thinning index, *n* on spreading length, *L* for tissue elasticity, $E_o$ = 9.96 kPa and λ = 6.05 and consistency, *m* = 400 $Psec^{n-1}$. ..... 78

Figure 3.19 Effect of consistency, *m* on spreading length, *L* for non-linear elastic parameters, $E_o$ = 0.994 kPa and λ = 8.66, shear-thinning index, *n* = 0.5. ..... 80

Figure 4.1 Contours of percentage change in spreading length, *L*, for 10% decrease in consistency, *m*, of a power-law model with linear elastic boundary condition. ..... 86

Figure 4.2 Contours of percentage change in spreading length for 10% increase in shear-thinning index, n of a power-law model with linear elastic boundary..... 89

Figure 4.3 Contours of percentage change in spreading length for 10% decrease in consistency, *m* and 10% increase in shear-thinning index, *n*, of a power-law model. ..... 91

Figure 4.4 Contours of percentage change in spreading length for 10% decrease in consistency, m of a power-law model with non-linear elastic boundary..... 94

Figure 4.5 Contours of percentage change in spreading length for 10% increase in shear-thinning index, *n* of a power-law model with linear elastic boundary..... 96

Figure 4.6 Contours of percentage change in spreading length for 10% decrease in consistency, *m* and 10% increase in shear-thinning index, *n* of a power-law model. ..... 97

# List of Tables

Table 1 List of cases shown to illustrate the effect of shear-thinning index, *n* of the power-law model with linear elastic boundary condition. ..... 52

Table 2: List of cases shown to illustrate the effect of shear-thinning number, $\alpha$ of an Ellis model with linear elastic boundary condition..... 63

Table 3 List of cases shown to illustrate the effect of shear-thinning index, *n* of the power-law model with a non-linear elastic boundary condition. ..... 75

Table 4: Estimated range of values for rheological properties for a specific tissue elasticity, application time and target length. ..... 103

# List of variables

| Variable | Definition | Units |
|---|---|---|
| $\tau$ | Shear stress | dynes/cm$^2$ |
| $\dot{\gamma}$ | Strain rate | Sec$^{-1}$ |
| $\eta_{app}$ | Apparent viscosity | Poise |
| $m$ | Consistency | Poise.sec$^{n-1}$ |
| $n$ | Shear-thinning index | dimensionless |
| $\eta_0$ | Zero shear stress viscosity | Poise |
| $\alpha$ | Shear-thinning number of Ellis model | dimensionless |
| $\tau_{1/2}$ | Shear stress at half viscosity | dynes/cm$^2$ |
| $\eta_\infty$ | Infinite shear stress viscosity | Poise |
| $\sigma_o$ | Yield stress | dynes/cm$^2$ |
| $p$ | Pressure acting on the fluid | dynes/cm$^2$ |
| ε | Strain | dimensionless |
| $E$ | Young's modulus of elasticity | kilo-Pascal |
| $T$ | Tissue thickness | cm |
| $h$ | Deformation in the tissue / height of the fluid bolus as a function of *x* and *t* | cm |
| $E_0$ | Model parameter for non-linear elasticity | kilo-Pascal |

| | | |
|---|---|---|
| $\lambda$ | Model parameter for non-linear elasticity | dimensionless |
| $\boldsymbol{u}$ | Velocity vector | cm/sec |
| $\boldsymbol{g}$ | Gravitational vector | cm/sec$^2$ |
| $\mathbb{T}$ | Stress tensor | dynes/cm$^2$ |
| $\rho$ | Density | g/cm$^3$ |
| $\mu$ | Viscosity | Poise |
| $H$ | Characteristic height | cm |
| $L$ | Characteristic length | cm |
| $q(x,t)$ | Flow rate per unit width | cm$^2$/sec |
| $\Delta x$ | Step size for spatial discretization | cm |
| $\Delta t$ | Step size for time discretization | seconds |

## Important Abbreviations

| | |
|---|---|
| AIDS | Acquired immune deficiency syndrome |
| ART | Anti-retrival therapy |
| HIV | Human immunodeficiency virus |
| MDS | Microbicide development strategy |
| SI | International system of units |
| STI | Sexually transmitted infection |
| HEC | Hydroxyethyl cellulose |

# Chapter 1

# Introduction

The flow of thin-films find wide range of applications, such as microchip fabrication, micro-fluidics and micro-electromechanical system (MEMS) devices (3), lining of mammalian lungs (4) and architectural coatings (5). Traditionally these flows have been studied with gravity as the driving force and a free surface boundary condition. Recent studies have paid much attention to the effect of film surface tension and the flow front instabilities (3). This thesis is another application of thin film flows where a non-Newtonian fluid flows between two elastic boundaries, rather than with a free surface. This study investigates the effect of fluid rheological properties and the driving forces - gravity and elasticity on the efficacy of anti-Human immunodeficiency virus (HIV) drug delivery systems popularly known as microbicides.

## 1.1 Introduction

Acquired immune deficiency syndrome (AIDS) has been a worldwide pandemic for over three decades now. UNAIDS global report 2010, estimated that by the end of the year 2009, 33.3 million people were living with HIV (6). Every year more than 2 million new HIV infection cases are reported (6).

The number of new infections annually has declined significantly, since the peak of the epidemic in the late 90s (6-7). Preventive measures such as condoms, awareness campaigns, and post-infection antiretroviral therapy (ART) have played a vital role in reducing new infections and increasing the life expectancy of those infected over the last decade (6). However, the total population living with HIV is increasing and hence there is a high risk for new infections (7-8).

Current measures to prevent HIV transmission are insufficient and ineffective in many parts of the world, especially in developing nations (9). An HIV vaccine would be the ultimate solution for the pandemic but experts believe that even a partially effective vaccine would take at least another 10 years or even more (10-11).

Globally more than 50% of the HIV infected population are women and 76% of these HIV positive women reside in sub-Saharan Africa (6). Young women aged 15-24 years living in sub-Saharan Africa are eight times more likely to be infected than men in the same region (6). In addition, women are more susceptible to sexually transmitted infections (STIs) due to their anatomy (12). Clearly, there is an urgent need for an alternative measure for women at high risk and those who often cannot negotiate the use of condoms due to socio-economic reasons.

## 1.2 What are microbicides?

A microbicide is a topical, prophylactic agent that acts as a barrier from transmission of HIV and other sexually transmitted infections (STIs). A microbicidal formulation consists of an anti-HIV active ingredient within a drug delivery vehicle such as, a foam, cream, “gel” (polymeric liquid), dissolving tablet, intravaginal ring, etc (13-14). Apart from acting as an effective barrier against STIs, a successful microbicide must be affordable, safe, user-friendly, physically, chemically and thermally stable, and acceptable to the end-user (9, 15).

A microbicidal formulation may be contraceptive or non-contraceptive in nature and can be combined with existing preventive measures (e.g. condoms) to provide better protection (16). Microbicides can potentially provide protection to those women who do not have access to existing means of protection.

Although microbicides hold great promise in preventing HIV, the process of developing them is highly complex. Most research in the field of microbicides has been limited to the development of the anti-HIV active ingredient (14). Many microbicidal trials have failed in the past possibly due to ineffective coating. Lack of delivery vehicle design has been identified as the current priority gap in Microbicide Development Strategy (MDS) (17). Thus, there is a need to design a delivery vehicle that optimizes the efficacy of a microbicidal agent.

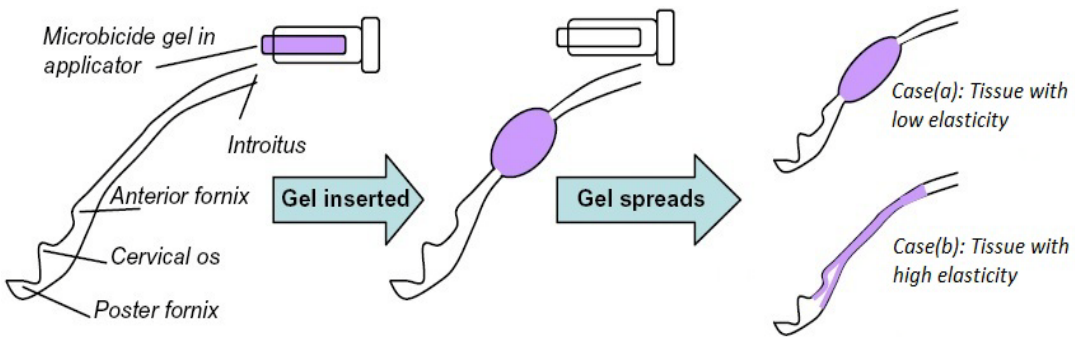


**Figure 1.1 Illustration of a microbicide gel being inserted using an applicator and the impact of elasticity and gravity on the gel distribution over the epithelium.**

Sketch of human vagina in supine position (traced from Netter Atlas of Human Anatomy) with microbicidal gel inserted using an applicator.

A microbicidal gel can be applied using an applicator near the fornix of the vagina (14). Once the applicator is removed, a number of factors may influence the gel distribution on the epithelium (see Figure 1.1). The effectiveness of the gel depends on the gel's rheological properties as well as the vaginal tissue properties, vaginal geometry, external forces like gravity and other factors like dilution, etc (14, 18-20). A good design must take all these factors into consideration and a better understanding of gel's flow behavior over the epithelium is needed before proceeding with clinical trials.

The overall objective of our lab group is to optimize the gel rheological properties to ensure efficacy of polymeric drug delivery systems under the influence of gravity, tissue elasticity, surface tension, shearing force, etc.

This thesis primarily focuses on the combined effect of gravity, tissue elasticity and rheological properties and their influence on the gel distribution. A parametric and sensitivity analysis of rheological properties with different elasticities is presented. The outcomes of this study will help achieve the long-term goal by determining which rheological property is important to the design of a delivery vehicle and how this depends on tissue elasticity.

## 1.3 Non-Newtonian fluids

Most prototype polymeric gels that can be used as delivery vehicles for microbicides are non-Newtonian and, in particular, shear-thinning in nature (18-19, 21). Gel distribution and retention are greatly influenced by its rheological properties (18). The non-Newtonian rheology makes the design of the delivery vehicle complex.

In a continuum, a constitutive relation characterizes any substance; it is defined as the relationship between the stress and deformation (22). For a Newtonian fluid, shear stress is directly proportional to shear rate at constant pressure and temperature (22) (see Figure 1.2). The constant of proportionality is defined as viscosity, which has the units (Pa-s) in international system (SI) of units. Examples of Newtonian fluids include, water, glycerin, air, etc.

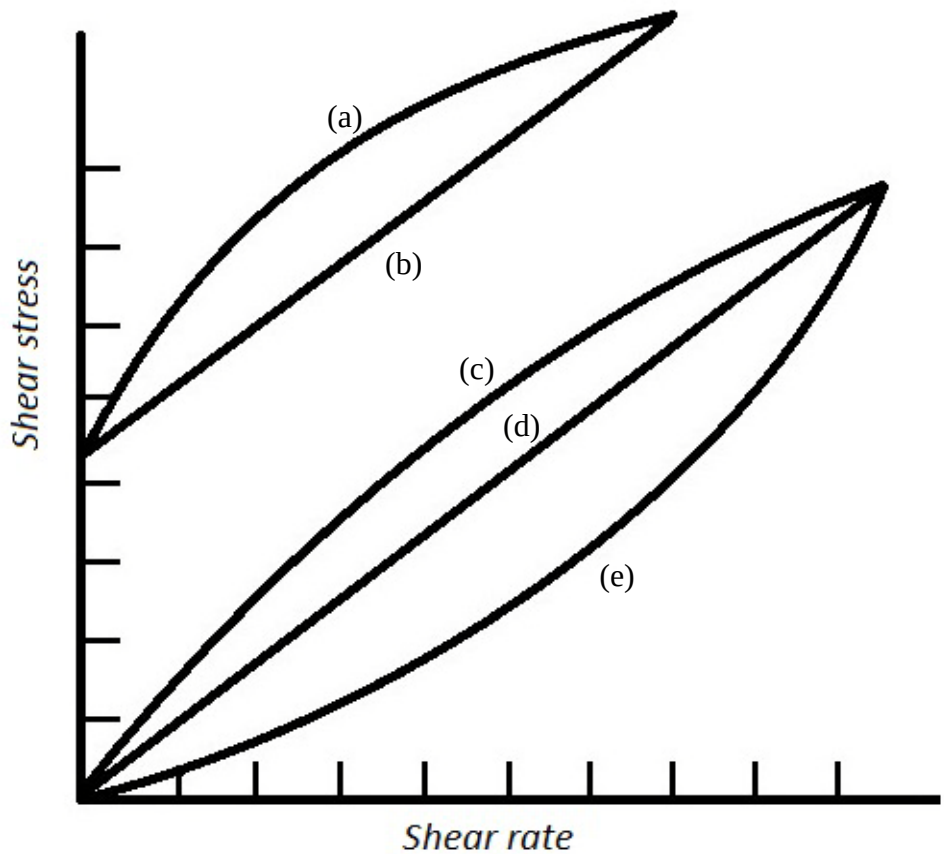


(a) Visco-plastic (Herschel –Bulkley), (b) Bingham Plastic, (c) Shear-thinning fluid (Pseudoplastic), (d) Newtonian fluid, (e) Shear-thickening fluid (Dilatant)

**Figure 1.2 Constitutive relationship for different kinds of fluids**

(modified from Rheology of Complex Fluids by R.P. Chabbra) (2). Schematic shows a linear relationship for a Newtonian fluid. All other fluids come in the category of non-Newtonian fluids.

The 1-D Newtonian constitutive equation is given by (22),

$$\sigma_{yx} = \eta \cdot \dot{\gamma} \tag{1.1}$$

where, $\sigma_{yx}$ is the shear stress acting on the fluid, $\dot{\gamma}$ is the shear rate and $\eta$ is the fluid viscosity which is a constant.

Conversely, a non-Newtonian fluid does not have a linear relationship between stress and deformation and can also be time dependent (2). Shear-thinning fluids are a class of non-Newtonian fluids, characterized by an apparent viscosity, which decreases with an increase in shear rate (2) (see Figure 1.2). Shear-thinning fluids are time independent unlike thixotropic fluids, for which the apparent viscosity decreases with the duration of shear (2). Other non-Newtonian fluids include viscoelastic fluids, shear-thickening fluids, Bingham plastic etc.

A generalized 2-D constitutive model for a shear-thinning fluid is given by,

$$\sigma_{yx} = \eta_{app} \cdot \dot{\gamma} \tag{1.2}$$

$$or, \qquad \eta_{app} = \frac{\sigma_{yx}}{\dot{\gamma}} \tag{1.3}$$

where, $\eta_{app}$ is the apparent viscosity.

There is no single mathematical constitutive relationship that truly defines the shear-thinning behavior of a fluid. In the literature, there are several constitutive models, which work well in different regimes of shear rates. The following constitutive models are relevant to this thesis. These do not consider the viscoelastic nature of polymeric liquids, which is outside the scope of this study.

### 1.3.1 Power-law or Ostwald de Waele model

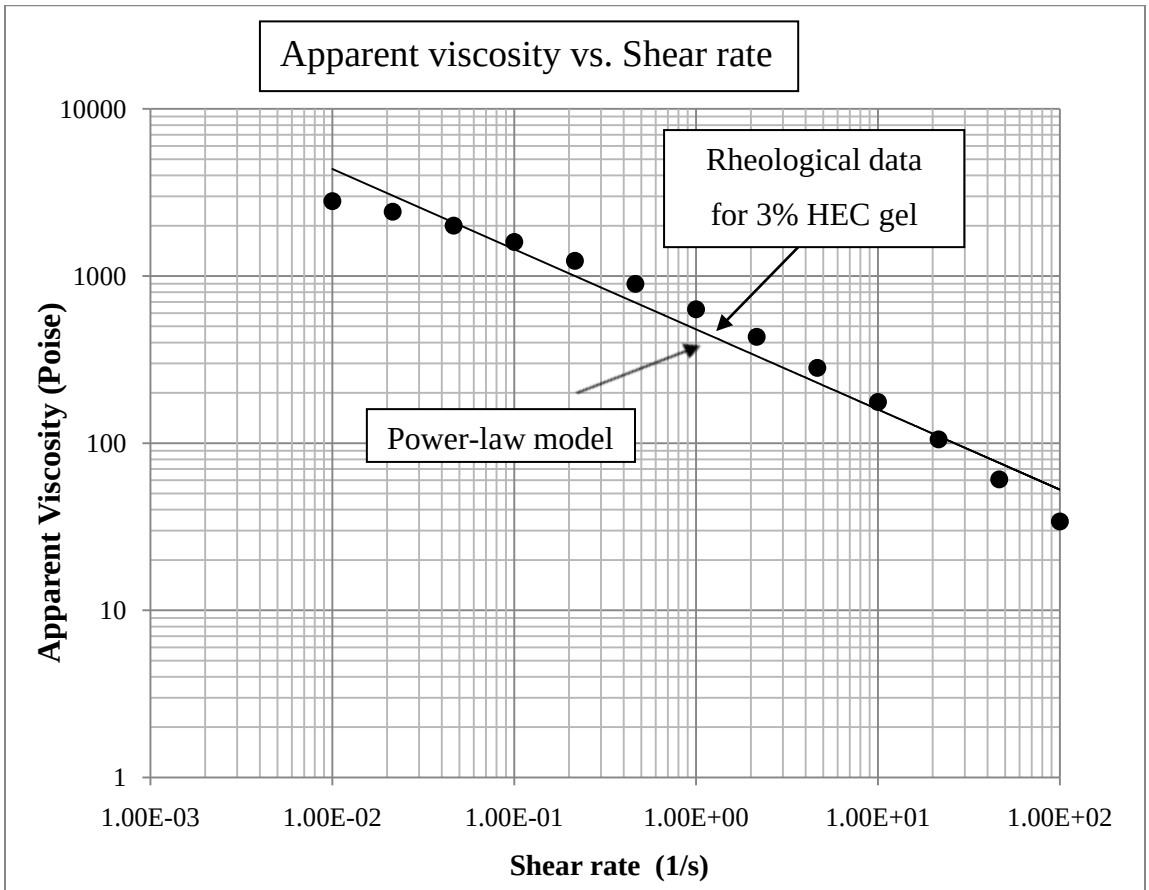


**Figure 1.3 A log-log plot showing the rheological data obtained using a plate and cone rheometer, for a 3% Hydroxyethyl cellulose sample.**

Plot illustrates the variation between actual rheological data and power-law constitutive model indicating its limitations.

The 1-D power-law constitutive equation is given by (2, 23),

$$\eta_{app} = m \cdot (\dot{\gamma})^{n-1} \tag{1.4}$$

where, $n$ is the shear-thinning index $0<n<1$ and $m$ is the consistency. The power-law model approximates the straight-line relationship of shear stress versus shear rate on a log-log plot (see Figure 1.3). The major limitation of the power-law model is that it does not predict lower and upper Newtonian plateaus in the limits of $\dot{\gamma} \to 0$ and $\dot{\gamma} \to \infty$.

### 1.3.2 Ellis model

The 1-D Ellis constitutive equation is given by (2),

$$\eta_{app} = \frac{\eta_0}{1 + \left(\frac{\tau}{\tau_{1/2}}\right)^{\alpha-1}} \tag{1.5}$$

where $\eta_0$ is the zero shear stress viscosity and $\tau_{1/2}$ is the value of shear stress for which the viscosity has been reduced by a factor of one-half. $\alpha$ controls the shear-thinning behavior of the model and is greater than unity. As $\tau_{1/2} \to \infty$, the equation reduces to the Newtonian model and when $\frac{\tau}{\tau_{1/2}} \gg 1$ the equation becomes power-law. This model can capture the low shear rate Newtonian plateau as well as the power-law behavior.

### 1.3.3 Carreau-Yasuda model

The 2-D Carreau-Yasuda constitutive model is given by (23),

$$\frac{\eta_{app} - \eta_\infty}{\eta_0 - \eta_\infty} = (1 + (\lambda \cdot \dot{\gamma})^a)^{\frac{n-1}{a}} \tag{1.6}$$

where, $\eta_0$ is the zero shear rate viscosity, $\eta_\infty$ is the infinite shear rate viscosity, $\lambda$ is a time constant, $n$ is the power-law exponent and $a$ is dimensionless parameter that describes the

transition region from the zero shear rate region to the power-law region. When $a$ = 2 it is called the Carreau model.

### 1.3.4 Herschel-Bulkley model

A Herschel-Bulkley fluid deforms and exhibits a shear-thinning behavior only after certain stress limit known as yield stress (see Figure 1.2).

The 1-D Herschel-Bulkley constitutive equation is given by (2),

$$\sigma = \sigma_o + m \cdot (\dot{\gamma})^n \ \ \forall \ \ \sigma > \sigma_o \tag{1.7}$$

$$\dot{\gamma} = 0 \ \forall \ \ \sigma \leq \sigma_o \tag{1.8}$$

where, $\sigma_o$ is the yield stress within the fluid, $m$ is the consistency and $n$ is the shear-thinning index similar to a power-law model. Common examples of yield-stress fluids include blood, yogurt, molten chocolate, etc (2).

In this study, the power-law constitutive model has been primarily used to describe the shear-thinning behavior of the microbicidal gels in the mathematical models. Although the power-law model has limitations at very low and high shear rates, it is widely used in engineering problems. Moreover, power-law model is a two parameter model and easier to fit with the rheological data. An Ellis fluid model has also been used with a linear elastic boundary condition for the mathematical models. However, a comparison between power-law and Ellis models has not been presented in this work.

The range of numerical values for the power-law model parameters and the Ellis model parameters were chosen based on the rheological data obtained for the hydroxyethylcellulose (HEC) gels, prepared by our lab group.

## 1.4 Vaginal anatomy

The female reproductive tract consists of four main regions: the introitus, the vaginal epithelium, the ectocervix and the endocervix (12). The human vagina is a thin-walled, collapsed fibro-muscular tube (7-10 cm long) which relaxes into a virtual cavity with H-shaped cross section (12, 21, 24). It consists of four layers: the mucosa, consisting of stratified squamous epithelial tissue; the submucosa, which is a vascularised connective tissue; the muscularis, consisting of smooth muscle and the adventitia, which is composed of loose connective tissue (25-27).

The biomechanical properties of vaginal tissue are strongly dependent on its composition, architecture and thickness (26). The vaginal wall thickness can range between 0.5 ~ 2.0 cm (26, 28). The tissue compliance or pressure from surrounding tissues, may significantly influence the distribution of a microbicidal gel between the anterior and posterior walls (19, 21). Thus, vaginal tissue properties are important in the design of vaginal drug delivery systems.

Modeling of soft tissues is a major challenge in the field of biomechanical research. All soft tissues including vaginal tissue, exhibit a strong non-linear, viscoelastic

behavior (1). Viscoelastic materials exhibit creep, hysteresis and are time dependent, which makes them difficult to model (1). Moreover, the model parameters and material constants have to be determined experimentally. Although most soft tissues have been studied extensively, there is limited data available on vaginal tissue properties. Most research on vaginal tissue has been limited to *ex vivo* assessment of tensile properties of prolapsed tissues.

Early studies to assess the tensile strength of vaginal tissue have assumed a linear elastic behavior for the tissue (29). Goh *et al.* investigated the biomechanical properties of prolapsed vaginal tissue samples *ex vivo,* obtained from pre and post-menopausal women (30). They concluded that the tissue properties in pre and post-menopausal women were similar and a little higher elastic modulus in postmenopausal vaginal tissue is attributed to age related changes (30).

Studies by Cosson *et al.* on prolapsed post-menopausal vaginal tissue samples *ex vivo*, showed that the maximum strength and elongation at rupture for the tissue varied greatly from one sample to another (31). Their results did not have any correlation with the age of the patients (31). Lei *et al.* preformed a similar study with a larger group of subjects and concluded that pre and post-menopausal vaginal tissue samples had variable properties and did not have any correlation with age (32), contradictory to Goh *et al.* (30). Rubod *et al.* developed an experimental protocol to determine the biomechanical properties of vaginal tissue under uni-axial tension (33). Rubod *et al.* illustrated that vaginal tissue exhibits a non-linear hyperelastic behavior for large strains (34). It was

highlighted that a linear elastic tissue model could not be used for vaginal tissue modeling in the treatment of pelvic order prolapse (POP) (34).

More recently, Martins *et al.* formulated a non-linear hyperelastic model based on their uni-axial tensile tests on prolapsed vaginal tissue samples (29). From the stress strain relations obtained, the linear elastic modulus was predicted to be 9.7MPa in tension (29). However, viscoelastic properties and parameters were not determined. Peňa *et al.* performed uni-axial tests on prolapsed vaginal tissue to determine the viscoelastic material parameters for their viscoelasic model (35). The tissue properties were measured only along the longitudinal direction and hence their study had limitations in determining all the viscoelastic parameters for the model (35). It was pointed out that the vaginal tissue properties were difficult to measure in transverse direction (34-35) and further information on multi-axial testing is needed to characterize vaginal tissue properties.

It is clear from the above listed literature that the biomechanical properties of vaginal tissue are unknown and are highly variable depending on parity (36-37), menopause (31-32), age (30), etc. Most of the studies have examined the *ex vivo* tensile strength of the tissue focusing on treatment of pelvic order prolapse (POP) whereas, the compressive strength of vaginal tissue or the forces due to pressure from surrounding tissue *in vivo* is the point of interest for this study. Although vaginal properties have not been measured under compression, it is estimated that the elastic modulus of vaginal tissue is about 12-36 kPa and the vaginal forces are about 2-12 N (20). A recent patent by Egorov *et al.* devised a vaginal probe to measure linear elasticity *in vivo*. They estimated

the vaginal elasticity to be 10 kPa near the regions where vaginal tissue is hard and 3 kPa in the region where vaginal tissue is soft (38).

To incorporate vaginal tissue elasticity into our numerical model of thin film flow between anterior and posterior vaginal walls, two tissue elasticity models have been considered: (i) linear elastic model and (ii) non-linear (exponential) elastic model. These models assume that the tissue is homogenous and isotropic.

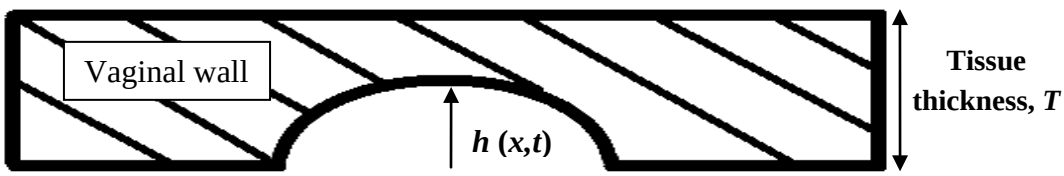


**Figure 1.4 Sketch shows the deformation *h*(*x*,*t*) in the vaginal wall.**

The linear elastic model assumes that the pressure, $p$ (or normal stress, $\sigma$) acting on the fluid boundary due to the tissue elasticity is directly proportional to strain, ($\varepsilon = h(x,t)/T$), in the tissue. Although the pressure acting is normal to the fluid surface and the strain is in the perpendicular direction, it is assumed that the pressure acting is proportional to the strain in the perpendicular direction since it is a thin film. The pressure acting on the fluid can be expressed as,

$$\sigma = E \cdot \varepsilon \tag{1.9}$$

$$or, \qquad p = E \cdot \frac{h(x,t)}{T} \tag{1.10}$$

where, $E$ is the tissue elasticity or young modulus, $T$ is the tissue thickness and $h(x,t)$ is the deformation in the tissue such that the strain in the tissue is $\epsilon = h(x,t)/T$. This approximation has been widely used in engineering problems related to elastohydrodynamic lubrication (39). Szeri *et al*. were the first to incorporated the linear elastic tissue model in vaginal drug delivery systems (28). However, most of their analysis was limited to a Newtonian fluid model and two elasticities. For this study, a wide range of values for the tissue elasticity ($E$=0.05-100kPa) have been chosen. This will account for variability of vaginal tissue elasticity and hence will help in determining optimal values for rheological parameters.

The linear elastic tissue model is an initial approximation in design of microbicidal delivery systems. As a next step, a non-linear (exponential) stress strain relationship has been introduced. Although, an exponential stress-strain relationship is not a true representation of the tissue, it is expected that an such a stress strain relationship is more close to the actual (non-linear) tissue behavior. The non-linear exponential form of stress strain relationship for vaginal tissue is assumed as:

$$p = E_o \cdot \varepsilon e^{\lambda\varepsilon} \tag{1.11}$$

such that, the elasticity of the tissue as a function of strain is given by the relation:

$$E(\varepsilon) = E_o e^{\lambda\varepsilon}(1 + \lambda\varepsilon) \tag{1.12}$$

where, $E_o$ and $\lambda$ are model parameters which need to be determined experimentally, $\varepsilon$ is the strain in the tissue, $\varepsilon = h(x,t)/T$ . For this study two sets of values for $E_o$ and $\lambda$ have been chosen which will be discussed further in Chapter 2.

According to Fung, the stress of a soft tissue is nearly an exponential function of strain at low ranges of stress (40). In addition, experimental data on vaginal tissue obtained by Rubod *et al.* (34), Martin *et al.* (29) and Peňa *et al.* (35) have shown near exponential stress strain relationship. Thus, the assumed exponential model is expected to model the tissue properties better than the linear elastic model.

Existing soft tissue hyperelastic models in the literature such as Mooney-Rivlin model (41) and non-linear Fung model (42), etc. are difficult to incorporate in the current model for vaginal drug delivery systems. In addition, these models are applicable at large strains (43), which is not the case for microbicides delivery. The assumed non-linear (exponential) stress strain relationship can be incorporated in the pressure term without a fluid structure interaction model.

In a future study, by our lab group, it is expect to experimentally determine the model parameters of our non-linear elastic model ($E_o$ and $\lambda$) using a vaginal probe which is under development by Mark Pacey (University of Kansas). A linear viscoelastic tissue model as a boundary condition is also presented. However, a numerical solution for the viscoelastic boundary condition is out of scope of this work.

## 1.5 Review of relevant literature for thin-film flows in microbicides

Studies on thin film flows for biological applications are growing in importance (44). Most common biological applications include lining of pleural surfaces of lungs (4), flow of synovial fluid between joints (44), and tear film between eye and eyelid (45). Only in the recent past have thin-film flows been applied to vaginal drug delivery systems.

Kieweg *et al.* first introduced an *in vitro* experimental model to investigate the effect of gravity on microbicidal gel coatings (14). They compared the surface wetability of six commercially available vaginal gels on hydrophobic and hydrophilic surfaces (14). They concluded that the presence of yield stress, surface wetability and shear-thinning, nature of the gels significantly affect the microbicidal gel coating. They also found that consistency did not play much role for coating over hydrophilic surfaces (14). This study was important as a first step in designing vaginal drug delivery systems.

Kieweg and Katz introduced the 2-D squeezing flow numerical model for power-law and Herschel-Bulkley fluids (19). They investigated the combined effect of a constant squeezing force (typical 4.45 N), shear-thinning behavior and yield stress of the fluid (19). They concluded that squeezing forces, shear-thinning and yield stress behavior play a significant role in gel coating. They validated these conclusions with their experimental results (19).

Kieweg *et al.* introduced a 2-D numerical model of gravity driven flow over an incline with a free surface for a power-law fluid as a supplement to their previous

experimental model (46). Kheyfets and Kieweg extended the 2-D free surface, gravity driven power-law model to 3-D. Their numerical results agreed better with the experimental studies indicating that lateral flow of the gel accounts for the error due to loss of mass in 2-D simulations (47).

Hu and Kieweg modified the 2-D free surface gravity driven model and incorporated surface tension (48). They concluded that surface tension does not affect the spreading speed but, fingering instabilities due to surface tension may cause ineffective or partial coating of the surface (48). Szeri *et al.* incorporated the combined effects of gravity and elastic forces from the vaginal walls to a 2-D channel flow (28). They considered a Carreau-like fluid model to account for the shear-thinning behavior but quantitative results were obtained primarily for a Newtonian fluid. They found a dimensionless number to characterize the relative effects of gravity and squeezing (28).

Previously developed mathematical models by Kheyfets and Kieweg (47), Hu and Kieweg (48), Kieweg *et al.* (46) and Kieweg and Katz (19) have focused on free surface flows and squeezing flows separately which are not realistic. A gravity-driven flow of a Carreau-like fluid with an linear elastic boundary was investigated by Szeri *et al*. (28). However, a systematic analysis of sensitivity of coating behavior to changes in non-Newtonian fluid properties for different elasticities combined with gravity has not been presented before. A parametric and sensitivity analysis of non-Newtonian gel parameters for a wide range of values for tissue elasticity has been incorporated in this thesis. In addition, a non-linear elastic model has been introduced in this work. This study

addresses the limitations of previously developed models in designing an optimal drug delivery vehicle.

## 1.6 Research objectives

The primary objective of this study is to examine the combined effect of vaginal tissue elasticity and gravity on the flow of a microbicidal gel. It is expected to see that the combined effect of gravity and tissue elastic forces will greatly affect the coating of a microbicidal gel. In addition, variations in tissue elasticity could greatly affect the gel coating.

The following research question are addressed in this work:

- Are gravitational and elastic forces comparable during spreading?
- How does gel behavior change with variability in tissue elasticity?
- Are shear-thinning index and consistency significant in the gel coating under the influence of gravitational and elastic forces?
- Do we need to incorporate better constitutive relation (Ellis model) for the gel?
- How does gel coating behavior change with non-linear tissue elasticity?
- Do we need to incorporate viscoelasticity of the tissue?

The overall objective of our lab group is to optimize the rheological properties and structure of a polymeric drug delivery vehicle, to ensure its efficacy on vaginal epithelium under the influence of forces like gravity, tissue compliance, shearing forces

etc. Ultimately, this model will be used to estimate target gel properties for use in groups of women with a specific measured tissue elasticity.

## 1.7 Guide to thesis document

*Chapter 2: Governing equations and numerical methods*

This chapter introduces the following mathematical models for the flow of a delivery vehicle:

- Flow of a power-law fluid with linear elastic boundary condition,
- Flow of an Ellis fluid with linear elastic boundary condition,
- Flow of a power-law fluid with non-linear elastic boundary condition,
- Flow of a power-law fluid with linear viscoelastic elastic boundary condition.

An evolution equation for the height of the fluid is derived from the conservation of momentum equation. A detailed description of the numerical method to solve the evolution equation is presented. In addition, a convergence study for spatial discretization is presented for power-law fluid with linear elastic boundary condition.

*Chapter 3: Results and discussion: Parametric study*

This chapter presents the results of parametric study of the models introduced in chapter 2. The goal of this chapter is to investigate the effect and relative importance of

rheological parameters on spreading length under the influence of gravitational and elastic forces.

*Chapter 4: Results and discussion: Sensitivity analysis*

This chapter presents the results of the sensitivity analysis of rheological properties. The goal of this chapter is to determine the sensitivity of spreading length for a percent change in rheological parameters for different spreading times and tissue elasticities.

*Chapter 5: Conclusions and future direction*

This chapter presents the overall conclusions of the study and the limitations of the current model. A set of optimal targets for the rheological properties estimates based on the parametric study are shown. This chapter provides a direction for future work in the field of microbicide delivery vehicle mathematical models.

# Chapter 2

# Governing Equations and Numerical Methods

This chapter presents a 2D mathematical model for flow of a microbicidal gel between anterior and posterior walls of the human vagina. Since the vagina is a collapsed tube, the width is not axi-symmetric, thus a 2D geometry has been chosen. The objective of this model is to examine the combined effect of gravitational force and tissue compliance on the overall coating of gels. An experimental setup for this flow problem is difficult, thus a numerical model was chosen to simulate the flow. Computational simulations have the advantage of being inexpensive and user-friendly. In addition, the experimental parameters can be varied conveniently.

An evolution equation for the height, $h$, of a finite bolus was derived as a function of spatial variable, $x$, and time, $t$, from the equations of motion. Appropriate boundary conditions and constitutive equations were used in each case. For all of the simulations the initial geometry of bolus is a parabola (see Figure 2.1) of length, $L$ = 3.5 cm and height, $H$ = 0.4 cm, such that the volume of the gel inserted 1.86 ml per unit width. The geometry of bolus is assumed to be symmetric about the vertical axis and the flow direction is along the vertical axis. It is assumed that the bolus remains symmetric at all times and hence the shear stress at the center is zero. Another advantage of a symmetric geometry is that the flow problem can be modeled of over half domain. The flow of the

bolus for different angles of inclination has not been addressed in this study, which is a limitation of this model.

## 2.1 Evolution equation for power-law model with linear elastic boundary

In this section, the evolution equation of a power-law model with a linear elastic boundary condition is derived. The derivation steps are as following:

### 2.1.1 Conservation of linear momentum

Applying conservation of linear momentum for the finite bolus,

$$\frac{d\boldsymbol{u}}{dt} + (\boldsymbol{u} \cdot \nabla)\boldsymbol{u} = -\frac{1}{\rho}\nabla \cdot p + \frac{\nabla \cdot \bar{\boldsymbol{\tau}}}{\rho} + \boldsymbol{g} \tag{2.1}$$

where, $\boldsymbol{u}$ is the velocity vector, $p$ is the pressure, $\rho$ is the density of the fluid, $\boldsymbol{g}$ is the gravitational vector and $\bar{\boldsymbol{\tau}}$ is the stress tensor.

### 2.1.2 Lubrication approximation

Lubrication approximation is a commonly used approximation in the theory of thin films. It assumes that the viscous terms dominate the flow when the characteristic length of the thin film is very large compared the characteristic height of the fluid film. Using the thin film lubrication approximation, the inertial terms can be neglected (49), when the equations (2.2) and (2.3) are satisfied.

$$H \ll L \tag{2.2}$$

$$\left(\frac{\rho u L}{\mu}\right)\left(\frac{H}{L}\right)^2 \ll 1 \tag{2.3}$$

where, $H$ is the characteristic height, $L$ is the characteristic length, $\mu$ is the viscosity of the fluid and $\rho$ is the density.

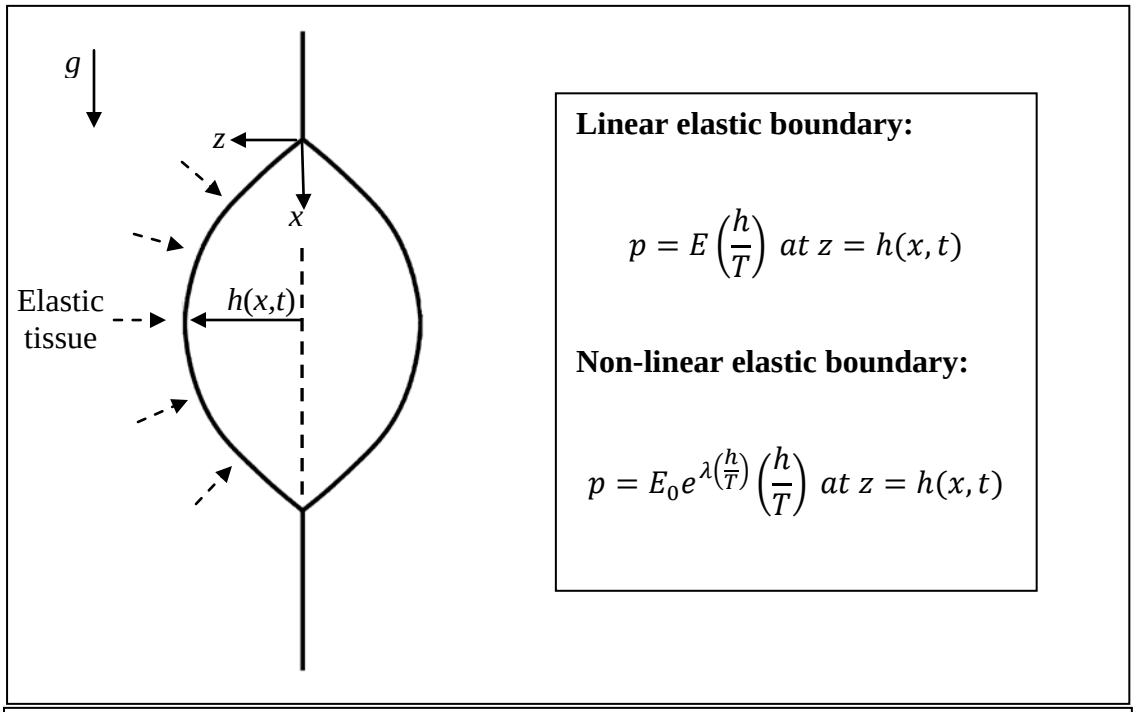


**Figure 2.1 Sketch showing the initial shape of the bolus.**

Initial shape of the bolus is a parabola of height, $H$=0.4 cm, length $L$=3.5cm

The highest ratio of $H/L$ in all of the simulations is 0.114. These flows usually have a Reynolds number of the order $10^{-2}$ to $10^{-4}$ (21). Therefore, lubrication theory is applicable to this flow model. Thus, the momentum equation (2.1) reduces to,

$$0 = -\frac{1}{\rho}\nabla \cdot p + \frac{\nabla \cdot \mathbb{T}}{\rho} + \boldsymbol{g} \tag{2.4}$$

The equation in $x$ and $z$ directions are given by

$x$ – direction:

$$0 = -\frac{\partial p}{\partial x} + \frac{\partial \tau_{zx}}{\partial z} + \rho g_x \tag{2.5}$$

$z$ – direction:

$$0 = -\frac{\partial p}{\partial z} \tag{2.6}$$

### 2.1.3 Boundary conditions

#### (a) Pressure boundary condition

The tissue elasticity is incorporated in the pressure term of the model. The pressure exerted by the tissue is directly proportional to the strain or deformation in the tissue assuming a linear elastic behavior. The tissue elasticity, $E$ is the constant of proportionality (described in Chapter 1).

$$p = E \cdot \frac{h(x,t)}{T} \quad \text{at} \quad z = h(x,t) \tag{2.7}$$

where $E$ is the elasticity of the tissue, $T$ is the tissue thickness and $h(x,t)$ is the height of the bolus at the tissue interface.

**(b) Symmetric (zero shear stress) boundary condition**

It is assumed that the bolus is symmetric at all times and there is no exchange of fluid mass across the vertical axis. Using this assumption, the shear stress at the center is specified with the following boundary condition,

$$\tau_{zx} = 0 \text{ at } \quad z = 0 \tag{2.8}$$

Since the geometry of the bolus is symmetric, the momentum equations are solved over the half domain.

**(c) No slip boundary condition**

A no slip boundary condition is introduced at the vaginal walls as:

$$u = 0 \text{ at } \quad z = h \tag{2.9}$$

Upon integration of the momentum equation in $z$-direction (2.6), an expression for pressure is obtained as, $p = f(x,t) + constant$.

Substitution of the pressure boundary condition equation (2.7) in the above expression yields, $p = \frac{E \cdot h}{T} + constant$.

Substituting this expression for $p$ into the $x$-direction momentum equation (2.5), gives:

$$0 = -\frac{E}{T}\frac{\partial h}{\partial x} + \frac{\partial \tau_{zx}}{\partial z} + \rho g_x \tag{2.10}$$

Integrating equation (2.10) with respect to *z*, and using the symmetric boundary condition (2.8), an expression for shear stress is obtained:

$$\tau_{zx}(x, z, t) = \left(\frac{E}{T}\frac{\partial h}{\partial x} - \rho g_x\right) z \tag{2.11}$$

### 2.1.4 Power-law constitutive model

The constitutive equation for a 1-D power-law fluid was discussed in Chapter 1, and is given by

$$\tau_{zx} = m\left(\frac{\partial u}{\partial z}\right)^n \tag{2.12}$$

where, *m* is the consistency and *n* is the shear-thinning index. To handle the absolute value terms we write the expression in the form(50),

$$\tau_{zx} = m\frac{\partial u}{\partial z}\left|\frac{\partial u}{\partial z}\right|^{n-1} \tag{2.13}$$

This avoids the complex form of the expression when the shear rate is negative. Substituting the constitutive equation (2.13) into equation (2.11), and integrating with respect to *z*, an expression for velocity is obtained:

$$u(x, z, t) = \frac{1}{m}\left(\frac{E}{T}\frac{\partial h}{\partial x} - \rho g_x\right)\left|\frac{1}{m}\left(\frac{E}{T}\frac{\partial h}{\partial x} - \rho g_x\right)\right|^{\frac{1}{n}-1}\left(\frac{|z|^{1+\frac{1}{n}}}{1+\frac{1}{n}}\right) + C1 \tag{2.14}$$

Using the no-slip boundary condition (2.9), the constant of integration is found as:

$$C1 = -\frac{1}{m}\left(\frac{E}{T}\frac{\partial h}{\partial x} - \rho g_x\right)\left|\frac{1}{m}\left(\frac{E}{T}\frac{\partial h}{\partial x} - \rho g_x\right)\right|^{\frac{1}{n}-1}\left(\frac{|h|^{1+\frac{1}{n}}}{1+\frac{1}{n}}\right) \tag{2.15}$$

Hence the expression for velocity $u(x,z,t)$ is given by:

$$u = \frac{1}{m}\left(\frac{E}{T}\frac{\partial h}{\partial x} - \rho g_x\right)\left|\frac{1}{m}\left(\frac{E}{T}\frac{\partial h}{\partial x} - \rho g_x\right)\right|^{\frac{1}{n}-1}\left(\frac{|z|^{1+\frac{1}{n}}}{1+\frac{1}{n}} - \frac{|h|^{1+\frac{1}{n}}}{1+\frac{1}{n}}\right) \tag{2.16}$$

Using this expression for velocity, the flow rate per unit width is given by,

$$q(x,t) = \int_0^{h(x,t)} u(x,z,t)\cdot dz \tag{2.17}$$

$$q(x,t) = \frac{-n\, m^{-\frac{1}{n}}}{(2n+1)}\left(\left(\frac{E}{T}\frac{\partial h}{\partial x} - \rho g_x\right)\left|\left(\frac{E}{T}\frac{\partial h}{\partial x} - \rho g_x\right)\right|^{\frac{1}{n}-1} h^{2+\frac{1}{n}}\right) \tag{2.18}$$

### 2.1.5 Evolution equation using law of conservation of mass

The conservation of mass was written as:

$$\frac{\partial h(x,t)}{\partial t} + \frac{\partial q(x,t)}{\partial x} = 0 \tag{2.19}$$

to obtain a nonlinear partial differential equation, that governs the evolution of the free surface $h(x,t)$:

$$\frac{\partial h(x,t)}{\partial t} - \frac{n\, m^{-\frac{1}{n}}}{(2n+1)} \frac{\partial}{\partial x}\left( \left(\frac{E}{T}\frac{\partial h}{\partial x} - \rho g_x\right) \left|\left(\frac{E}{T}\frac{\partial h}{\partial x} - \rho g_x\right)\right|^{\frac{1}{n}-1} h^{2+\frac{1}{n}} \right) = 0 \qquad (2.20)$$

Thus, this is the "evolution equation" of a power-law model with a linear elastic boundary condition. In the further sections of this chapter, a numerical method is described to solve this equation. For the power-law model with linear elastic boundary condition, we chose the range of values for elasticity, $E$ = 0.05 - 100 kPa. The range of values for consistency, $m$ = 100 - 600 Psec$^{n-1}$ and shear- thinning index, $n$ = 0.5 - 1.0. These range of values for non-Newtonian gel parameters were chosen based on rheological data obtained for hydroxyethyl cellulose (HEC) gels synthesized by our lab group. In total 396 simulations/cases were run for the power-law fluid model with linear elastic boundary condition.

## 2.2 Evolution equation for Ellis model with linear elastic boundary condition

The initial steps involved in the derivation for an Ellis model are same as sections 2.1.1, 2.1.2 and 2.1.3. Hence, this derivation directly begins from the constitutive equation for the fluid.

### 2.2.1 Ellis fluid constitutive model

The 1D constitutive equation for Ellis model was described in Chapter 1, and is given by,

$$\eta_{app} = \frac{\eta_0}{\left(1 + \left|\frac{\tau_{zx}}{\tau_{1/2}}\right|^{\alpha-1}\right)} \tag{2.21}$$

where $\eta_0$ is the zero shear stress viscosity and $\tau_{1/2}$ is the value of shear stress for which the viscosity has been reduced by a factor of one-half. $\alpha$ controls the shear-thinning behavior of the model.

The expression for shear stress is,

$$\tau_{zx} = \eta_{app} \frac{\partial u}{\partial z} \tag{2.22}$$

An expression for velocity is obtained by substituting the constitutive model into the expression (2.11) for shear stress $\tau_{zx}(x, z, t)$ derived in the previous section and integrating with respect to $z$. The constant of integration is determined using the no-slip boundary condition (2.9)

$$u = \frac{1}{\eta_0}\left(\left(\frac{E}{T}\frac{\partial h}{\partial x} - \rho g_x\right)\frac{z^2 - h^2}{2} + \frac{z^{\alpha+1} - h^{\alpha+1}}{\alpha + 1}\left|\frac{\left(\frac{E}{T}\frac{\partial h}{\partial x} - \rho g_x\right)}{\tau_{1/2}}\right|^{\alpha-1}\right) \tag{2.23}$$

Using the expression for velocity, the flow rate per unit width is obtained using the steps described in section 2.1.4 using equation (2.17)

$$q(x,t) = \frac{-1}{\eta_0}\left(\left(\frac{E}{T}\frac{\partial h}{\partial x} - \rho g_x\right)\left(\frac{h^3}{3}\right) + \frac{h^{\alpha+2}}{(\alpha+2)}\left|\frac{\left(\frac{E}{T}\frac{\partial h}{\partial x} - \rho g_x\right)}{\tau_{1/2}}\right|^{\alpha-1}\right) \tag{2.24}$$

### 2.2.2 Evolution equation from law of conservation of mass

The evolution equation for $h(x,t)$ of an Ellis fluid model with linear elastic boundary condition is obtained by following the steps described in section 2.1.5:

$$\frac{\partial h}{\partial t} - \frac{1}{\eta_0}\frac{\partial}{\partial x}\left(\left(\frac{E}{T}\frac{\partial h}{\partial x} - \rho g_x\right)\frac{h^3}{3} + \frac{h^{\alpha+2}}{(\alpha+2)}\left|\frac{\left(\frac{E}{T}\frac{\partial h}{\partial x} - \rho g_x\right)}{\tau_{1/2}}\right|^{\alpha-1}\right) = 0 \tag{2.25}$$

The range of values for the rheological parameters were taken as zero shear stress viscosity, $\eta_0$ = 944.1 - 3120 P, shear-thinning number, $\alpha$ = 1.0 - 2.1 and shear stress at half value of viscosity $\tau_{1/2}$ = 141.7 - 170.4 dynes/cm$^2$. These were the range of values for Ellis model parameters obtained from data fit of 2.4 - 3.0% HEC gels by our lab group. The range of elasticities considered for this model were elasticity, $E$ = 0.1 - 50 kPa. In total 432 simulations/cases were run for the Ellis fluid model with linear elastic boundary condition.

## 2.3 Evolution equation for power-law model with non-linear elastic boundary condition

The initial steps for the derivation of the evolution equation are same as in sections 2.1.1 and 2.1.2 but the boundary conditions for this model are modified to account for the non-linear stress-strain relationship.

### 2.3.1 Boundary conditions

Vaginal tissue exhibits a non-linear behavior and a linear function cannot approximate this very well. There is experimental evidence showing that the tissue may exhibit exponential behavior (29, 34-35). The non-linear elasticity is incorporated as an exponential function of the deformation, $h$ in the pressure term such that the pressure, $p$ is an exponential function of strain ($\varepsilon = h/T$) of the tissue. Although, this model does not represent the actual non-linear elasticity of vaginal tissue, we expect to see an exponential form of non-linearity for the tissue.

$$p = E_o \cdot e^{\lambda\varepsilon}\varepsilon \quad \text{at} \quad z = h(x,t) \tag{2.26}$$

The elasticity of the tissue is given by:

$$E(\varepsilon) = \frac{dp}{d\varepsilon} = E_o e^{\lambda\varepsilon}(1 + \lambda\varepsilon) \tag{2.27}$$

where $E_0$ and $\lambda$ are model parameters for non-linear elastic model which need to be determined experimentally, strain $\varepsilon = h/T$, $T$ is the tissue thickness and $h(x,t)$ is the height of the bolus at the tissue interface (the deformation in the tissue).

Since there is no experimental data available for vaginal tissue under compression, two set of values were chosen for elasticity parameters, based on the

operating pressure ranges for vaginal tissue using a vaginal probe which ranges from 1-20 kPa (38). For the 1st case, $\underline{E_o}$ = 0.994 kPa and λ = 8.66 such that, the pressure is $p$ = 2.5 kPa when the deformation in the tissue is $h(x,t)$ = 0.4 cm (see Figure 2.2) and the tissue elasticity, $E$ =1 kPa when the deformation in the tissue is $h(x,t)$ = 0.001 cm. In the 2nd case, $E_o$ = 9.96 kPa and λ = 6.05 such that, the pressure is $p$ = 13.3 kPa when the deformation in the tissue $h(x,t)$ = 0.4 cm (see Figure 2.2) and the elasticity of the tissue $E$ = 10 kPa when the deformation in the tissue, $h(x,t)$ = 0.001 cm.

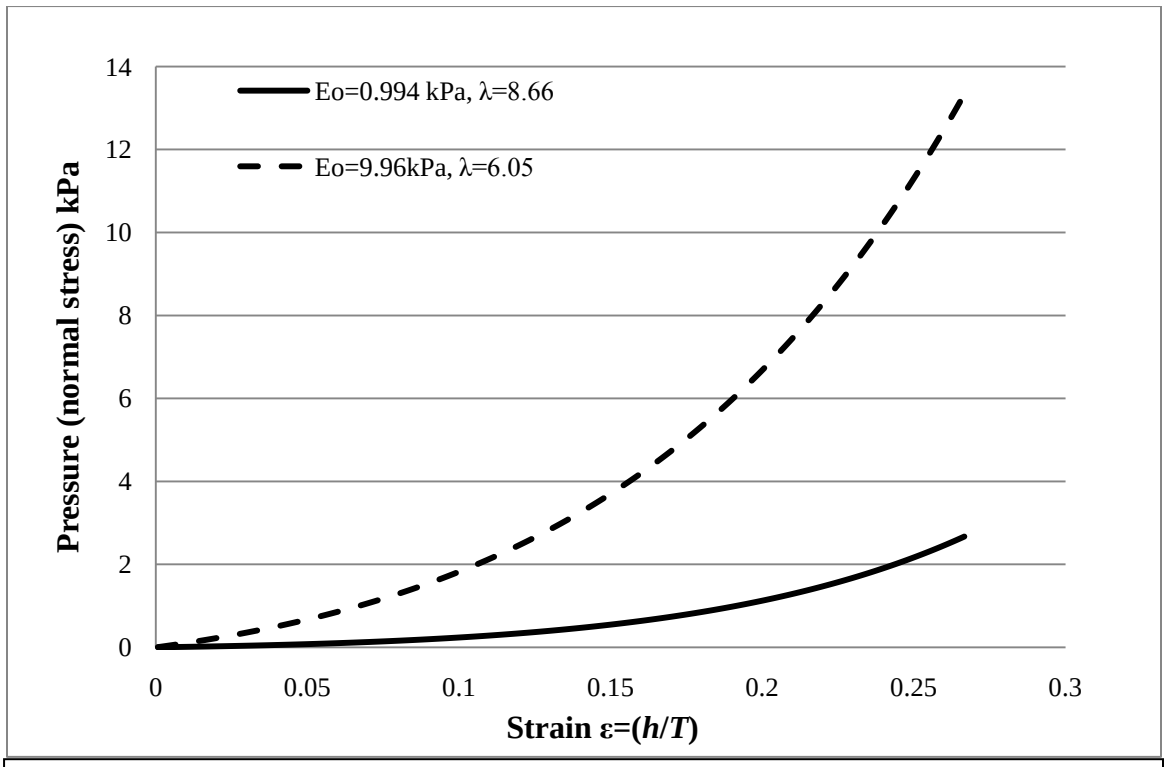


**Figure 2.2 Plot showing how the parameters for non-linear elastic model were chosen based on stress-strain relationship.**

The use of symmetric boundary condition (2.8) and no-slip boundary condition (2.9) are similar to section 2.1.3

Substituting the expression for $p$ in the $z$-direction momentum equation (2.6), integrating with respect to $z$, and using the symmetric boundary condition (2.8), an expression for shear stress is obtained:

$$\tau_{zx}(x,z,t) = \left(\frac{E_0 e^{\lambda \cdot \frac{h}{T}}}{T}\left(1+\frac{\lambda h}{T}\right)\frac{\partial h}{\partial x} - \rho g_x\right) z \qquad (2.28)$$

Using power-law constitutive model and integrating the shear stress with respect to z, an expression for velocity is obtained. The constant of integration was determined by the no-slip boundary condition (2.9).

$$u = \frac{n m^{-\frac{1}{n}}}{(n+1)}\left(\frac{E_0 e^{\lambda \cdot \frac{h}{T}}}{T}\left(1+\frac{\lambda h}{T}\right)\frac{\partial h}{\partial x} - \rho g_x\right)\left|\left(\frac{E_0 e^{\lambda \cdot \frac{h}{T}}}{T}\left(1+\frac{\lambda h}{T}\right)\frac{\partial h}{\partial x} - \rho g_x\right)\right|^{\frac{1}{n}-1}\left(|z|^{1+\frac{1}{n}} - |h|^{1+\frac{1}{n}}\right) \qquad (2.29)$$

The flow rate per unit width is obtained by the same method as in section 2.1.4, equation (2.17) to find:

$$q(x,t) = -\frac{n\, m^{-\frac{1}{n}}}{m(2n+1)}\left(\frac{E_0 e^{\lambda\cdot\frac{h}{T}}}{T}\left(1+\frac{\lambda h}{T}\right)\frac{\partial h}{\partial x}\right.$$

$$\left.-\rho g_x\right)\left|\frac{1}{m}\left(\frac{E_0 e^{\lambda\cdot\frac{h}{T}}}{T}\left(1+\frac{\lambda h}{T}\right)\frac{\partial h}{\partial x}-\rho g_x\right)\right|^{\frac{1}{n}-1}\left(h^{2+\frac{1}{n}}\right) \qquad (2.30)$$

### 2.3.2 Evolution equation from law of conservation of mass

The evolution equation for $h(x,t)$ of a power-law fluid model with non-linear elastic boundary condition was obtained by following the steps described in section 2.1.5:

$$\frac{\partial h(x,t)}{\partial t} - \frac{n\, m^{-\frac{1}{n}}}{(2n+1)}\frac{\partial}{\partial x}\left(\left(\frac{E_0 e^{\lambda\cdot\frac{h}{T}}}{T}\left(1+\frac{\lambda h}{T}\right)\frac{\partial h}{\partial x}\right.\right.$$

$$\left.\left.-\rho g_x\right)\left|\left(\frac{E_0 e^{\lambda\cdot\frac{h}{T}}}{T}\left(1+\frac{\lambda h}{T}\right)\frac{\partial h}{\partial x}-\rho g_x\right)\right|^{\frac{1}{n}-1} h^{2+\frac{1}{n}}\right) = 0 \qquad (2.31)$$

The range of power-law parameters were taken same as the linear elastic boundary condition. In total 72 simulations/cases were run for the power fluid model with non-linear elastic boundary condition. Upon Substituting $\lambda = 0$ in the equation 2.31, it reduces to the evolution equation of linear elastic boundary condition. The numerical code for non-linear elastic boundary condition was also validated for $\lambda = 0$ which gave the same solution for the corresponding linear elastic boundary condition numerical solution

## 2.4 Evolution equation for power-law model with linear viscoelastic boundary condition

The derivation for the power-law fluid with linear viscoelastic boundary condition is presented in this section. This is an initial attempt to incorporate tissue viscoelasticity in the existing drug delivery model. A numerical solution to this model is out of scope of this thesis.

### 2.4.1 Viscoelastic boundary condition

Viscoelasticity is the true tissue behavior and difficult to model. The viscoelasticy of the tissue is introduced as a pressure term such that the pressure acting on the fluid is equal to the viscoelastic stress in the tissue. Here the Voigt model was used to describe the linear viscoelastic nature of the tissue model.

Although this model does not represent the actual viscoelasticity of vaginal tissue, this is an initial approximation in an attempt to incorporate viscoelasticity into the current model as a fluid pressure term. A standard linear model consisting of both Maxwell and Voigt models would be a better representation of the tissue, but the stress term cannot be expressed explicitly in terms of strain and strain rate, hence it cannot be incorporated as fluid pressure.

The viscoelastic stress acting on the tissue for a Voigt model is given by (see Figure 2.3):

$$p = \frac{E \cdot h}{T} + \frac{\eta}{T}\frac{\partial h}{\partial t} \quad at \quad z = h(x,t) \tag{2.32}$$

where, $E$ is the elastic parameter, $\eta$ is the viscous parameter of the tissue, $T$ is the tissue thickness and $h(x,t)$ is the height of the bolus at the tissue interface. The elastic and viscous parameters need to be determined experimentally.

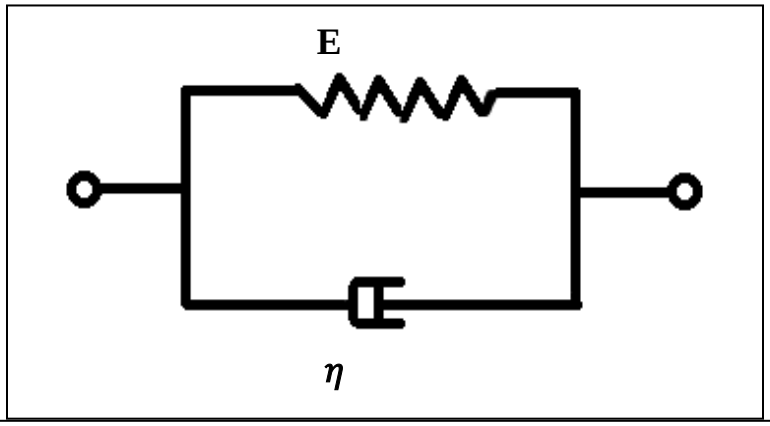


**Figure 2.3 Sketch of aVoigt viscoelastic model**

The classical viscoelastic Kelvin voigt model consists of a spring and a dashpot connected in parallel. (modified from Biomechanics: Material properties of living tissues by Y.C. Fung)

The above boundary condition is substituted into the $z$-direction momentum equation (2.6) to get an expression for pressure. This expression for pressure when substituted in $x$-direction momentum equation (2.5), gives a relation for shear stress:

$$\tau_{zx}(x,z,t) = \left(\frac{E}{T}\frac{\partial h}{\partial x} + \frac{\eta}{T}\frac{\partial^2 h}{\partial x \partial t} - \rho g_x\right) z \tag{2.33}$$

Using the power-law constitutive model, in the expression for shear stress (2.32) and integrating with respect to $z$ an expression for velocity is obtained. The constant of integration is determined using no-slip boundary condition (2.9). The velocity is given by:

$$u(x,z,t) = \frac{1}{m}\left(\frac{E}{T}\frac{\partial h}{\partial x} + \frac{\eta}{T}\frac{\partial^2 h}{\partial x \partial t} - \rho g_x\right)\left|\frac{1}{m}\left(\frac{E}{T}\frac{\partial h}{\partial x} + \frac{\eta}{T}\frac{\partial^2 h}{\partial x \partial t} - \rho g_x\right)\right|^{\frac{1}{n}-1}\left(\frac{|z|^{1+\frac{1}{n}}}{1+\frac{1}{n}} - \frac{|h|^{1+\frac{1}{n}}}{1+\frac{1}{n}}\right) \tag{2.34}$$

The flow rate per unit width is obtained using equation (2.17):

$$q(x,t) = \frac{n\, m^{-\frac{1}{n}}}{(2n+1)}\left(\left(\frac{E}{T}\frac{\partial h}{\partial x} + \frac{\eta}{T}\frac{\partial^2 h}{\partial x \partial t} - \rho g_x\right)\left|\left(\frac{E}{T}\frac{\partial h}{\partial x} + \frac{\eta}{T}\frac{\partial^2 h}{\partial x \partial t} - \rho g_x\right)\right|^{\frac{1}{n}-1} h^{2+\frac{1}{n}}\right) \tag{2.35}$$

### 2.4.2 Evolution equation applying law of conservation of mass

The evolution equation is obtained by following the steps described in section 2.1.5:

$$\frac{\partial h(x,t)}{\partial t} - \frac{n\, m^{-\frac{1}{n}}}{(2n+1)} \frac{\partial}{\partial x}\left( \left( \frac{E}{T}\frac{\partial h}{\partial x} + \frac{\eta}{T}\frac{\partial^2 h}{\partial x \partial t} - \rho\, g \right) \left| \left( \frac{E}{T}\frac{\partial h}{\partial x} + \frac{\eta}{T}\frac{\partial^2 h}{\partial x \partial t} - \rho g_x \right) \right|^{\frac{1}{n}-1} h^{2+\frac{1}{n}} \right)$$

$$= 0 \tag{2.36}$$

## 2.5 Numerical methods and solution

An implicit finite difference scheme was used to solve the evolution equation for *h(x,t)* obtained in the previous sections 2.1, 2.2, 2.3. The numerical scheme is implemented on a C code used previously by Dr. Kieweg for a free surface gravity-driven flow model. This work incorporated tissue elasticity in the pressure acting on the fluid as an extra term in the existing code. Numerical solution to the viscoelastic model is not presented in this study. All the numerical simulations were performed on the ITTC computing cluster, University of Kansas.

### 2.5.1 Discretization

Based on Taylor's polynomial expansion, a central difference scheme was used to discretize the evolution equation (2.19), to obtain the equation of the form:

$$\frac{h_i^{n'+1} - h_i^{n'}}{\Delta t} = -\frac{q_{i+\frac{1}{2}}^{n'+1} - q_{i-\frac{1}{2}}^{n'+1}}{\Delta x} \tag{2.37}$$

where, $i$, represents the spatial position and $n'$ is current time point, $\Delta t$ is the time step and $\Delta x$ is the spatial step size. The order of error of this scheme is $(\Delta x)^2$.

For the power-law model with linear elastic boundary, the discretization terms are given by:

$$q_{i+\frac{1}{2}}^{n'+1} = \frac{-nm^{-\frac{1}{n}}}{(2n+1)}\left(\frac{E}{T}\frac{h_{i+1}^{n'+1} - h_i^{n'+1}}{\Delta x} - \rho\, g\right)\left|\left(\frac{E}{T}\frac{h_{i+1}^{n'+1} - h_i^{n'+1}}{\Delta x} - \rho\, g\right)\right|^{\frac{1}{n}-1}\left(\frac{h_{i+1}^{n'+1} + h_i^{n'+1}}{2}\right)^{2+\frac{1}{n}} \tag{2.38}$$

$$q_{i-\frac{1}{2}}^{n'+1} = \frac{-nm^{-\frac{1}{n}}}{(2n+1)}\left(\frac{E}{T}\frac{h_i^{n'+1} - h_{i-1}^{n'+1}}{\Delta x} - \rho\, g\right)\left|\left(\frac{E}{T}\frac{h_i^{n'+1} - h_{i-1}^{n'+1}}{\Delta x} - \rho\, g\right)\right|^{\frac{1}{n}-1}\left(\frac{h_i^{n'+1} + h_{i-1}^{n'+1}}{2}\right)^{2+\frac{1}{n}} \tag{2.39}$$

For the Ellis fluid model with linear elastic boundary, the discretization terms are given by:

$$q_{i+\frac{1}{2}}^{n'+1} = \frac{-1}{\eta_0}\left(\frac{1}{3}\left(\frac{E}{T}\frac{h_{i+1}^{n'+1} - h_i^{n'+1}}{\Delta x} - \rho g_x\right)\left(\frac{h_{i+1}^{n'+1} + h_i^{n'+1}}{2}\right)^3\right.$$

$$+ \frac{1}{(\alpha+2)}\left|\frac{1}{\tau_{1/2}}\left(\frac{E}{T}\frac{h_{i+1}^{n'+1} - h_i^{n'+1}}{\Delta x}\right.\right.$$

$$\left.\left.\left. - \rho g_x\right)\right|^{\frac{1}{n}-1}\left(\frac{h_{i+1}^{n'+1} + h_i^{n'+1}}{2}\right)^{\alpha+2}\right) \tag{2.40}$$

$$q_{i-\frac{1}{2}}^{n'+1} = \frac{-1}{\eta_0}\left(\frac{1}{3}\left(\frac{E}{T}\frac{h_i^{n'+1} - h_{i-1}^{n'+1}}{\Delta x} - \rho g_x\right)\left(\frac{h_i^{n'+1} + h_{i-1}^{n'+1}}{2}\right)^3\right.$$

$$+ \frac{1}{(\alpha+2)}\left|\frac{1}{\tau_{1/2}}\left(\frac{E}{T}\frac{h_i^{n'+1} - h_{i-1}^{n'+1}}{\Delta x}\right.\right.$$

$$\left.\left.\left. - \rho g_x\right)\right|^{\frac{1}{n}-1}\left(\frac{h_i^{n'+1} + h_{i-1}^{n'+1}}{2}\right)^{\alpha+2}\right) \tag{2.41}$$

For the power-law model with non-linear elastic boundary, the discretization terms are given by:

$$q_{i+\frac{1}{2}}^{n'+1} = \frac{-nm^{-\frac{1}{n}}}{(2n+1)}\left(\frac{E_0 e^{\lambda\cdot\frac{h_{i+1}^{n'+1}+h_i^{n'+1}}{2T}}}{T}\left(1+\frac{\lambda}{T}\frac{h_{i+1}^{n'+1}+h_i^{n'+1}}{2}\right)\frac{h_{i+1}^{n'+1}-h_i^{n'+1}}{\Delta x}\right.$$

$$\left.-\rho g_x\right)\left|\frac{E_0 e^{\lambda\cdot\frac{h_{i+1}^{n'+1}+h_i^{n'+1}}{2T}}}{T}\left(1+\frac{\lambda}{T}\frac{h_{i+1}^{n'+1}+h_i^{n'+1}}{2}\right)\frac{h_{i+1}^{n'+1}-h_i^{n'+1}}{\Delta x}\right.$$

$$-\rho g_x\Bigg|^{\frac{1}{n}-1}\left(\frac{h_{i+1}^{n'+1}+h_i^{n'+1}}{2}\right)^{2+\frac{1}{n}} \tag{2.42}$$

$$q_{i-\frac{1}{2}}^{n'+1} = \frac{-nm^{-\frac{1}{n}}}{(2n+1)}\left(\frac{E_0 e^{\lambda\cdot\frac{h_i^{n'+1}+h_{i-1}^{n'+1}}{2T}}}{T}\left(1+\frac{\lambda}{T}\frac{h_i^{n'+1}+h_{i-1}^{n'+1}}{2}\right)\frac{h_i^{n'+1}-h_{i-1}^{n'+1}}{\Delta x}\right.$$

$$\left.-\rho g_x\right)\left|\left(\frac{E_0 e^{\lambda\cdot\frac{h_i^{n'+1}+h_{i-1}^{n'+1}}{2T}}}{T}\left(1+\frac{\lambda}{T}\frac{h_i^{n'+1}+h_{i-1}^{n'+1}}{2}\right)\frac{h_i^{n'+1}-h_{i-1}^{n'+1}}{\Delta x}\right.\right.$$

$$\left.-\rho g_x\right)\Bigg|^{\frac{1}{n}-1}\left(\frac{h_i^{n'+1}+h_{i-1}^{n'+1}}{2}\right)^{2+\frac{1}{n}} \tag{2.43}$$

The non-linear system of equations were solved using Newton's search method. The number of maximum allowable iterations for Newton's search method to converge was 10 iterations. The convergence criteria was monitored by the reduction of the error to a specific value (in this case the maximum allowable error was $10^{-13}$). A time adaptive

scheme was used with an initial time step value of $\Delta t$ = 0.001 sec. The time adaptive scheme reduces the time step to a factor of 0.8 if the error of the Newton's method does not reduce to the maximum allowable error. The total error tolerance for the simulation was $10^{-8}$ throughout the study.

## 2.6 Convergence study

A convergence study was performed for the spatial discretization, to verify that the mesh size chosen for this study was small enough to obtain a converged solution. The convergence study was performed only for the linear elastic model. with two different elasticities $E$ = 10 kPa and $E$ = 100 kPa. The consistency, $m$, and shear-thinning index, $n$, were kept constant. Figure 2.4 and Figure 2.5 show how the spreading characteristics were affected by the mesh size.

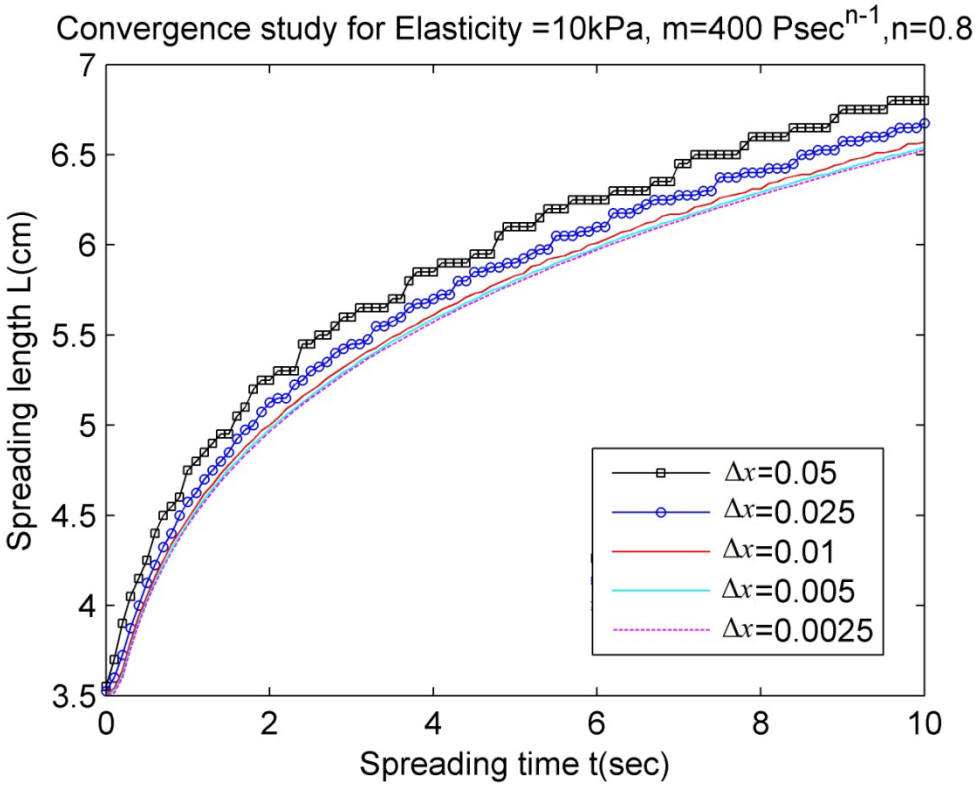


**Figure 2.4 Convergence study of spatial discretization for tissue elasticity, *E* = 10 kPa, consistency, *m* = 400 Psec$^{n-1}$ and shear-thinning index, *n* = 0.8.**

Plot illustrates the effect of mesh size, comparing $\Delta x$ = 0.05, 0.025, 0.01, 0.005 and 0.0025 cm. The step size of $\Delta x$ = 0.01 cm gave a converged solution

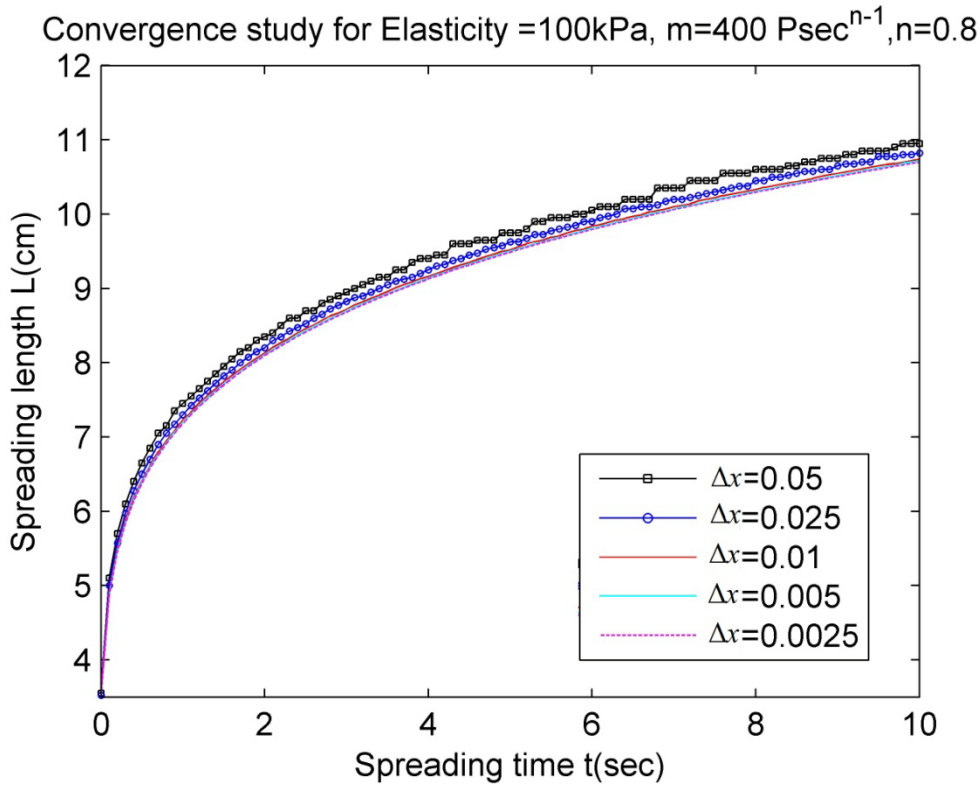


**Figure 2.5 Convergence study of spatial discretization for tissue elasticity, *E* = 100 kPa, consistency, *m* = 400 Psec$^{n-1}$ and shear-thinning index, *n* = 0.8.**

Plot illustrates the effect of mesh size, comparing $\Delta x$ =0.05, 0.025, 0.01, 0.005 and 0.0025 cm. The step size of $\Delta x$ = 0.01 cm gave a converged solution

The results obtained from the convergence study showed that $\Delta x$ = 0.01 cm was sufficiently refined mesh size to obtain a converged solution. Further refinement would largely increase the computational time with no significant improvement in the results. Hence step size of $\Delta x$ = 0.01 cm was chosen for all our computations.

# Chapter 3

# Results and Discussion: Parametric Study

This chapter presents the results of the parametric study for (a) the power-law fluid model with a linear elastic boundary condition, (b) the Ellis fluid model with linear elasticity boundary condition and (c) the power-law fluid with non-linear elastic boundary condition. The parametric study explores the relative influence of tissue elasticity & gravity and the effect of rheological properties on gel spreading. These results are needed four our long term goal of design of a vaginal drug delivery vehicle. For all of the simulations, the fluid density, $\rho$, was taken as 1 g/cm$^3$. The tissue thickness, $T$ (see Figure 1.4), was assumed to be 1.5 cm. The total computational time was 100 seconds. The length of the computational domain was taken as 20 cm and the maximum allowable spreading length was 15 cm. The bolus was positioned such that, the gel does not exceed the computational domain in each case.

## 3.1 Parametric study for power-law fluid model with linear elastic boundary condition

A parametric study for a linear elastic tissue model with a power-law fluid was performed. Since the vaginal tissue elasticity is unknown and thought to be highly

variable (summarized in chapter 1 and 2), a large range of values for tissue elasticitiy were chosen between $E$ = 0.05 to 100 kPa. For the gel rheological properties, the consistency ranged from $m$ = 100 to 600 $Psec^{n-1}$ and the shear-thinning index ranged from $n$ = 0.5 to 1.0.

### 3.1.1 Effect of elastic and gravitational forces

To illustrate the effect of elastic and gravitational forces, the flow profiles of gel for a range of elasticities has been presented (see Figure 3.1). The plots show the flow profiles at intervals of 10 seconds, starting from the initial state at $t$ = 0.001 seconds to $t$ = 50 seconds. In all of these cases, the gravitational force is constant and the tissue elasticity was varied. The shear-thinning index and consistency were taken as $n$ = 0.7 and $m$ = 500 $Psec^{n-1}$ respectively.

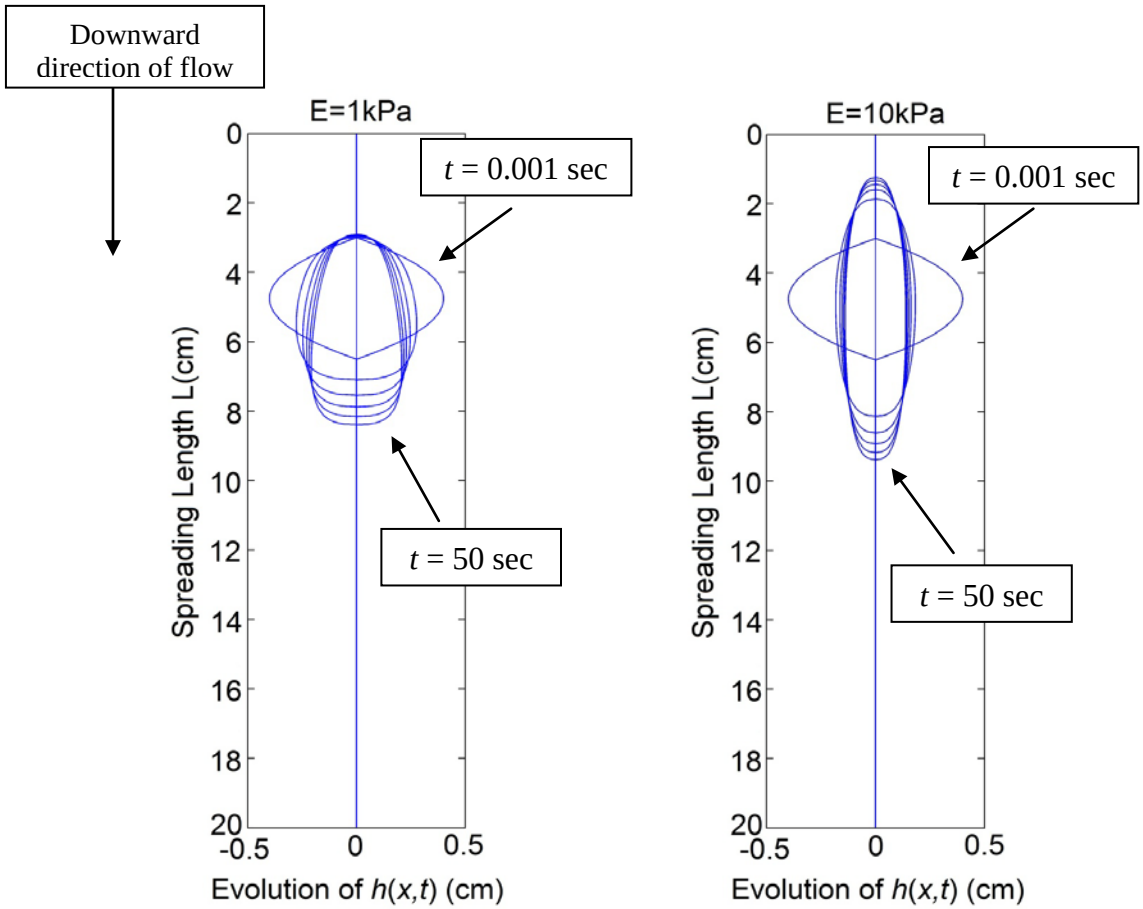


**Figure 3.1(a) Spreading profile for *E* = 1 kPa**

**Figure 3.1(b) Spreading profile for *E* = 10 kPa**

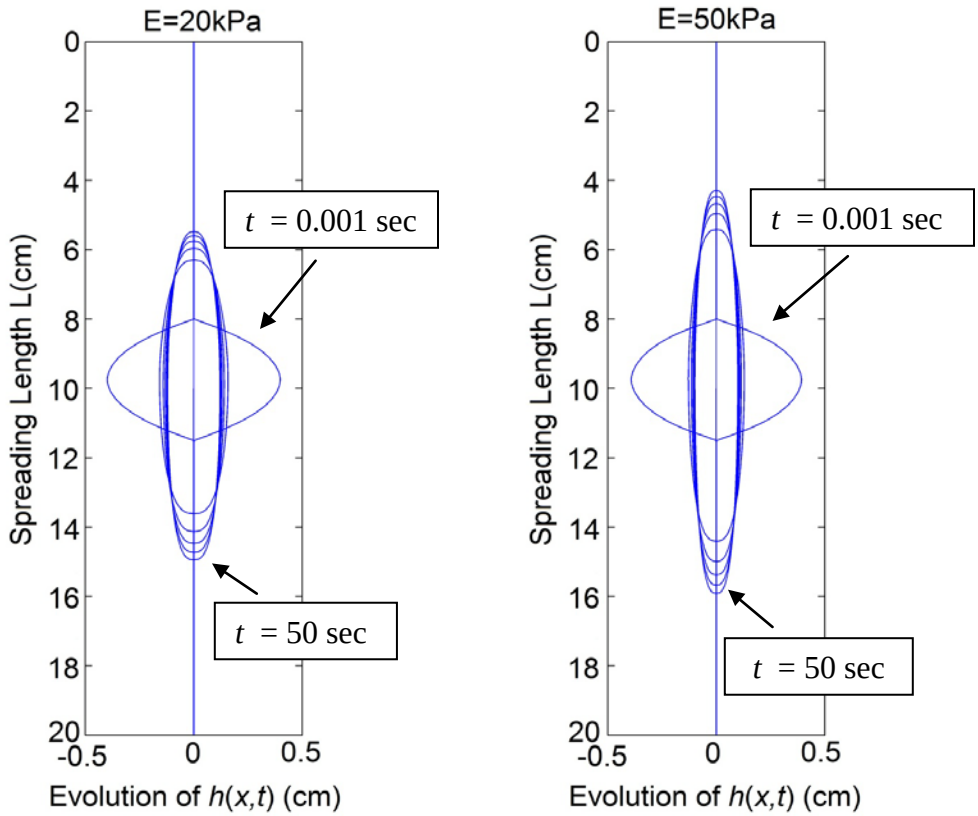


**Figure 3.1(c) Spreading profile for *E* = 20 kPa**

**Figure 3.1(d) Spreading profile for *E* = 50 kPa**

**Figure 3.1 Flow profiles of power-law fluid with different elasticities (linear elasticity), illustrating the effect of tissue elasticity, *E* on coating of the gel.**

Plots comparing the flow profiles of $E$ = 1 kPa, $E$ = 10 kPa, $E$ = 20 kPa and $E$ = 50 kPa for 50 seconds of flow time at intervals of 10 seconds. The shear-thinning index and consistency were $n$ = 0.7 and $m$ = 500 Psec$^{n-1}$ respectively. The bolus is positioned such that it does not exceed the computational domain during spreading in each case.

In the above Figure 3.1(a), the tissue elasticity was low ($E$ = 1 kPa) and the flow profile is in the downward direction. As the tissue elasticity increased in Figures 3.1(b),

(c) and (d), an upward flow was observed. In Figure 3.1(d) when the tissue elasticity was as high as $E$ = 50 kPa, the amount of spreading in the upward direction was nearly equal to the spreading in downward direction. An increase in the spreading rates was also observed as the elasticity increased. From the above observations it can be concluded that a higher elasticity results in faster spreading rates. When the elasticity was high, an upward flow was observed indicating that the squeezing forces due to the tissue elasticity are significantly large compared to gravitational force. As the tissue elasticity increased, the relative effect of gravity decreased.

This result is important to the overall objective of this study by indicating the relative importance of the forces acting on the drug delivery vehicle. This result can be important in choosing the application spot for women with different elasticities. For a woman with higher tissue elasticity the gel may be applied near the fornix. Conversely, for a woman with low tissue elasticity, the gel might have to be applied closer to the cervix.

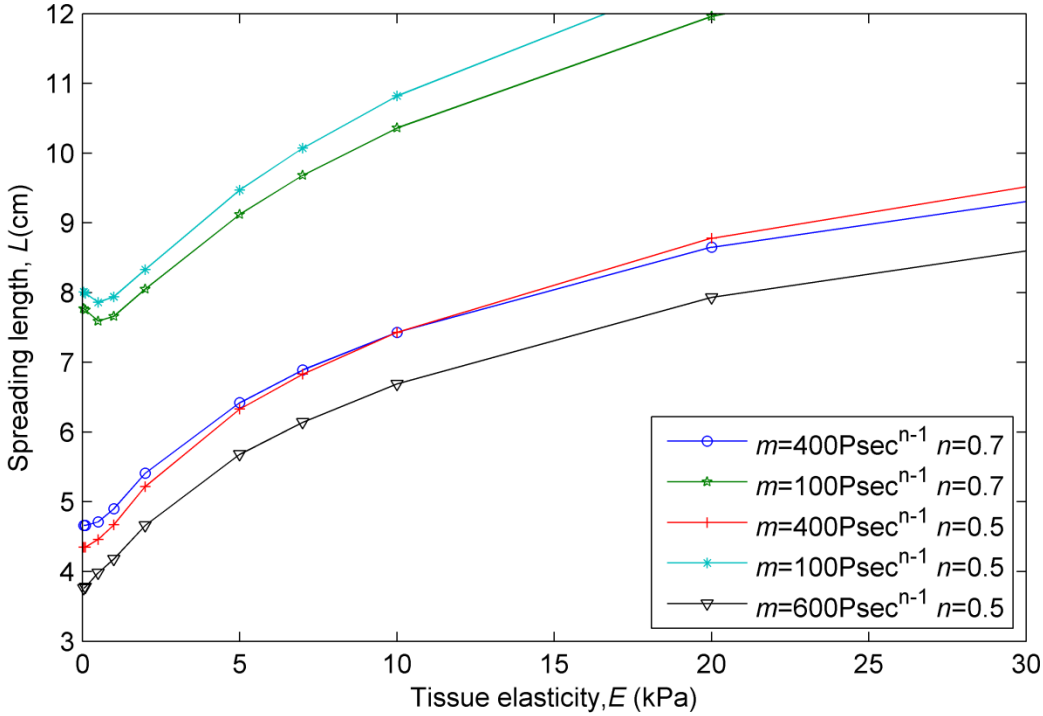


**Figure 3.2 Plot illustrates the gel coating behavior for different tissue elasticities.**

Plot shows a decrease in spreading length, *L* for increase in tissue elasticity, *E* at low tissue elasticity.

An interesting behavior of spreading length was observed for very low tissue elasticity. The spreading length decreased with increase in elasticity (see Figure 3.2). When the elasticity is low, the gravitational force is dominant and there is no upward flow. In addition, tissue elasticity tends to hold the gel intact whereas the gravity pulls the gel down. When the tissue elasticity exceeds a threshold value, beyond which the spreading length increases with increase in elasticity, an upward flow is observed, indicating the dominance of elasticity which squeezes the gel in both upward and downward directions.

### 3.1.2 Effect of shear-thinning index *n*

Shear-thinning index is an important rheological property in the design of a delivery vehicle. In order to investigate the effect of shear-thinning index a parametric study was performed with *n* varying from 0.5 to 1.0. In this section, a comparison of the effect of shear-thinning index *n* for two different tissue elasticities ($E$ = 1 kPa and $E$ = 50kPa) and gel consistency values (100 $Psec^{n-1}$ and 400 $Psec^{n-1}$) has been presented (see Table 1). Figures 3.3, 3.4 and 3.5 present plots of spreading length versus spreading time for different values of shear-thinning index, *n*.

**Table 1 List of cases shown to illustrate the effect of shear-thinning index, *n* of the power-law model with linear elastic boundary condition.**

| Case | Elasticity, *E* kPa | Consistency, *m* $Psec^{n-1}$ | Shear-thinning index, *n* | Figure number |
|---|---|---|---|---|
| Case 1 | 1 | 100 | 0.5-1.0 | Figure 3.3 |
| Case 2 | 1 | 400 | 0.5-1.0 | Figure 3.4 |
| Case 3 | 50 | 400 | 05-1.0 | Figure 3.5 |

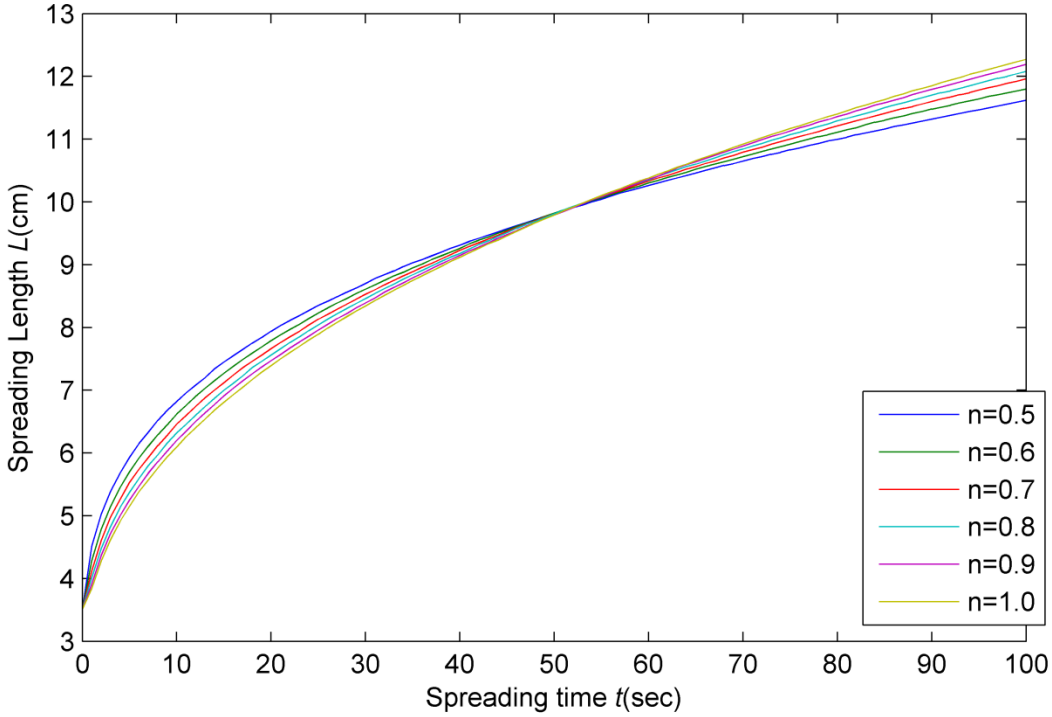


**Figure 3.3 Effect of shear-thinning index, *n* on spreading length, *L* for low tissue elasticity, *E* = 1 kPa and low gel consistency, *m* = 100 Psec$^{n-1}$.**

Spreading length, *L* vs. spreading time, *t* for different values of shear-thinning index, *n*. A lower value of *n* indicates greater shear-thinning behavior, *n* = 1.0 for a Newtonian fluid.

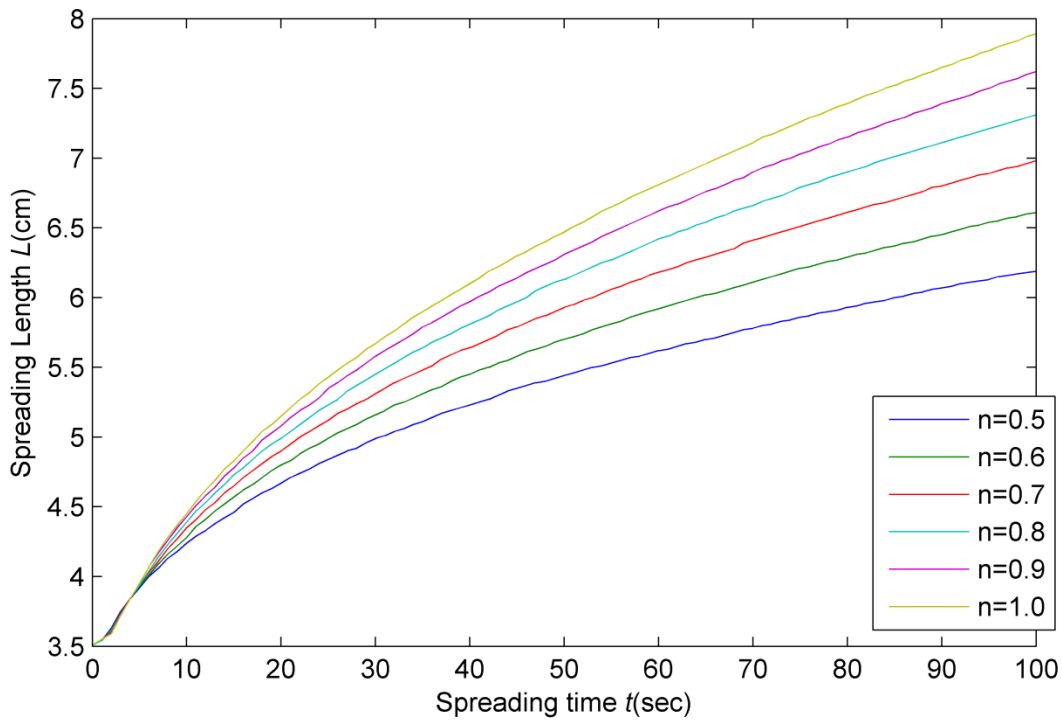


**Figure 3.4 Effect of shear-thinning index, *n* on spreading length, *L* for low tissue elasticity, *E* = 1 kPa and high gel consistency, *m* = 400 Psec$^{n-1}$.**

Spreading length, *L* vs. spreading time, *t* for different values of shear-thinning index, *n*. A lower value of *n* indicates greater shear-thinning behavior, *n* = 1.0 for a Newtonian fluid.

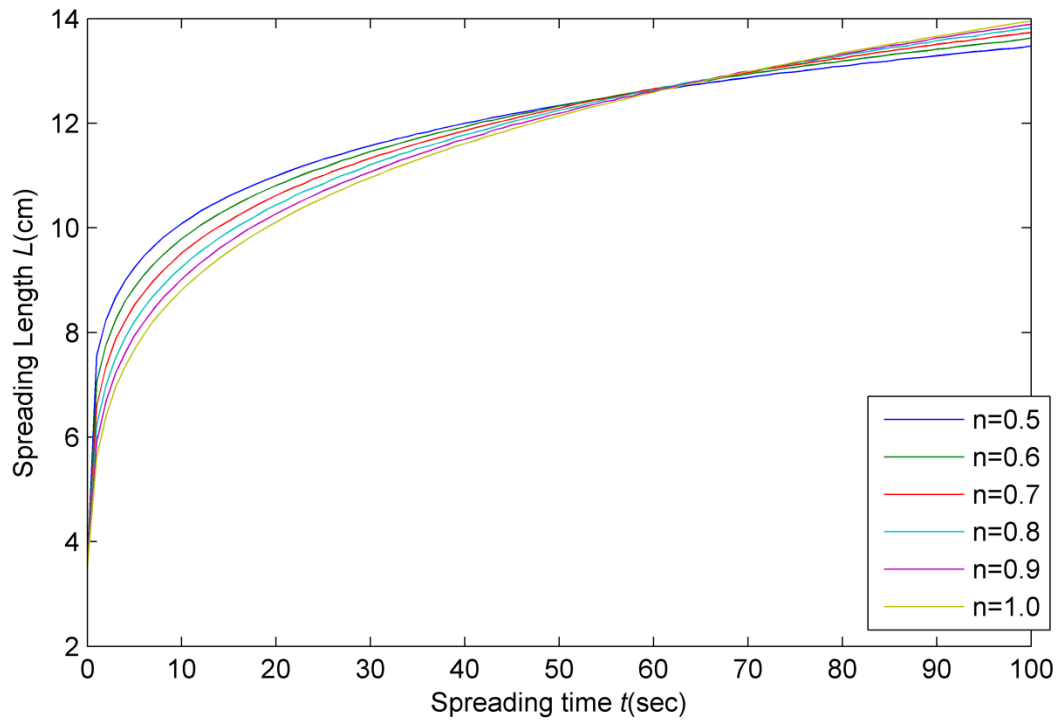


**Figure 3.5 Effect of shear-thinning index, *n*, on spreading length, *L* for high elasticity, *E* = 50 kPa and high consistency, *m* = 400 Psec$^{n-1}$.**

Spreading length, *L* vs. spreading time, *t* for different values of shear-thinning index, *n*. A lower value of *n* indicates greater shear-thinning behavior, *n* = 1.0 for a Newtonian fluid.

Figures 3.3, 3.4 and 3.5 compared the effect of shear-thinning index for different cases of tissue elasticity, *E*, and gel consistency, *m*. The spreading lengths for different values of shear-thinning index *n* are closely packed (Figure 3.3) indicating that shear-thinning index had little impact in the coating of the gel for the time duration of this study. The plot for *E* = 50 kPa and *m* = 100 Psec$^{n-1}$ has not been illustrated here because from the cases shown above, the effect of change in elasticity and change in consistency

can be determined. A synergistic change only adds up the individual effect and hence self-explanatory.

For all the cases a more shear-thinning fluid (lower $n$) flowed faster during initial spreading whereas at longer times a more Newtonian fluid flowed faster ($n \rightarrow 1$). Comparing Figures 3.3 and 3.4, it was observed that, a more shear-thinning fluid spreads faster for a very short period of time for higher consistency. In Figure 3.4, it was observed that for a higher elasticity the shift where Newtonian fluid flows faster occurs at a longer time.

From these observations, it is inferred that a more shear-thinning fluid flows faster during initial spreading, while the Newtonian fluid flows faster at longer times. This shift greatly depends on the consistency and elasticity of the tissue. A fluid with lower consistency has this shift at a later time point and for a fluid with higher consistency at a shorter time. Higher the elasticity the shift is at a later point of time.

The shear-thinning index does not affect the spreading length for shorter spreading times (simulation time in this thesis is small compared to actual application time of microbicidal gel) except when the tissue elasticity is low and the consistency is high. However, there is a shift in trend from a shear-thinning fluid flowing faster to a Newtonian fluid flowing faster which is diverging. Thus, the shear-thinning index may play a vital role for longer times. This is an important result for the design of a delivery vehicle. Especially, the shift in the trend must be considered which is highly dependent on consistency and elasticity of the tissue. This can significantly influence the coating for

long application times. The optimal target values for shear-thinning index for a delivery vehicle should be chosen by keeping this result in mind.

### 3.1.3 Effect of consistency, *m*

To illustrate the effect of consistency a range of parameters for *m* were chosen between $m$ = 100 to 600 $Psec^{n-1}$. The trend for consistency is similar for all elasticities and shear-thinning indices (although impact may be more), hence only one plot showing spreading length versus spreading time has been presented for tissue elasticity, $E$ = 1kPa and shear-thinning index, $n$ = 0.5.

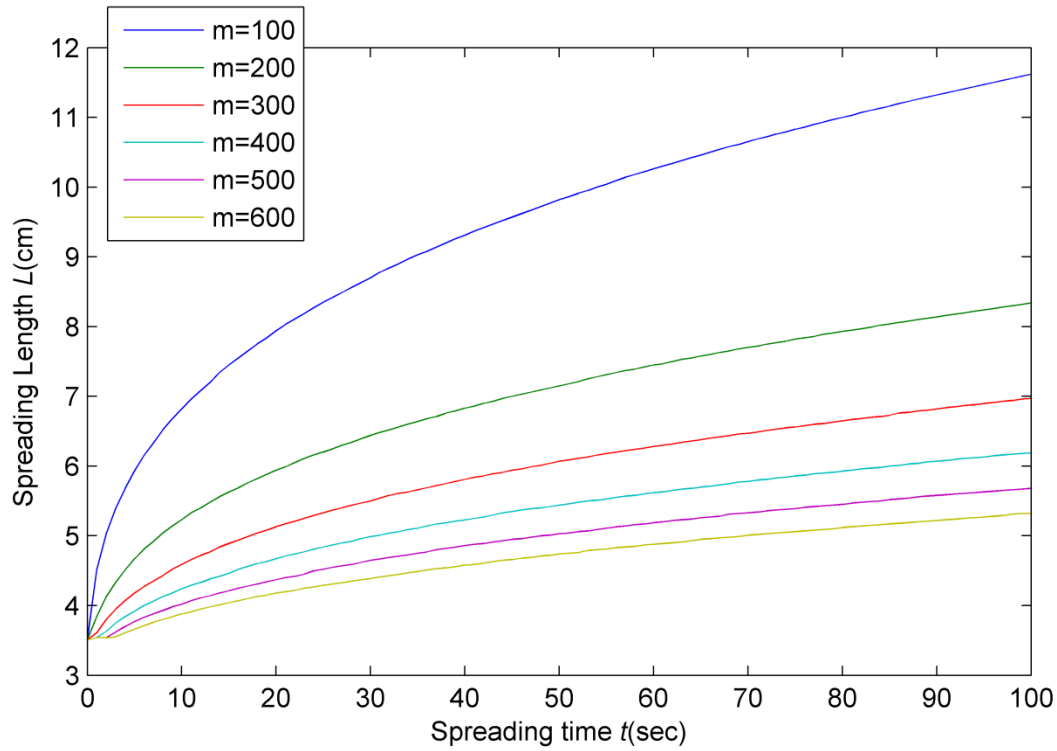


**Figure 3.6 Effect of gel consistency, *m* on spreading length, *L* for tissue elasticity, *E* = 1kpa and shear-thinning index, *n* = 0.5.**

Spreading length, *L* vs. spreading time, *t* for different values of consistency, *m*.

As the consistency of the fluid increased the spreading rate decreased (see figure 3.5). This effect of consistency does not change with spreading time unlike shear-thinning index. At any point of time, a fluid with lower consistency flows faster. The lines showing spreading lengths for different consistencies are widely spaced indicating that consistency has greater impact on the flow than shear-thinning index. However at longer times the slope of spreading length is decreasing and hence the impact at longer times may not be significant compared to initial spreading. Based on this result an

appropriate value of consistency, m can be determined for a potential delivery vehicle depending on application time and tissue elasticity.

An interesting point to be noted is that for a fluid with high value of consistency, the spreading length increases only after a few seconds and the fluid does not flow during that time (negligible change in spreading length) (see Figure 3.6) . This is because there is a change in the shape of the bolus of at this time without increase in spreading length (see Figure 3.7)

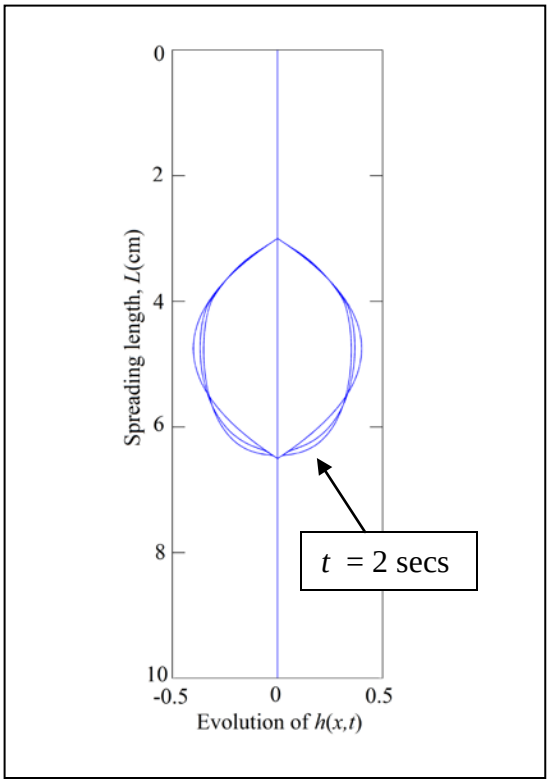


**Figure 3.7 Spreading profile for flow time of t=2 seconds, tissue elasticity, *E* = 1kPa, consistency, *m* = 600 Psec$^{n-1}$ and shear-thinning index, *n* = 0.5.**

Plots illustrates the change in the shape of the bolus without increase in spreading length

### 3.1.4 Summary of results for parametric study of power-law model with linear elastic boundary condition

The results obtained from the parametric study of power-law model with linear elastic boundary condition presented a comparison between the driving forces gravity and tissue elasticity which greatly influence the gel coating. When the tissue elasticity was low, gravity was the dominant force and hence the flow direction was downhill. As the elasticity increased, the squeezing forces resulted in flow in both uphill and downhill directions showing the dominance of elastic forces. When the elasticity was as high as 50 kPa, the spreading length was symmetric in both directions (upward and downward).

Summary of results for parametric study of rheological parameters and elasticity showed that tissue elasticity and gel consistency had great impact on spreading characteristics. As the tissue elasticity increased and gel consistency decreased the spreading length increased. Although shear-thinning fluid has little impact on the spreading characteristics except for at low elasticity and high consistency, the shear-thinning index may play an important role at later spreading times.

## 3.2 Parametric study for an Ellis model with linear elastic boundary condition

An Ellis fluid model does not have limitations at low shear rates unlike power-law model and may be a better constitutive model as summarized in Chapter 1. In this

section, results of the parametric study for the Ellis model have been presented. The range of parameters for the Ellis model were taken from rheological data obtained for 2.4 - 3% HEC gels measured by our lab group. The results of this model have not been compared to the power-law model and only a parametric study for the influence of the Ellis model parameters is presented. The range of tissue elasticities were chosen between $E$ = 0.1 kPa to 100 kPa. The range of parameters for zero shear stress viscosity, $\eta_o$, shear stress for which viscosity is reduced to one-half of its value, $\tau_{1/2}$, and shear-thinning, number for Ellis model, $\alpha$, were taken as $\eta_o$ = 944.1 – 3120 P, $\tau_{1/2}$ = 141.7 – 170.4 dynes/cm$^2$ and $\alpha$ = 1.0 – 2.1 respectively.

### 3.2.1 Effect of elastic and gravitational forces

In this section flow profiles for an Ellis fluid under the influence of tissue elasticity and gravity have been presented with fixed zero shear rate viscosity, $\eta_o$ = 2000 P, shear stress for which viscosity is reduced to one-half of its value, $\tau_{1/2}$ = 160Dynes/cm$^2$ and shear-thinning, number for Ellis model, $\alpha$ = 1.5. The evolution of the gel under the influence of three different elasticities has been presented.

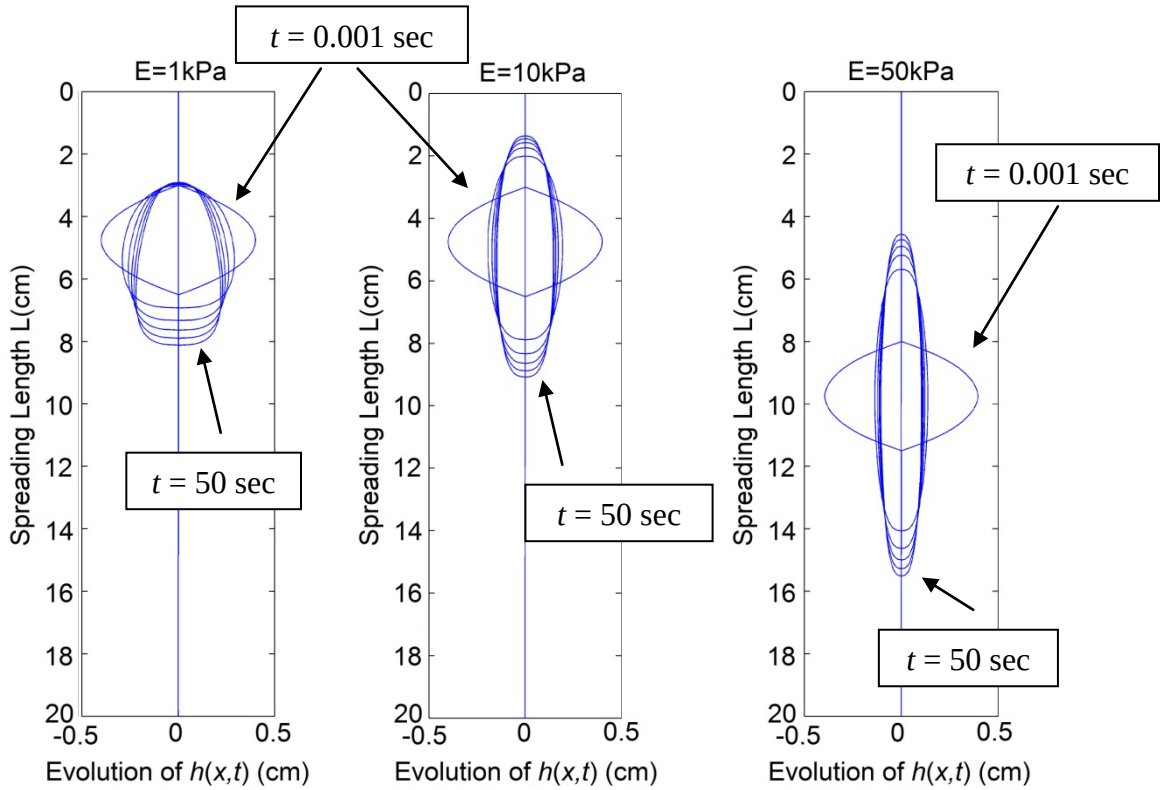


| | | |
|---|---|---|
| **Figure 3.8(a) Spreading profile for *E* = 1 kPa** | **Figure 3.8(b) Spreading profile for *E* = 10 kPa** | **Figure 3.8(a) Spreading profile for *E* = 50 kPa** |

**Figure 3.8 Flow profiles of Ellis fluid with different tissue elasticities (linear elasticity), illustrating the effect of tissue elasticity on coating of the gel.**

Plots comparing the flow profiles of $E$ = 1 kPa, $E$ = 10 kPa and $E$ = 50 kPa for flow time of 50 seconds, at intervals of 10 seconds. The zero shear rate viscosity, $\eta_o$ = 2000 P, shear stress for which viscosity is reduced to one-half of its value, $\tau_{1/2}$ = 160 dynes/cm$^2$ and shear-thinning, number for Ellis model, $\alpha$ = 1.5. The bolus is positioned such that it does not exceed the computational domain during spreading in each case.

Figure 3.8 shows that as the tissue elasticity increased, the spreading rate of the gel increased. This result is similar to the one obtained for the power-law model. Upward flow was observed when the tissue elasticity was higher (see Figure 3.8 (b), (c)). When the tissue elasticity was low, there was no upward flow observed (see Figure 3.8 (a)). The relative importance of gravitational and elastic forces is an important result, which is helpful for the design of a microbicidal gel. The upward flow of the gel of the gel is important in choosing the right application spot for a women depending the tissue elasticity. This result shows that tissue elasticity is a very important parameter in the design of delivery vehicle.

### 3.2.1 Effect of shear-thinning, number, $\alpha$

The effect of shear-thinning, number, $\alpha$ of the Ellis model is illustrated for variations in tissue elasticity, zero shear rate viscosity and shear stress at half value of viscosity.

**Table 2: List of cases shown to illustrate the effect of shear-thinning number, $\alpha$ of an Ellis model with linear elastic boundary condition.**

| Case | Elasticity, $E$, kPa | Zero shear stress viscosity, $\eta_o$ P | Shear-thinning, number, $\alpha$ | Shear stress at half viscosity, $\tau_{1/2}$ dynes/cm$^2$ | Figure |
|---|---|---|---|---|---|
| Case 1 | 1 | 944.1 | 1.0-2.1 | 141.7 | Figure 3.9 |
| Case 2 | 1 | 944.1 | 1.0-2.1 | 170.4 | Figure 3.10 |
| Case 3 | 1 | 3120 | 1.0-2.1 | 141.7 | Figure 3.11 |
| Case 4 | 50 | 3120 | 1.0-2.1 | 141.7 | Figure 3.12 |

Figure 3.9 shows a plot of spreading length versus spreading time for different $\alpha$ for the 1st case of $E$, $\eta_o$ and $\tau_{1/2}$ (see Table 2). The spreading length lines are closely packed indicating that shear-thinning, number doesn't have much influence on the spreading length. However, during initial spreading a more shear-thinning fluid (higher $\alpha$) flows faster and at later times a more Newtonian fluid ($\alpha \rightarrow 1.0$) flows faster. Due to this shift the shear-thinning, number may play an important role for longer spreading times.

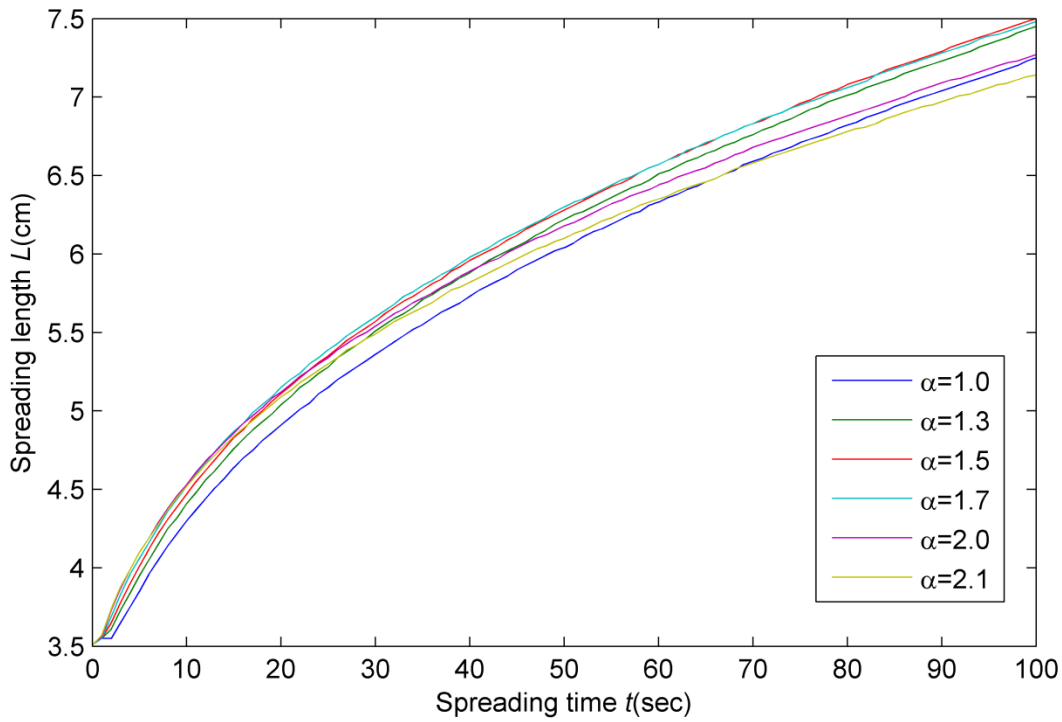


**Figure 3.9 Effect of shear-thinning, number $\alpha$ of an Ellis fluid on spreading length, $L$.**

Spreading length, $L$ vs. spreading time, $t$ for elasticity, $E$ = 1 kPa, zero shear rate viscosity, $\eta_o$ = 944.1 P and shear stress for which viscosity is reduced to one half of its value, $\tau_{1/2}$ = 141.7 dynes/cm$^2$. A greater value of $\alpha$ indicates more shear-thinning behavior, $\alpha$ = 1.0 for a Newtonian fluid.

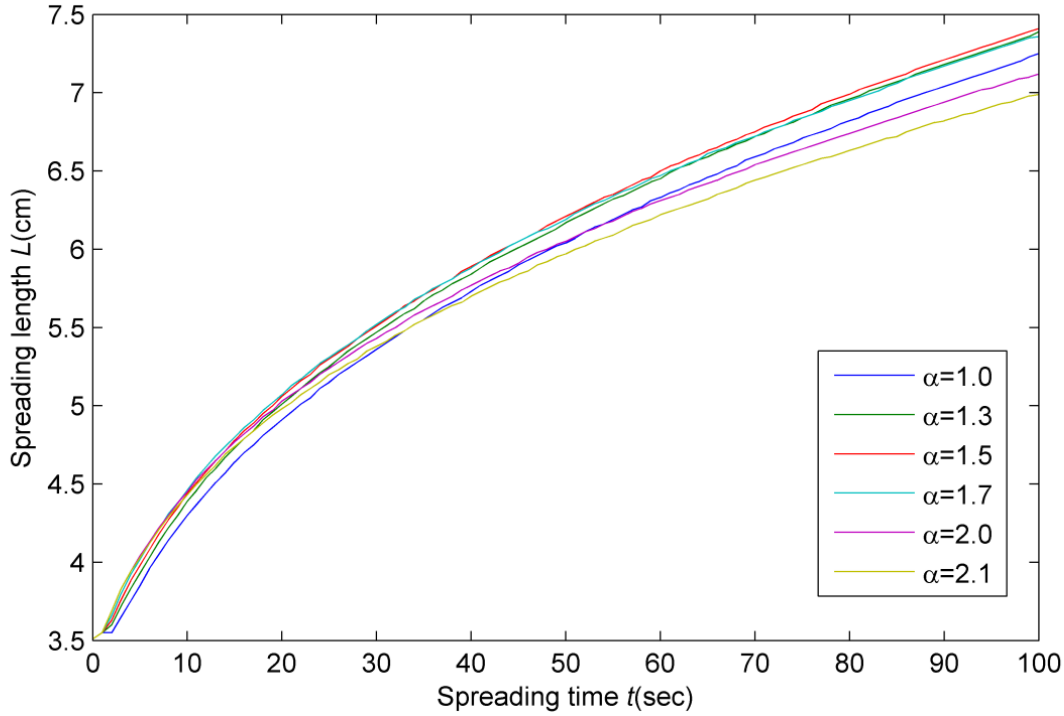


**Figure 3.10 Effect of shear-thinning number, $\alpha$ of an Ellis fluid on spreading length, $L$ for change in shear stress at half value of viscosity, $\tau_{1/2}$.**

Spreading length, $L$ vs. spreading time, $t$ for elasticity $E$ = 1 kPa, zero shear rate viscosity, $\eta_o$ = 944.1 P and shear stress for which viscosity is reduced to one half of its value, $\tau_{1/2}$ = 170.4 dynes/cm$^2$. A greater value of $\alpha$ indicates more shear-thinning behavior, $\alpha$ = 1.0 for a Newtonian fluid.

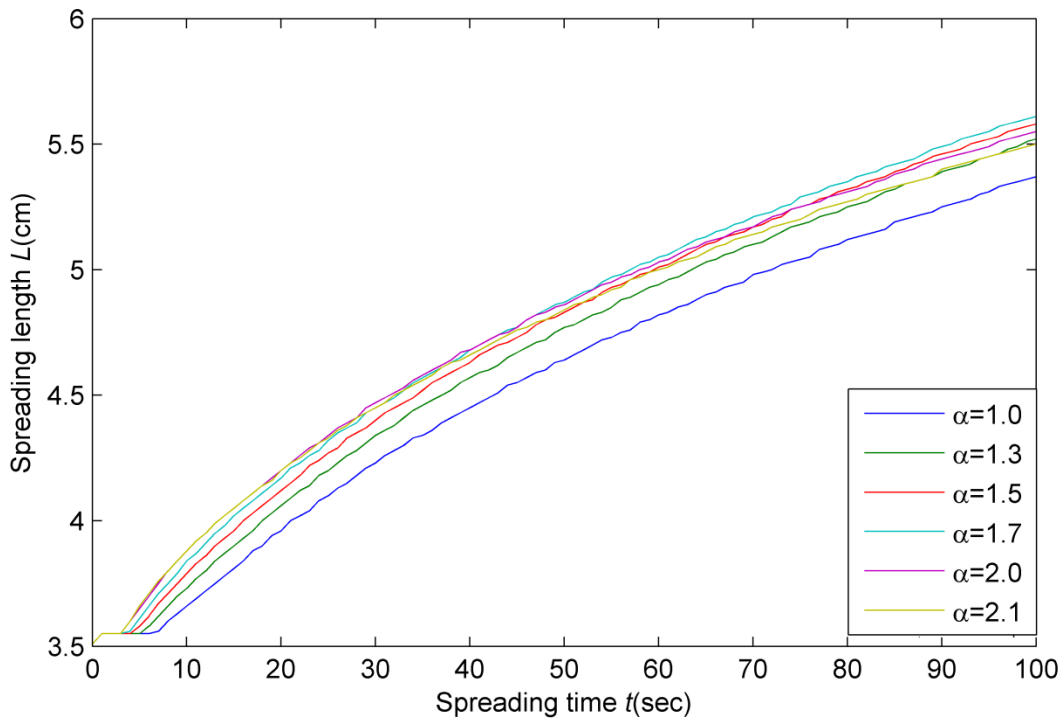


**Figure 3.11 Effect of shear-thinning number, $\alpha$ of Ellis fluid on spreading length L for change in zero shear rate viscosity.**

Spreading length, $L$ vs. spreading time, $t$ for elasticity $E$ = 1 kPa, zero shear rate viscosity, $\eta_o$ = 3120 P and shear stress for which viscosity is reduced to one half of its value, $\tau_{1/2}$ = 141.7 dynes/cm$^2$. A greater value of $\alpha$ indicates more shear-thinning behavior; $\alpha$ = 1.0 for a Newtonian fluid.

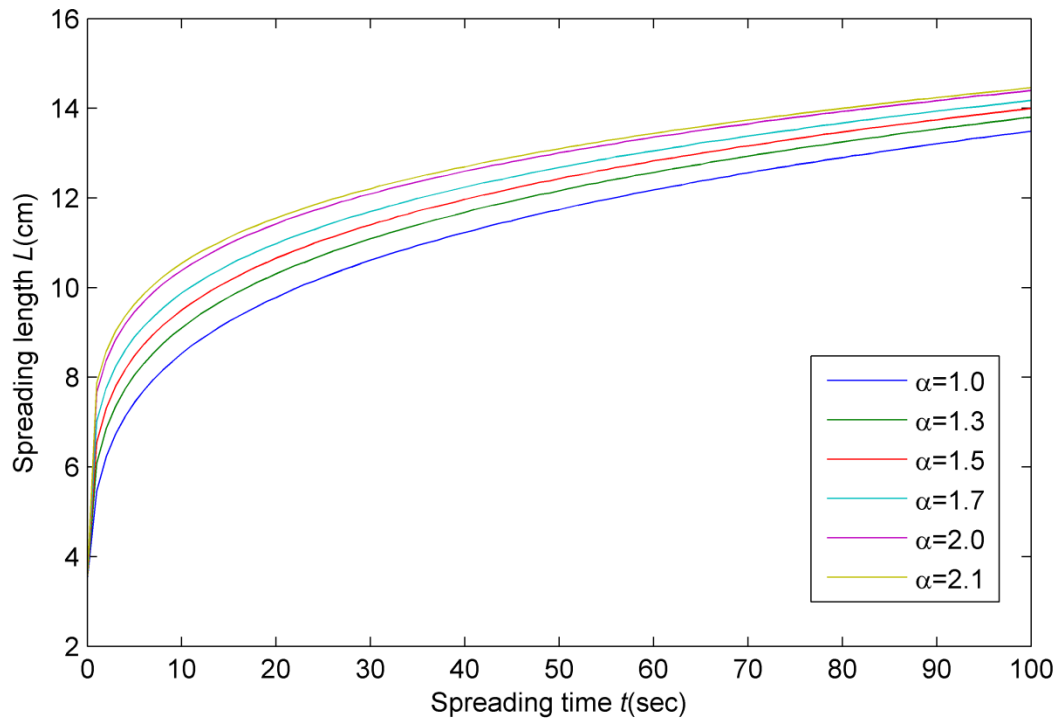


**Figure 3.12 Effect of shear-thinning number, *α* of Ellis fluid on spreading length, *L*, for change in tissue elasticity, *E*.**

Spreading length, *L* vs. spreading time, *t* for tissue elasticity, *E* = 50 kpa, zero shear rate viscosity, $\eta_o$ = 3120 P and shear stress for which viscosity is reduced to one half of its value, $\tau_{1/2}$ = 141.7 dynes/cm$^2$. A greater value of *α* indicates more shear-thinning behavior, *α* = 1.0 for a Newtonian fluid.

The shear stress at half value of viscosity, $\tau_{1/2}$, has negligible effect on the shift of shear-thinning index number trend (compare Figure 3.9 and Figure 3.10 where only $\tau_{1/2}$ differs). Conversely, the zero shear rate viscosity, $\eta_o$, and tissue elasticity, *E* greatly influence the shift in the trend from more shear-thinning fluid flowing faster to Newtonian flowing faster (compare Figures 3.9 and 3.11 for effect of $\eta_o$ and compare

Figures 3.9 and 3.12 for the effect of $E$) . Higher elasticity and lower zero shear stress viscosity led to shift in this trend at later times (see Figures 3.11 and 3.12). This result is helpful in understanding when a shear-thinning fluid starts flowing slower. A shear-thinning fluid would have higher spreading rate during initial spreading, but would flow slower than a Newtonian after a point of time. This must be kept in mind while choosing optimized values for a delivery vehicle in order to have effective coatings. These results are similar to the effect of shear-thinning index in the power-law model.

### 3.2.2 Effect of zero shear stress viscosity, $\eta_o$

The effect to zero shear stress viscosity on spreading length, is illustrated by Figure 3.13 for tissue elasticity, $E$ = 1 kPa, shear-thinning number, $\alpha$ = 1.5, and shear stress at half viscosity $\tau_{1/2}$ = 160 dynes/cm$^2$. Here only one case is shown for the effect of $\eta_o$ because this trend is similar for all variation in rheological properties, however the impact may increase for increase in elasticity.

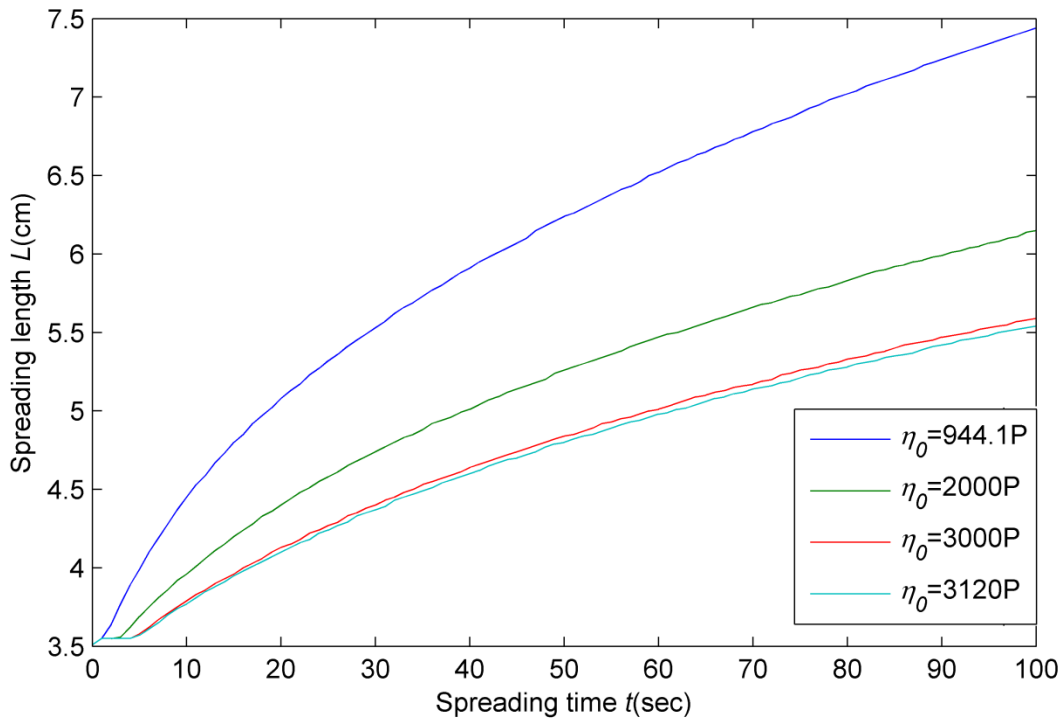


**Figure 3.13 Effect of zero shear rate viscosity $\eta_o$ of an Ellis fluid on spreading length, *L*.**

Spreading length, *L* vs. spreading time, *t* for elasticity, *E* = 1 kPa, shear-thinning, number, $\alpha$ = 1.5 and shear stress for which viscosity is reduced to one half of its value, $\tau_{1/2}$ = 160 dynes/cm$^2$.

Figure 3.13 shows the zero shear stress viscosity has a great impact on spreading length. As the zero shear stress viscosity increased the spreading length decreased (similar to consistency of power-law model). Thus, zero shear stress viscosity is an important rheological parameter in the design of delivery vehicle using an Ellis fluid model. The impact of $\eta_o$ increases with increase in tissue elasticity.

### 3.2.3 Effect of shear stress at half value of viscosity $\tau_{1/2}$

Figure 3.14 illustrates the effect of shear stress at half value of viscosity, $\tau_{1/2}$. Spreading length $L$ versus spreading time $t$ plot has been shown for elasticity, $E$ = 10 kPa, shear-thinning, number $\alpha$ = 2.1 and zero shear stress viscosity $\eta_o$ = 944.1 P. Clearly, $\tau_{1/2}$ has negligible effect on the spreading length from the range of parameters chosen in this study (see Figure 3.14). Moreover, as shear-thinning, number approaches unity, the effect of shear stress at half value of viscosity vanishes. This trend is same for all variation in other rheological parameters.

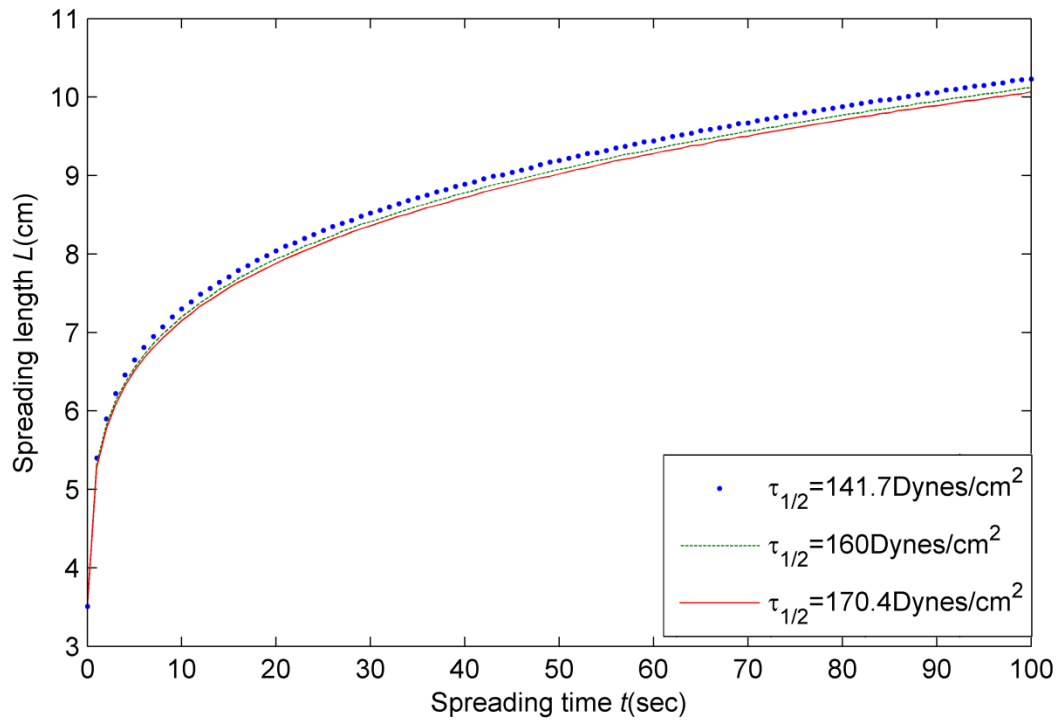


**Figure 3.14 Effect of shear stress for half viscosity, $\tau_{1/2}$ of an Ellis fluid model on spreading length, *L*.**

Spreading length, *L* vs. Spreading time, *t* for elasticity $E$ = 10 kPa, shear-thinning number, $\alpha$ = 2.1 and zero shear rate viscosity, $\eta_o$ = 944.1 P.

### 3.2.4 Summary of results for parametric study of an Ellis fluid model with linear elastic boundary condition.

The results from the parametric study of rheological parameters an Ellis fluid model and linear elasticity of the tissue showed that tissue elasticity, $E$ and zero shear stress viscosity $\eta_o$, had great impact on spreading length. As the elasticity increased and zero shear stress viscosity decreased the spreading length increased. The shear stress at

half value of viscosity, $\tau_{1/2}$ had negligible effect on spreading length for the range of values chosen for this study. The shear-thinning number $\alpha$ had little impact on spreading length for low elasticity and more impact when the tissue elasticity is high. There is a shift in more shear-thinning fluid flowing faster to a more Newtonian fluid flowing faster with spreading time as seen in power-law model.

The comparison of elastic and gravitational forces was similar to the power-law model. An upward flow was observed as the tissue elasticity increased indicating that tissue elasticity is the dominant force. When the tissue elasticity is low, there is no upward flow observed.

## 3.3 Parametric study for a power-law fluid model with non-linear elastic boundary condition

In this section, a parametric study for a power-law model with non-linear elastic boundary condition has been presented. The range for consistency and shear-thinning index were taken as $m$ = 100 to 600 Psec$^{n-1}$ and $n$ = 0.5 to 1.0. Two sets of non-linear elastic parameters $\underline{E_o}$ = 0.994 kPa and $\lambda$ = 8.66 and $E_o$ = 9.96 kPa and $\lambda$ = 6.05 are chosen (as discussed in Chapter 2).

### 3.3.1 Effect of elastic and gravitational forces

The flow profiles for non-linear elastic parameters, $E_o$ = 0.994 kPa and $\lambda$ = 8.66 and $E_o$ = 9.96 kPa and $\lambda$ = 6.05 have been presented in Figure 3.15 for 50 seconds of flow

time in the interval of 10 seconds. The consistency and shear-thinning index were fixed as $m$ = 500 Psec$^{n-1}$ and $n$ = 0.7 respectively.

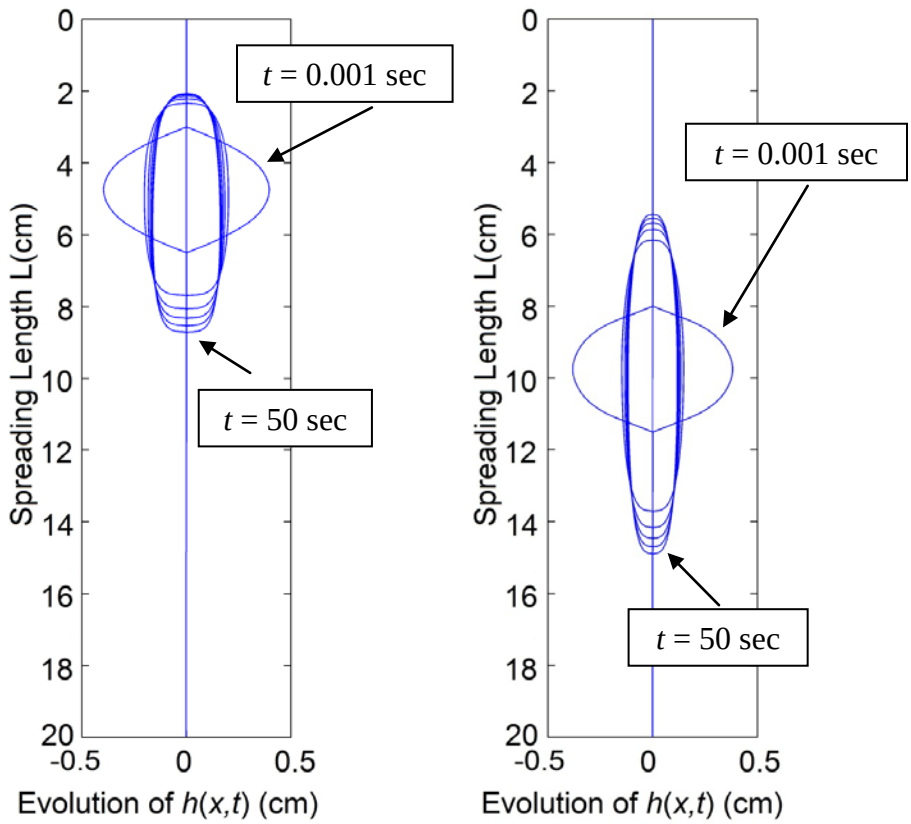


**Figure 3.15 (a) Spreading profile for $E_o$ = 0.994 kPa and λ = 8.66.**

**Figure 3.15 (b) Spreading profile for $E_o$ = 9.96 kPa and λ = 6.05**

**Figure 3.15 Flow profiles of power-law fluid with different elasticities (non-linear elasticity), illustrating the effect of tissue elasticity on coating of the gel.**

Plots comparing the flow profiles of $E_o$ = 0.994 kPa and λ = 8.66, $E_o$ = 9.96 kPa and λ = 6.05 for 50 seconds of flow time at intervals of 10 seconds. The shear-thinning index, $n$ and consistency, $m$ were $n$ = 0.7 and $m$ = 500 Psec$^{n-1}$ respectively.

The tissue elasticity is an important parameter in effective coating of the gel. When the tissue elasticity is high, the gravitational force is negligible compared to elastic forces due to tissue and hence an upward flow is observed. All the results for the effect of tissue elasticity for a non-linear elastic boundary condition are same as the one obtained for linear elastic boundary in section 3.1.1.

Importantly, the spreading lengths are smaller compared to linear elastic model. The non-linearity of the tissue is important. By incorporating the non-linear boundary, the pressure exerted by the tissue decreases exponentially with the height which is more realistic for a soft tissue. A non-linear model tends to retain the gel compared to linear elastic model.

### 3.3.2 Effect of shear-thinning index, *n*

To illustrate the effect of shear-thinning index, n spreading length versus spreading time plots have been shown for change in consistency and change in elastic parameters for non-linear elastic boundary. The following cases are considered (see Table 3)

**Table 3 List of cases shown to illustrate the effect of shear-thinning index, *n* of the power-law model with a non-linear elastic boundary condition.**

| Case | Model parameters | Consistency, *m* $Psec^{n-1}$ | Shear-thinning index, *n* | Figure number |
|---|---|---|---|---|
| Case 1 | $\underline{E_o}$ = 0.994 kPa and λ = 8.66 | 100 | 0.5-1.0 | Figure 3.16 |
| Case 2 | $\underline{E_o}$ = 0.994 kPa and λ = 8.66 | 400 | 0.5-1.0 | Figure 3.17 |
| Case 3 | $E_o$ = 9.96 kPa and λ = 6.05 | 400 | 05-1.0 | Figure 3.18 |

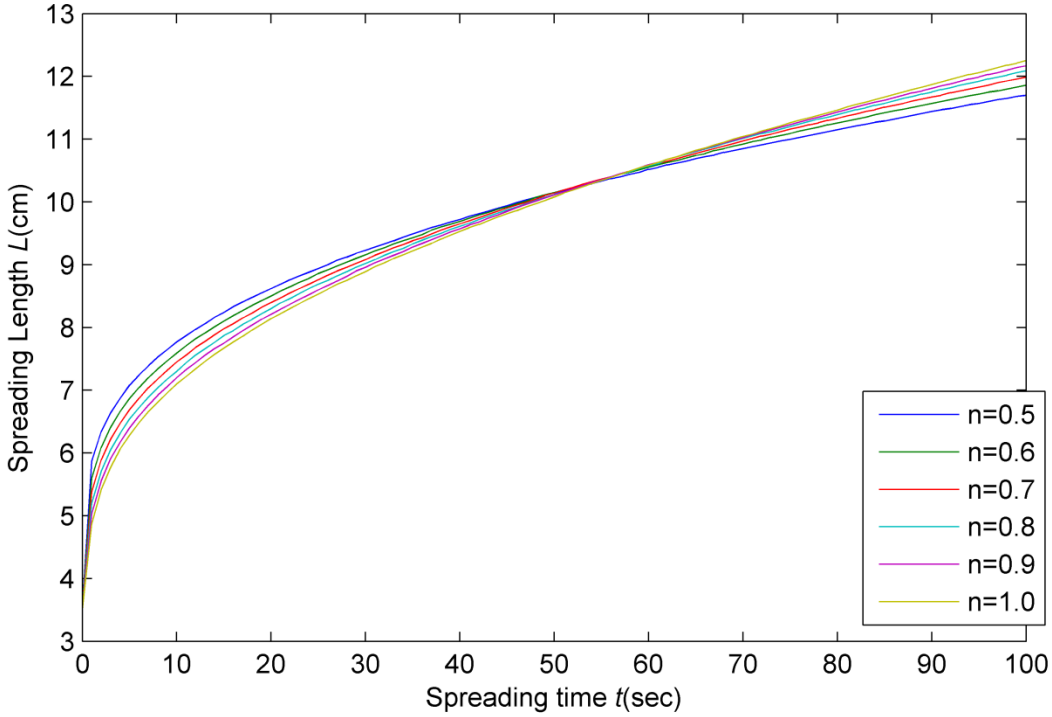


**Figure 3.16 Effect of shear-thinning index, *n*, on spreading length, *L*, for tissue elasticity, $E_o$ = 0.994 kPa and λ = 8.66 and consistency, *m* = 100 Psec$^{n-1}$.**

Spreading length, *L* vs. spreading time, *t* for different values of shear-thinning index, *n*.

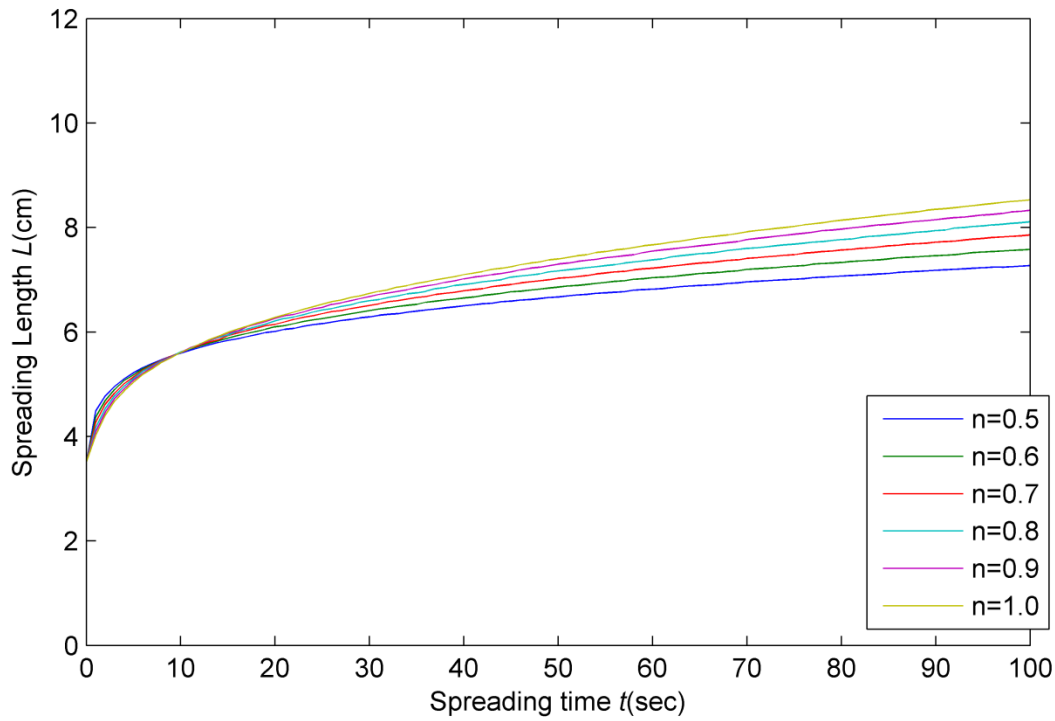


**Figure 3.17 Effect of shear-thinning index, *n*, on spreading length, *L*, for elastic parameters, $E_o$ = 0.994 kPa and λ = 8.66 and consistency, *m* = 400 Psec$^{n-1}$.**

Spreading length, *L* vs. spreading time, *t* for different values of shear-thinning index, *n*.

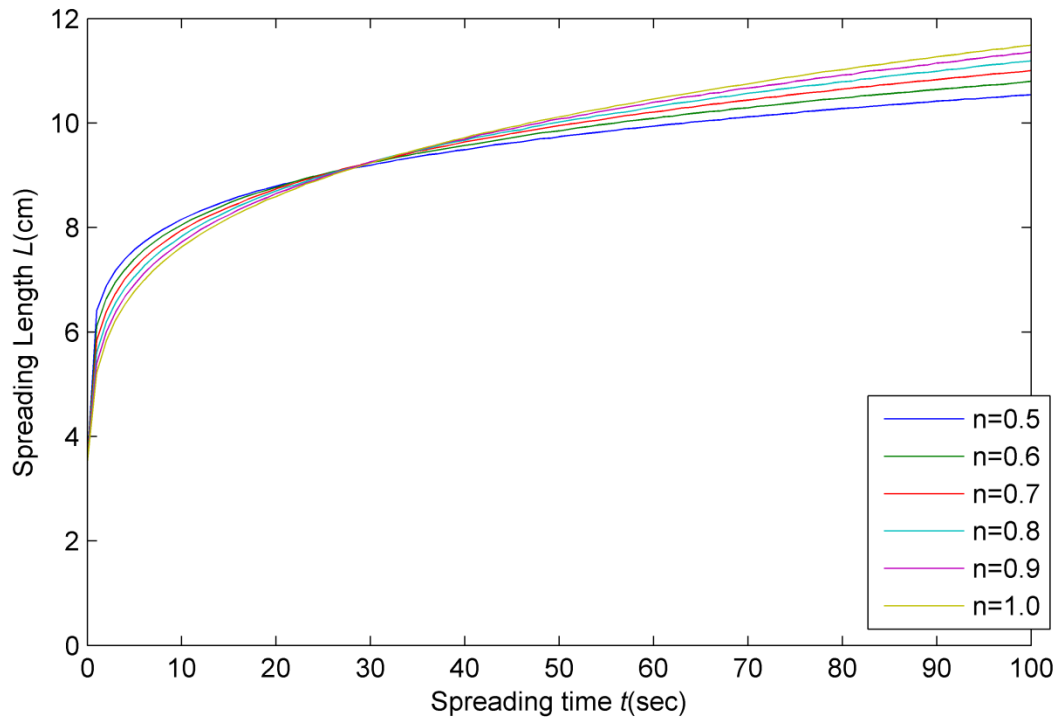


**Figure 3.18 Effect of shear-thinning index, *n* on spreading length, *L* for tissue elasticity, $E_o$ = 9.96 kPa and λ = 6.05 and consistency, *m* = 400 Psec$^{n-1}$.**

Spreading length, *L* vs. spreading time, *t* for different values of shear-thinning index, *n*.

The results obtained for the effect of shear-thinning index *n*, are similar to the ones obtained for the linear elastic model. The spreading length lines for different shear - thinning indices are closely packed indicating that shear-thinning index does not affect the flow for the simulation time of this study (see Figure 3.16). However, there is a shift in trend from a more shear-thinning fluid flowing faster during initial spreading to more Newtonian fluid flowing faster at later times which can be an important design consideration. Compared to the linear elastic model, the effect of change in consistency

on shear-thinning index has little impact for non-linear elastic model (compare Figure 3.19 and Figure 3.17). As the elasticity increased, the shift from shear-thinning fluid flowing faster to a Newtonian fluid flowing faster occurred at a later point of time (see Figure 3.18). This effect of elasticity is the same as that of linear elasticity.

### 3.3.3 Effect of consistency, *m*.

To illustrate the effect of consistency for non-linear elastic boundary, spreading length versus spreading time has been presented in Figure 3.19. The elasticity parameters were taken as $E_o$ = 0.994 kPa and $\lambda$ = 8.66, shear-thinning index was taken as $n$ = 0.5. The behavior of consistency is similar for all spreading times and elasticities hence only one plot is shown here.

The consistency is an important rheological parameter, which greatly affects the spreading of the gel. The results obtained for non-linear elastic model are similar to the ones obtained for the linear elastic boundary model. As the consistency, m of the fluid decreases, the spreading length and spreading rate of the fluid increases.

Compared to the linear elastic boundary condition, the spreading lengths and spreading rates are smaller for a non-linear model. These results are more realistic since the elasticity of the tissue greatly depends on the strain and as the tissue relaxes, the pressure or the stress exerted, also decreases exponentially.

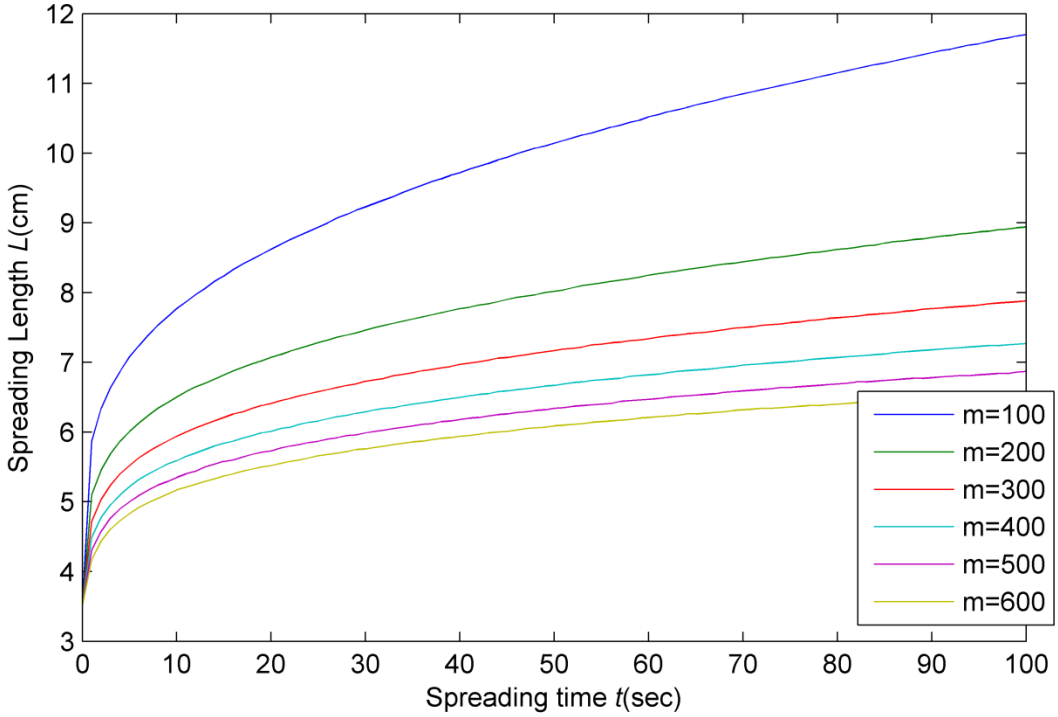


**Figure 3.20 Effect of consistency, *m* on spreading length, *L* for non-linear elastic parameters, $E_o$ = 0.994 kPa and λ = 8.66, shear-thinning index, *n* = 0.5.**

Spreading length, *L* vs. spreading time, *t* for different values of consistency, *m*.

### 3.3.4 Summary of results for parametric study of power-law model with non-linear elastic boundary condition

The comparison between elastic and gravitational forces for the non-linear elastic model showed similar results like the linear elastic model. The higher tissue elasticity dominated the flow.

The parametric study for rheological parameters power-law model with non-linear elastic boundary showed that elasticity and consistency greatly influence the spreading characteristics of the gel. As the non-linear parameter, $E_o$ increased and consistency decreased, the spreading length increased. The behavior of shear-thinning index was observed to be the same as linear elastic boundary. However, a change in consistency had little impact on the behavior of shear-thinning index compared to linear elastic model.

## 3.4 Summary of parametric study

In this chapter a comparison of elastic and gravitational forces is presented, when the gravitational force was dominant, the fluid flow direction was downward, with subsequent increase in tissue elasticity, the spreading length greatly increased as a consequence of squeezing forces which resulted in flow in both directions (upward and downward). This result can be important in choosing the application spot for women with different elasticities. For a woman with higher tissue elasticity the gel may be applied near the fornix. Conversely, for a woman with low tissue elasticity, the gel might have to be applied closer to the cervix.

The parametric study for the power-law fluid with linear and non-linear elastic models in this study showed that, the tissue elasticity and gel consistency had greater impact on spreading compared to shear-thinning index. The shear-thinning index has an interesting behavior that depends on spreading time. During initial spreading, a more

shear-thinning fluid flows faster and at a longer spreading times, a more Newtonian fluid flows faster. This shift greatly depends on tissue elasticity and consistency for a linear elastic model, however consistency has relatively less impact on the behavior of shear-thinning index for a non-linear elastic model. The shift in trend can greatly change the sensitivity of the gel and hence an important design consideration especially for longer spreading times.

The parametric study for an Ellis model showed that zero shear stress viscosity had greatest impact compared to shear stress at half value of viscosity and shear-thinning number. The shear stress at half value of viscosity had the least impact and its effect can be neglected. The behavior of shear-thinning number, $\alpha$ is similar to shear-thinning index of the power law model. Since, the shear stress at half value of viscosity had no effect on spreading characteristics of the gel. The incorporation of Ellis model did not give any advantage to our simulations. Hence, a sensitivity analysis for power-law model alone is presented in Chapter 4.

The results from this chapter help in determining the relative importance of each parameter involved in the design of the delivery vehicle. This study can also help in predicting target values for specific tissue elasticity, application time and target application length. An example application of this study is presented in Chapter 5.

# Chapter 4

# Results and Discussion: Sensitivity Analysis

In this chapter, a sensitivity analysis of the power-law model parameters is presented for linear elastic and non-linear elastic boundary conditions. A comparison of sensitivities for two different elasticities (low and high elasticities) is provided at two different spreading times. The parametric study for an Ellis model is not presented because there was no notable advantage or variation in results observed for an Ellis model compared to the power-law model for the range of values chosen in this study. Moreover, power-law model is a two parameter model and hence the it is convenient to choose for the design of delivery vehicle. In addition many previous study in the design of delivery vehicle for microbicides have used the power-law model (14, 19, 47-48) and hence the results obtained can be correlated and compared.

The results obtained from the parametric study (Chapter 3) gave an overview of the general behavior of the rheological parameters under the influence of gravitational and elastic forces. The optimal target values can be predicted from the parametric study based on the application time, target coverage length and tissue elasticity. However, it is difficult to synthesize gels with a specific value of consistency and shear-thinning index. In addition, once the gel is applied there may be other factors particularly dilution, which

may change the gel properties. As a result of the change in gel properties, a gel may behave differently for different tissue elasticities.

The parametric study did not give a quantitative estimate of change in spreading length for a percentage change of parameters. Sensitivity analysis is important in determining percentage change in spreading length for a change in a parameter. It can also determine which property ranges are more sensitive to a change, whether that change is due to synthesis/formulation or dilution effects. Thus, the sensitivity study is also required for designing gels with target properties and performance.

Here, the percent sensitivity of the spreading length is defined as,

$$\%\, Sensitivity\ spreading\ length = \frac{(L_{new} - L_{old})}{L_{old}} \times 100\ \%$$

where, $L_{new}$ is the spreading length after a 10% change in the parameter, $L_{old}$ is the spreading length without any change to the parameter.

## 4.1 Sensitivity analysis for the power-law model with linear elastic boundary condition

In this section, the sensitivity of spreading length for 10% change in rheological parameters of the power-law fluid for a linear elastic model has been presented. Once the gel is applied, its properties may change significantly when diluted by vaginal fluids. In such a scenario, the fluid becomes more Newtonian, i.e. its consistency decreases and

shear-thinning index increases. Thus, the optimal target values predicted from the parametric study may not work as one would expect. A gel with high sensitivity towards spreading length is highly undesirable even if its properties are optimal for a target length, application time and tissue elasticity. Thus, a sensitivity analysis is important for the design of delivery vehicle.

Here, each power-law parameter is considered individually and then synergistically at the following points $m$ = 100, 200, 300, 400, 500, 600 $Psec^{n-1}$ and $n$=0.5, 0.6, 0.7, 0.8, 0.9, 1.0. (Note in some plots data points $m$ = 100 $Psec^{n-1}$ and $n$ = 0.5 are missing because the spreading length reached 15 cm before the spreading time shown in the plots).

### 4.1.1 Percent sensitivity of spreading length, *L* for 10% decrease in consistency, *m*.

The percent sensitivity of the spreading length for 10% decrease in consistency is presented for two different tissue elasticities, $E$ = 1 kPa and $E$ = 50 kPa and two spreading times, $t$ = 50 seconds and $t$ = 100 seconds. The sensitivity for tissue elasticity, $E$ = 50 kPa at $t$ = 100 seconds is not shown here, because many of the data sets for spreading length (at $m$ and $n$ values) are unavailable at $t$ = 100 seconds. This is because the spreading length reached 15 cm, which is the maximum allowable spreading length for all the simulations way before $t$ = 100 seconds.

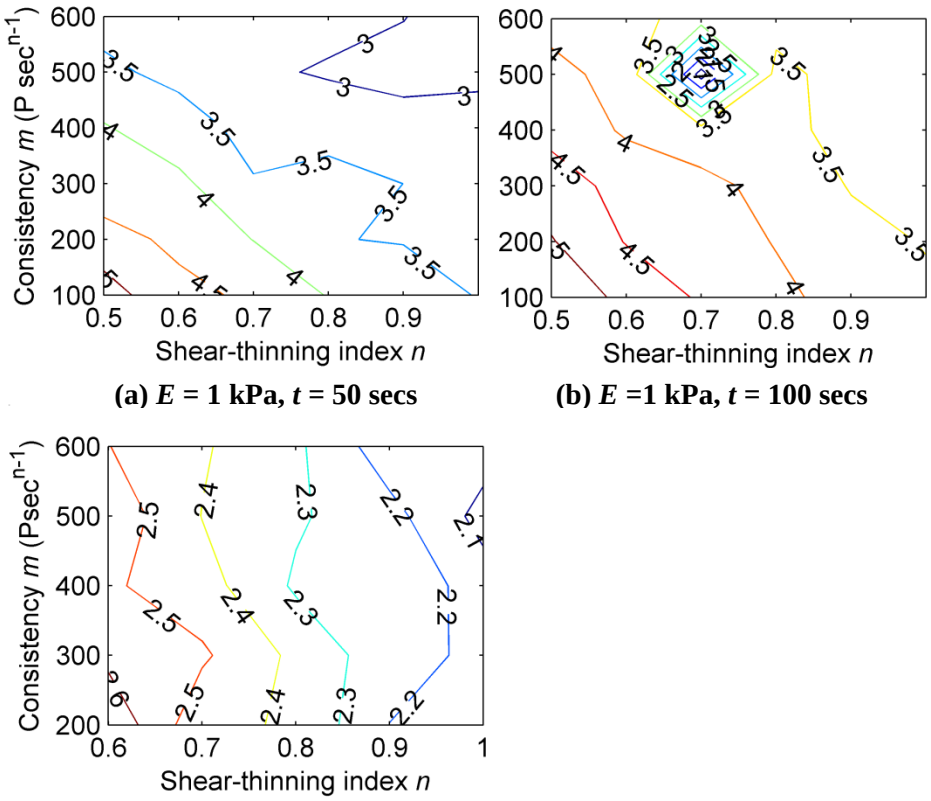


**(a) $E$ = 1 kPa, $t$ = 50 secs** **(b) $E$ =1 kPa, $t$ = 100 secs**

**(c) $E$ = 50 kPa, $t$ = 50 secs**

**Figure 4.1 Contours of percentage change in spreading length, *L*, for 10% decrease in consistency, *m*, of a power-law model with linear elastic boundary condition.**

The contours show the percent sensitivity of spreading length over the *m* and *n* parameter space for several cases. **(a)** Percent sensitivity at 50 seconds flow time for elasticity $E$ = 1 kPa **(b)** Percent sensitivity at 100 seconds flow time for elasticity $E$ = 1 kPa. **(c)** Percent sensitivity at 50 seconds flow time for elasticity $E$ = 50 kPa.

In Figure 4.1, contours showing percentage change in spreading length for 10% decrease in consistency have been presented. The spreading length is more sensitive to change in consistency at low consistency ($m \rightarrow 100$ Psec$^{n-1}$) and low shear-thinning index

($n \rightarrow 0.5$) (see Figure 4.1(a)). The spreading length is more sensitive at 100 seconds of spreading compared to 50 seconds of spreading time. (compare Figure 4.1 (a) and (b)).

The spreading length is less sensitive to change in consistency when the tissue elasticity is higher (compare Figure 4.1 (a) and (c)). An interesting pattern is observed for 100 seconds spreading for $E$ = 1 kPa near $m$ = 500 Psec$^{n-1}$ and $n$ = 0.7 (see Figure 4.1 (b)). A sudden decrease in percent sensitivity of spreading length is observed. This might be due to a shift from Newtonian flowing faster than a shear-thinning fluid. There was no specific pattern in all of these cases for the sensitivity of spreading length. Overall, the spreading length is about 2-5% sensitive to 10% change in consistency. This shows spreading length is quite sensitive to changes in consistency. Thus, a large value of consistency is more favorable for the design because in this region the sensitivity is reduced.

### 4.1.2 Percent sensitivity of spreading length for 10% increase in shear-thinning index, *n*

This section presents percent sensitivity of spreading length for 10% increase in shear-thinning index for two different elasticities, $E$ = 1 kPa and $E$ = 50 kPa and two different time points $t$ = 50 seconds and $t$ = 100 seconds. The sensitivity for tissue elasticity, $E$ = 50 kPa at $t$ = 100 seconds is not shown here, because many of the data sets for spreading length (at $m$ and $n$ values) are unavailable at $t$ = 100 seconds. This is

because the spreading length reached 15 cm, which is the maximum allowable spreading length for all the simulations way before $t$ = 100 seconds.

For a percentage change in shear-thinning index, there was no change in sensitivity for all the values of shear-thinning index, $n$ at lower tissue elasticity, $E$ and lower gel consistency, $m$ (see Figure 4.2(a) and (b)). Sensitivity is higher for larger values of consistency, when the elasticity is low (see Figure 4.2 (a) and (b)). Conversely, the sensitivity is lower for larger values of consistency when the elasticity is high (see Figure 4.2 (c)). This shows that elasticity has a dominant effect on spreading length and sensitivity of rheological parameters.

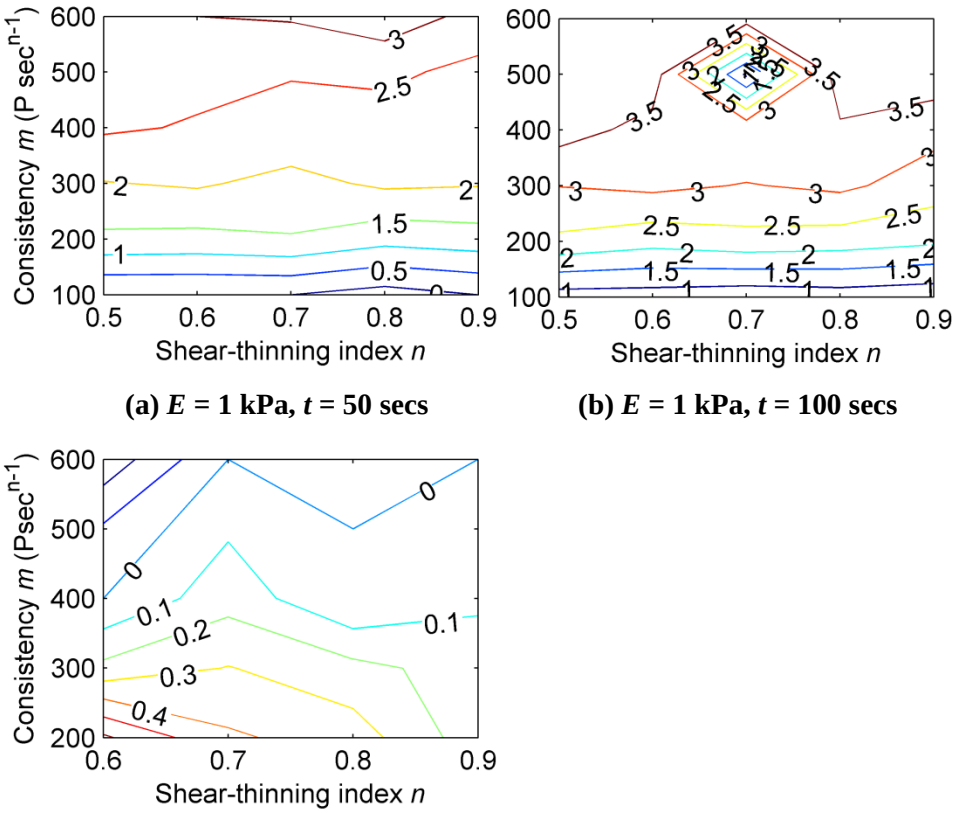


**(a) $E$ = 1 kPa, $t$ = 50 secs** **(b) $E$ = 1 kPa, $t$ = 100 secs**

**(c) $E$ = 50 kPa, $t$ = 50 secs**

**Figure 4.2 Contours of percentage change in spreading length for 10% increase in shear-thinning index, n of a power-law model with linear elastic boundary.**

The contours show the percent sensitivity of spreading length over the $m$ and $n$ parameter space for several cases. **(a)** Percent sensitivity at 50 seconds flow time for elasticity $E$ = 1 kPa **(b)** Percent sensitivity at 100 seconds flow time for elasticity $E$ = 1 kPa **(c)** Percent sensitivity at 50 seconds flow time for elasticity $E$ = 50 kPa.

Although, the spreading length increases with increase in elasticity, the percent sensitivity of spreading length is less for a tissue with higher elasticity because, the sensitivity is a percentage change with respect to the old spreading length. Since the old

spreading length for higher tissue elasticity is itself a large number, even a large change would make the sensitivity small.

The magnitude of percent sensitivity is lower when the tissue elasticity is high and vice versa (see Figure 4.2 (a) and (c)). The possible reason for a very low sensitivity for high tissue elasticity in Figure 4.2 (c) is due to the shift from a shear-thinning fluid flowing faster to a Newtonian fluid flowing faster. The spreading length is more sensitive at longer spreading times.

The magnitude of sensitivity of spreading length for 10% change is about 0-3%. The sensitivity of spreading length for a change in shear-thinning index is less compared to change in consistency.

### 4.1.3 Percent sensitivity of spreading length for 10% decrease in consistency, m and 10% increase in shear-thinning index, *n*

This section illustrates the synergistic sensitivity of spreading length for both 10% decrease in consistency and 10% increase in shear-thinning index for two different elasticities, $E$ = 1 kPa and $E$ = 50 kPa and two different time spreading times $t$ = 50 seconds and $t$ = 100 seconds.

The sensitivity for tissue elasticity, $E$ = 50 kPa at $t$ = 100 seconds is not shown here, because many of the data sets for spreading length (at $m$ and $n$ values) are unavailable at $t$ = 100 seconds. This is because the spreading length reached 15 cm,

which is the maximum allowable spreading length for all the simulations way before $t$ = 100 seconds.

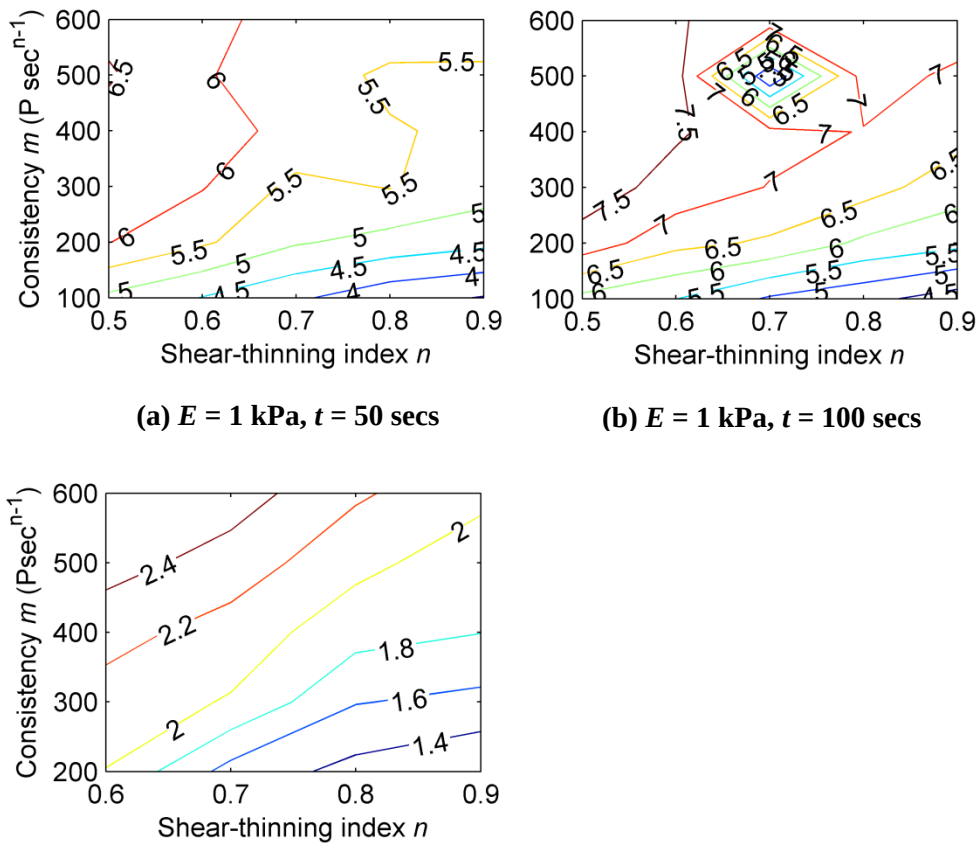


**(a) $E$ = 1 kPa, $t$ = 50 secs**

**(b) $E$ = 1 kPa, $t$ = 100 secs**

**(c) $E$ = 50 kPa, $t$ = 50 secs**

**Figure 4.3 Contours of percentage change in spreading length for 10% decrease in consistency, *m* and 10% increase in shear-thinning index, *n*, of a power-law model.**

The contours show the percent sensitivity of spreading length over the $m$ and $n$ parameter space for several cases. **(a)** Percent sensitivity at 50 seconds flow time for elasticity $E$ = 1 kPa. **(b)** Percent sensitivity at 100 seconds flow time for elasticity $E$ = 1 kPa. **(c)** Percent sensitivity at 50 seconds flow time for elasticity $E$ = 50 kPa.

As expected, the combined change in consistency and shear-thinning index resulted in higher sensitivity of spreading length compared to the previous sections. The spreading length is most sensitive for high consistency ($m \rightarrow 600$ Psec$^{n-1}$) and low shear-thinning index ($n \rightarrow 0.5$) (see Figure 4.3(a)). The spreading length of the gel is least sensitive for low consistency ($m \rightarrow 100$ Psec$^{n-1}$) and high shear-thinning index ($n \rightarrow 1.0$). The spreading length is more sensitive for longer spreading times and less sensitive when the elasticity is high (see Figure 4.3 (b) and (c)). The spreading length is up to 7.5% sensitive for 10% changes in consistency and shear-thinning index, which is quite high.

This shows that for a percent sensitivity for synergistic changes in both consistency and shear-thinning index has a great impact on gel coating and this behavior changes with spreading time and variability in tissue elasticity. These results are important in choosing target values for rheological parameters which are less sensitive. These results also suggest that there is a need to measure tissue elasticities in groups of women, so that the gel synthesized based on the vaginal tissue properties, which can greatly change the coating behavior.

## 4.2 Sensitivity analysis for the power-law model with non- linear elastic boundary condition

In this section, sensitivity analysis for the power-law model with non-linear elastic boundary condition is presented. In the previous section 4.1, it was concluded that tissue elasticity affects the sensitivity of the spreading length for change in rheological

properties. Hence, it is expected that the non-linearity of the tissue may change the results of the sensitivity analysis. In each of the following sub-sections, percent sensitivity of spreading length for two different non-linear elastic parameters $E_o$ = 0.994 kPa and $\lambda$ = 8.66 and $E_o$ = 9.96 kPa and $\lambda$ = 6.05 is presented. The sensitivity is illustrated at two different spreading times $t$ = 50 seconds and $t$ = 100 seconds. Contours of percent sensitivity over the parameter space consistency, $m$ and shear-thinning index, $n$, are shown.

### 4.2.1 Percent sensitivity of spreading length for 10% decrease in consistency, *m*

In Figure 4.4(a), it is observed that the spreading length is most sensitive for low consistency ($m \rightarrow 100$ kPa) and low shear-thinning index ($n \rightarrow 0.5$). This trend is similar to the result obtained for linear elastic boundary condition. The sensitivity of spreading length increased with increase in time (see Figure 4.4 (a) to (b) and Figure 4.4 (c) to (d)). The sensitivity of spreading length ranged between 2-4% for 10% change in consistency which is quite high. For all cases, the sensitivity varied over the entire parametric space $m$ and $n$.

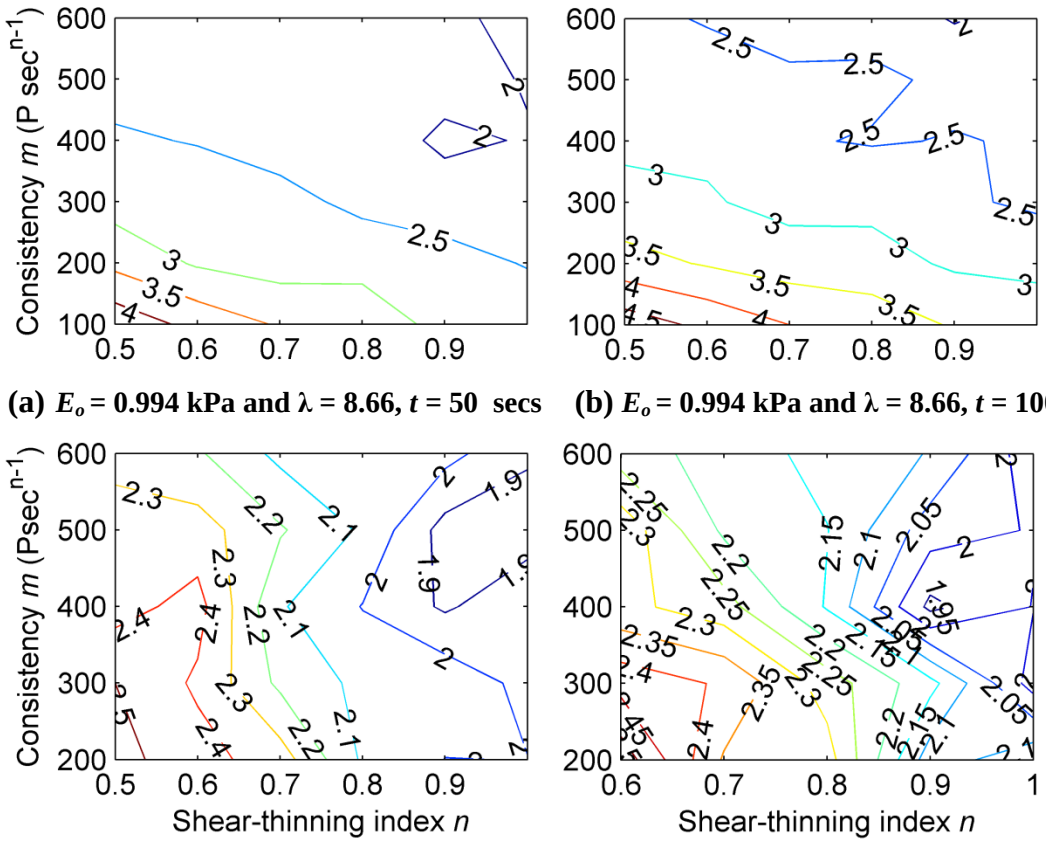


**(a)** $E_o$ **= 0.994 kPa and λ = 8.66,** $t$ **= 50 secs** **(b)** $E_o$ **= 0.994 kPa and λ = 8.66,** $t$ **= 100 secs**

**(c)** $E_o$ **= 9.96 kPa and λ = 6.05,** $t$ **= 50 secs** **(d)** $E_o$ **= 9.96 kPa and λ = 6.05,** $t$ **= 100 secs**

**Figure 4.4 Contours of percentage change in spreading length for 10% decrease in consistency, m of a power-law model with non-linear elastic boundary.**

The contours show the percent sensitivity of spreading length over the *m* and *n* parameter space for several cases. **(a)** Percent sensitivity at 50 seconds flow time for $E_o$ = 0.994 kPa and λ = 8.66. **(b)** Percent sensitivity at 100 seconds flow time for elasticity $E_o$ = 0.994 kPa and λ = 8.66. **(c)** Percent sensitivity at 50 seconds flow time for elasticity $E_o$ = 9.96 kPa and λ = 6.05. **(d)** Percent sensitivity at 100 seconds flow time for elasticity $E_o$ = 9.96 kPa and λ = 6.05.

### 4.2.2 Percent sensitivity of spreading length for 10% increase in shear-thinning index, *n*

Figure 4.5 illustrates the sensitivity of spreading length for 10% increase in shear-thinning index, *n*. It is observed that sensitivity of spreading length is more for large values of consistency (see Figure 4.5 (a)). The sensitivity increased with increase in spreading time for both low and high elasticities (see Figure 4.5 (b) and (d)). The percent sensitivity is lower for higher elasticity (see Figure 4.5 (c) and (d)). The magnitude of percent sensitivity of spreading length for change in shear-thinning index are less compared to change in consistency.

Compared to the linear elastic model the sensitivities are lower for low elasticity. For a higher elasticity the sensitivity of linear elastic model is lower, this may be because of a shift from shear-thinning fluid flowing faster to a Newtonian fluid flowing faster and hence the sensitivity behavior cannot be compared. Moreover, the linear elastic model elasticities are not an equivalent (or comparable in magnitude) to the non-linear model and hence they cannot be compared quantitatively but overall behavior can be assessed.

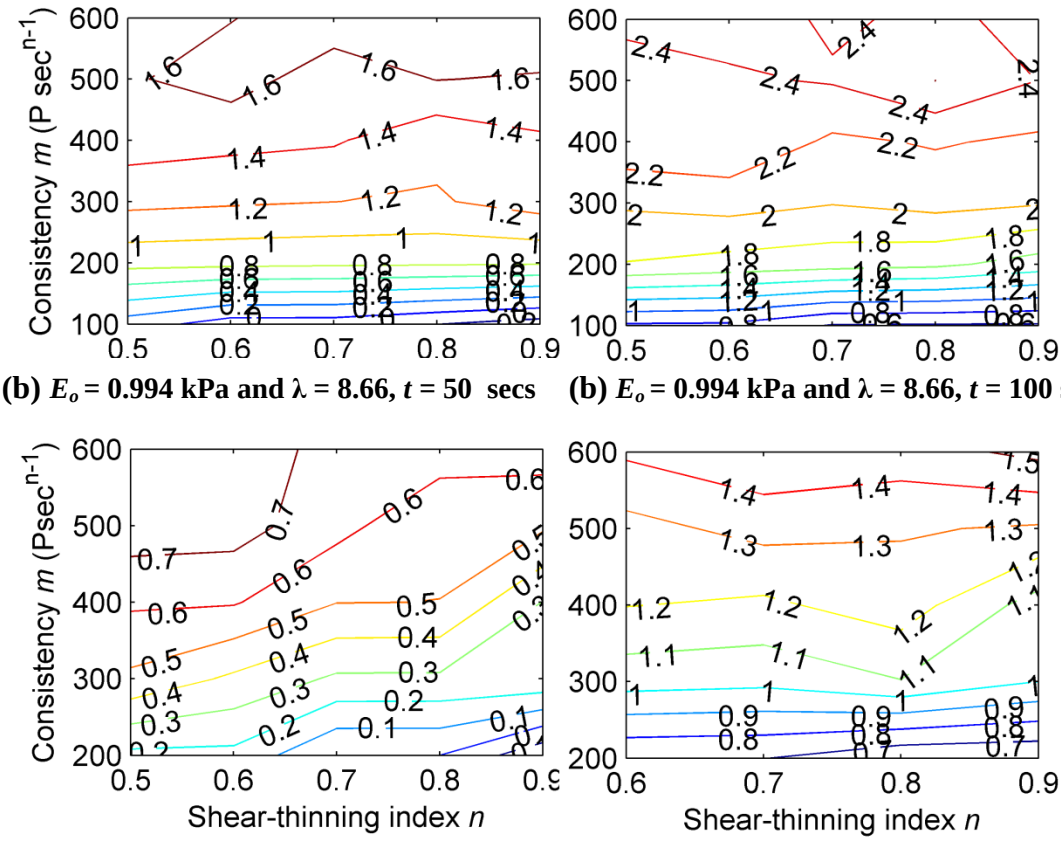


**(b)** $E_o$ **= 0.994 kPa and** $\lambda$ **= 8.66,** $t$ **= 50 secs** **(b)** $E_o$ **= 0.994 kPa and** $\lambda$ **= 8.66,** $t$ **= 100 secs**

**(c)** $E_o$ **= 9.96 kPa and** $\lambda$ **= 6.05,** $t$ **= 50 secs** **(d)** $E_o$ **= 9.96 kPa and** $\lambda$ **= 6.05,** $t$ **= 100 secs**

**Figure 4.5 Contours of percentage change in spreading length for 10% increase in shear-thinning index, *n* of a power-law model with linear elastic boundary.**

**(a)** Percent sensitivity at 50 seconds flow time for $E_o$ = 0.994 kPa and $\lambda$ = 8.66. **(b)** Percent sensitivity at 100 seconds flow time for elasticity $E_o$ = 0.994 kPa and $\lambda$ = 8.66. **(c)** Percent sensitivity at 50 seconds flow time for elasticity $E_o$ = 9.96 kPa and $\lambda$ = 6.05. **(d)** Percent sensitivity at 100 seconds flow time for elasticity $E_o$ = 9.96 kPa and $\lambda$ = 6.05.

### 4.2.3 Percent sensitivity of spreading length for both 10% decrease in consistency, *m*, and 10% increase in shear-thinning index, *n*

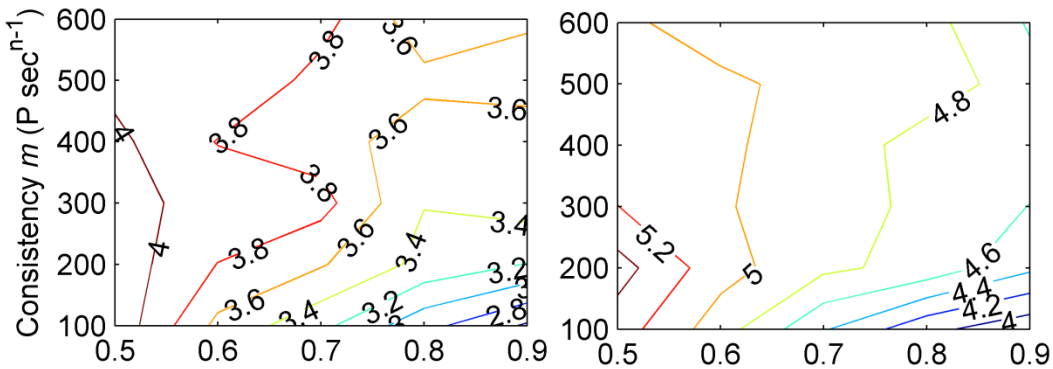


**(c)** $E_o$ **= 0.994 kPa and** $\lambda$ **= 8.66,** $t$ **= 50 secs** **(b)** $E_o$ **= 0.994 kPa and** $\lambda$ **= 8.66,** $t$ **= 100 secs**

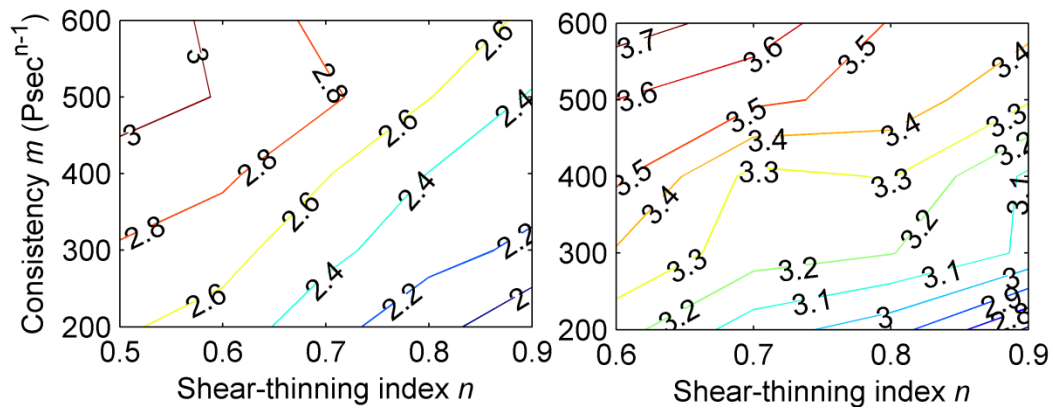


**(c)** $E_o$ **= 9.96 kPa and** $\lambda$ **= 6.05,** $t$ **= 50 secs** **(d)** $E_o$ **= 9.96 kPa and** $\lambda$ **= 6.05,** $t$ **= 100 secs**

**Figure 4.6 Contours of percentage change in spreading length for 10% decrease in consistency, *m* and 10% increase in shear-thinning index, *n* of a power-law model.**

**(a)** Percent sensitivity at 50 seconds flow time for $E_o$= 0.994 kPa and $\lambda$ = 8.66, **(b)** Percent sensitivity at 100 seconds flow time for elasticity $E_o$= 0.994 kPa and $\lambda$ = 8.66, **(c)** Percent sensitivity at 50 seconds flow time for elasticity $E_o$ = 9.96 kPa and $\lambda$ = 6.05, **(d)** Percent sensitivity at 100 seconds flow time for elasticity $E_o$ = 9.96 kPa and $\lambda$=6.05.

Figure 4.6 illustrates the percent change in spreading length for 10% change in both consistency and shear-thinning index. The trend observed are similar to linear elastic boundary condition in section 4.1. The sensitivity of spreading length is more for high consistency and low shear-thinning index (see Figure 4.6). The sensitivity of spreading length increased for longer spreading times (see Figure 4.6 (b)). The sensitivity is lower for higher elasticity (see figure 4.6 (c)). The magnitude of sensitivity of spreading length for a synergistic change in consistency and shear-thinning index is higher compared to percent change in consistency and shear-thinning index individually.

## 4.3 Summary of sensitivity analysis

The sensitivity of spreading length for a change in rheological properties is highly variable depending on spreading time, tissue elasticity and the rheological properties itself. Although there was no specific pattern observed for the contours of percent sensitivities of spreading length, a higher tissue elasticity resulted in lower sensitivity. The spreading length is more sensitive to changes in consistency than shear-thinning index. The sensitivity is high at high consistency and low shear-thinning index in most cases. The combined change in consistency and shear-thinning index resulted in greater sensitivity of spreading length. The results of sensitivity analysis for linear and non-linear elastic models cannot be compared quantitatively because the elasticities are not equivalent. However, as a general trend, the sensitivities were lower for non-linear elastic model.

A low sensitivity is desired but at the same time, the structure and properties of the polymeric gels should be kept in mind. Although a more Newtonian fluid has less sensitivity, most polymeric delivery vehicles are shear-thinning in nature. Thus, an optimization of all the parameters involved in the design process is needed. The estimated target values for rheological parameters for a specific tissue elasticity, application time and target length can be predicted using the parametric study, however the changes in the gel parameters under the influence of dilution etc. can be addressed only by knowing the sensitivity of the gel. An important point to be noted for this study is that the sensitivity is defined with respect to the initial spreading length at that time. If the initial spreading length were very small, even a slight increase in the spreading length would make it very sensitivity. On the other hand, if the initial spreading length were large then even a large change would result in less sensitivity.

# Chapter 5

# Conclusions and Future work

## 5.1 Summary of major findings

The results obtained for the numerical simulations presented in this study showed that the combined effect of gravitational and elastic forces greatly influence the coating of a microbicidal gel. Higher tissue elasticity resulted in faster spreading rates and an upward flow, indicating that the elastic forces were dominant. For a tissue with low elasticity, the spreading rates were slower and there was no flow in the upward direction, showing that gravitational and elastic forces were comparable. These results are important in choosing the right insertion location and application time. It also demonstrates the need to measure the elasticity of vaginal tissue for different groups of women.

The consistency, *m*, of the gel had greater impact on spreading compared to shear-thinning index, *n*. The spreading rates increased with decrease in consistency. The percent sensitivity of spreading length was greatest for a fluid with high consistency. The effect of shear-thinning index on spreading of the gel was dependent on the spreading time. A more shear-thinning fluid flowed faster during initial spreading and a Newtonian fluid flowed faster at longer times. For a fluid with low shear-thinning index, the sensitivity of spreading length is more. Although shear-thinning index did not have much

effect on spreading length for the small simulation time in this study, it is expected that it may play a significant role considering that the microbicidal gels will have longer application time. These results are important in choosing optimal rheological parameters of a delivery vehicle. The effect of change in volume of the bolus has not been presented in this thesis; however, simulations with larger volume were performed for power-law fluid with linear elastic boundary condition. An increase in volume leads to higher spreading rates; it also affects the trend of shear-thinning index on spreading length.

The results obtained for the Ellis model show that the shear-thinning, number $\alpha$, of an Ellis model had a similar behavior to that of shear-thinning index $n$ of a power-law model. The zero shear stress viscosity, $\eta_o$, had greater impact on spreading. As the zero shear stress viscosity increased the spreading rate decreased. The shear stress at half value of viscosity, $\tau_{1/2}$, had negligible effect for the range of values that were considered in this study.

The results from the non-linear elastic model showed that the linear elastic model overestimated spreading rates. It is expected that the spreading rate would decrease as the tissue relaxed and hence the spreading rate would decrease over time. A linear elastic model assumes a linear decrease in tissue pressure as the tissue relaxes, which is a very crude assumption considering vaginal tissue is a soft tissue exhibiting viscoelastic behavior. The non-linear model incorporated an exponential stress strain relationship, which is expected to be more close to the actual tissue behavior.

The results for the viscoelastic tissue model were not presented in this study. The viscoelasticity of the tissue has been neglected in previous studies assuming small relaxation times for application in vaginal delivery system (28). To predict if the viscoelasticity of the tissue is important, the tissue viscoelastic parameters have to be determined and a numerical simulation should be performed. A comparison between results for the viscoelastic models with the current models can determine if the viscoelasticity of the tissue is important.

## 5.2 Application of results obtained from the parametric study of a power-law fluid with linear elastic model

In this section, an example of how the results from the parametric study can be used to predict target gel properties is shown. Table 4 presents an estimate of gel consistency, *m* and and shear-thinning index, *n* values for a given tissue elasticity, application time and target length from the parametric simulations.

For example, if a target length of 15 cm is to be coated in 50 seconds for a women with vaginal tissue elasticity of 50 kPa, the estimated gel consistency and shear-thinning index are $m$ = 180-200 $Psec^{n-1}$ and $n$ = 0.5 - 0.6 respectively (as highlighted in Table 4). These values do not consider the effect of sensitivity to changes in rheological properties. The target values shown are based on the data obtained for spreading length from the simulations of the parametric study in the interval of one second. The spreading lengths

for longer time points can be calculated based on non-dimensional form of the evolution equation (see Appendix I).

**Table 4: Estimated range of values for rheological properties for a specific tissue elasticity, application time and target length.**

| Elasticity, *E* (kPa) | Application Time (approx) (seconds) | Approximate target lengths *L* (cm) | Estimated gel consistency, *m* ($Psec^{n-1}$) | Estimated shear-thinning index, *n* |
|---|---|---|---|---|
| 50 | 100 | 15 | 250-300 | 0.4-0.5 |
| 50 | 50 | 15 | 180-200 | 0.5-0.6 |
| 50 | 25 | 15 | 100 | 0.7-0.8 |
| 50 | 100 | 12 | 600-650 | 0.4-0.5 |
| 50 | 50 | 12 | 400-450 | 0.9-1.0 |
| 50 | 25 | 12 | 280-320 | 0.55-0.65 |
| 10 | 100 | 15 | 50-100 | 0.9-1.0 |
| 10 | 50 | 15 | N.A | N.A |
| 10 | 25 | 15 | N.A | N.A |
| 10 | 100 | 12 | 180-200 | 0.9-1.0 |
| 10 | 50 | 12 | 75-100 | 0.9-1.0 |
| 10 | 25 | 12 | N.A | N.A |

From the parametric study, a relative low shear thinning and high consistency index is more suitable as a target drug delivery vehicle between two elastic tissues for a long application time. A low shear-thinning index *n* ensures a quick initial spreading and then spreads slowly. A moderate or relatively high consistency index would ensure controlled amount of spreading without the gel being over flow from the target surface.

However, the sensitivity of consistency, *m* and shear-thinning index, *n* is very high in this range and hence there is a high chance of the coating of the gel may be very different than what was expected. This makes the design quite complex and suggests that there is a need for a specific target application time. This also shows the need and importance of a sensitivity analysis before clinical trials.

## 5.3 Limitations and Future work

The major limitation of this model is that it is a 2D model. Studies by Kheyfets has shown that 2D models overestimate spreading rates and lateral spreading may affect the overall coating (51). Another limitation is that the simulation time in this model is small (100 seconds) compared to the time for which the microbicidal gel may be inserted in a human vagina. In a real life situation, the gel may be applied for several hours.

The geometry of the bolus was assumed to be symmetric and vertical at all times which is a limitation considering the posture of women might change that will change the direction gravitational force. The results obtained from linear elastic and non-linear elastic models were not compared quantitatively. In addition, the non-linear model parameters need to be determined experimentally.

Future work should incorporate the 3rd dimension to account for lateral spreading. The angle of inclination for the flow must be incorporated. The simulations should be performed for longer times, closer to actual application time. The

viscoelasticity of the vaginal tissue should be considered and also better constitutive models for the fluid should be used which account for the viscoelasticity of the polymeric gels. A 3D fluid structure interaction FEA model incorporating the tissue and gel, viscoelastic constitutive equations for long spreading times and also incorporating the effect of dilution would be the ultimate model. In addition to the numerical simulations, an *in vivo* experimental setup should validate the results.

## 5.4 Conclusion

All the research questions have been addressed in this thesis. The relative importance of each parameter has been qualitatively determined. Optimal target gel properties can be predicted from the parametric study for a desired application time and tissue elasticity. The sensitivity analysis quantitatively determined percent changes in the spreading length for a change in a rheological parameter.

This study helped in achieving the overall goal of optimizing the parameters for the design of a delivery vehicle by providing a framework for overall gel behavior under the influence of gravity. The introduction of non-linear tissue elasticity was an initial step to incorporate the effect of tissue properties on spreading. An important design consideration that has been addressed in this thesis is the application time and how with spreading time the coating is affected. The mathematical tool and the results presented in this thesis with further investigation of tissue properties will ultimately help in determining optimal gel properties for microbicidal drug delivery systems.

# Appendix I

## A.1 Non-dimensional plot for linear elastic boundary condition

The evolution equation for power-law fluid with linear elastic boundary condition is given by (as derived in chapter 2):

$$\frac{\partial h(x,t)}{\partial t} - \frac{n\, m^{-\frac{1}{n}}}{(2n+1)} \frac{\partial}{\partial x}\left( \left(\frac{E}{T}\frac{\partial h}{\partial x} - \rho g_x\right) \left|\left(\frac{E}{T}\frac{\partial h}{\partial x} - \rho g_x\right)\right|^{\frac{1}{n}-1} h^{2+\frac{1}{n}} \right) = 0 \qquad (A.1)$$

The equation can be non-dimensionalized using the following transformations:

$$h' = \frac{h}{H} \qquad (A.2)$$

$$x' = \frac{x}{H} \qquad (A.3)$$

$$t' = t\left(\frac{EH}{Tm}\right)^{1/n} \qquad (A.4)$$

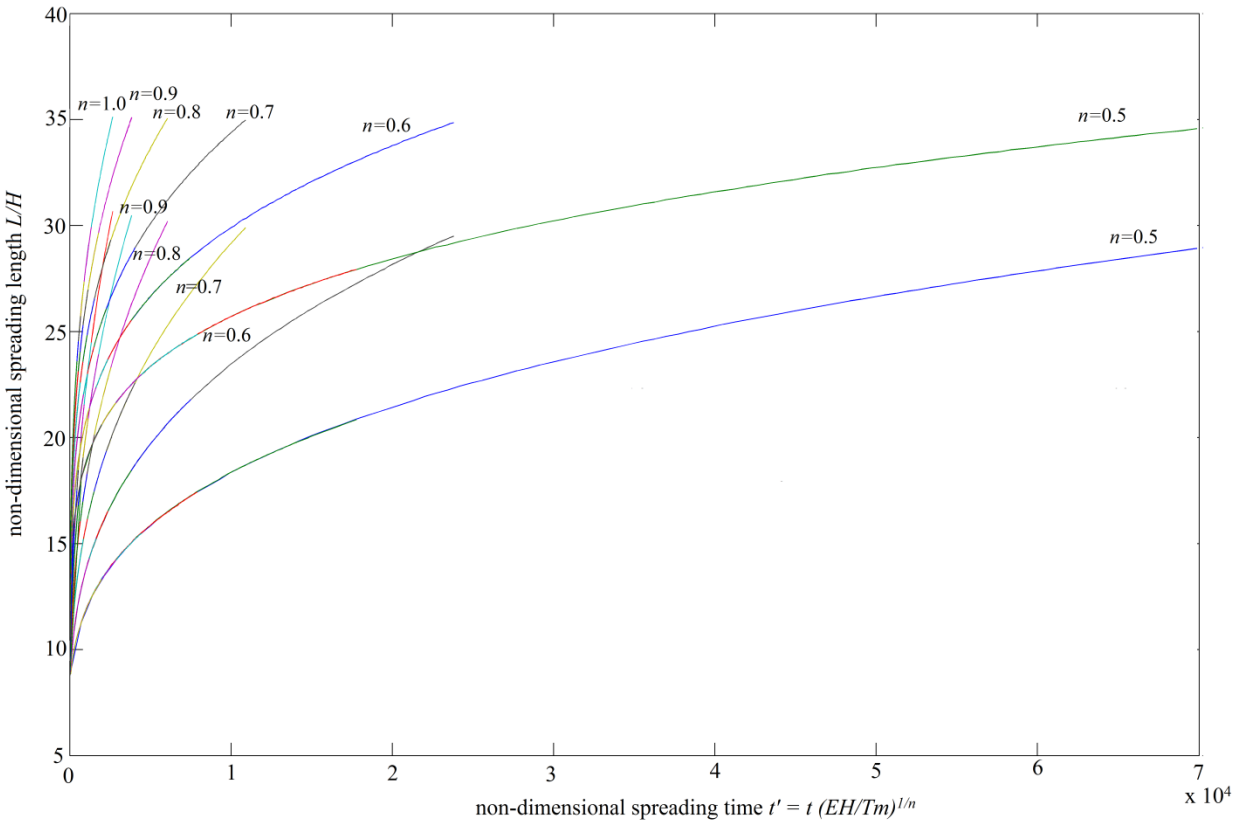


**Figure A1: Non-dimensional spreading length vs. non-dimensional spreading time:** Plot illustrates the data for non-dimensional spreading length for consistency $m$ = 100 - 600 Psec$^{n-1}$, shear-thinning index $n$ = 0.5 - 1.0, and tissue elasticity $E$ = 1 kPa and 10 kPa.

The above plot is helpful in interpreting spreading lengths data for spreading times which are not available from our simulations. This plot shows that non-dimensional spreading length has a similar curve for all values of gel consistency. The curve can be interpolated to obtain spreading lengths at desired point of time.

## Bibliography:


1. Fung YC. Biomechanics: Mechanical Properties of Living Tissues. 2nd ed ed. New york: Springer-Verlag; 1993.

2. Chhabra RP. Non-Newtonian Fluids: An Introduction. In: Krishnan JM, Deshpande AP, Kumar PBS, editors. Rheology of Complex Fluids: Springer New York; 2010. p. 3-34.

3. Diez JA, Kondic L. Contact Line Instabilities of Thin Liquid Films. Physical Review Letters. 2001;86(4):632.

4. Gouldstone A, Brown RE, Butler JP, Loring SH. Elastohydrodynamic separation of pleural surfaces during breathing. Respiratory Physiology & Neurobiology. 2003;137(1):97-106.

5. Schwartz LW, Eley RR. Flow of architectural coatings on complex surfaces; theory and experiment. Journal of Engineering Mathematics. 2002;43(2):153-71.

6. Global report: UNAIDS report on the global AIDS epidemic 2010 [database on the Internet]. WHO Library Cataloguing-in-Publication Data. 2010. Available from: http://www.unaids.org/globalreport/Global_report.htm.

7. UNAIDS, AIDS at 30: Nations at the Crossroads. WHO Library Cataloguing-in-Publication Data; 2011 [updated 2011; cited]; Available from: http://www.unaids.org/unaids_resources/aidsat30/aids-at-30.pdf.

8. Shattock RJ, Warren M, McCormack S, Hankins CA. AIDS. Turning the tide against HIV. Science. 2011;333(6038):42-3.

9. Nuttall J, Romano J, Douville K, Galbreath C, Nel A, Heyward W, et al. The future of HIV prevention: prospects for an effective anti-HIV microbicide. Infect Dis Clin North Am. 2007;21(1):219-39, x.

10. Tonks A. Quest for the AIDS vaccine. BMJ. 2007;334(7608):1346-8. PMCID: 1906671.

11. Will there be an HIV vaccine in the next 10 years? Nat Med. 2007;13(5):518.

12. Rohan LC, Sassi AB. Vaginal drug delivery systems for HIV prevention. AAPS J. 2009;11(1):78-87. PMCID: 2664883.

13. Ramjee G, Doncel GF, Mehendale S, Tolley EE, Dickson K. Microbicides 2008 conference: from discovery to advocacy. AIDS Res Ther. 2008;5:19. PMCID: 2546423.

14. Kieweg SL, Geonnotti AR, Katz DF. Gravity-induced coating flows of vaginal gel formulations: in vitro experimental analysis. J Pharm Sci. 2004;93(12):2941-52.

15. Stone A. Microbicides: a new approach to preventing HIV and other sexually transmitted infections. Nat Rev Drug Discov. 2002;1(12):977-85.

16. Friend DR, Doncel GF. Combining prevention of HIV-1, other sexually transmitted infections and unintended pregnancies: Development of dual-protection technologies. Antiviral Research. 2010;88(Supplement 1):S47-S54.

17. Silver Spring M. The Microbicide Development Strategy. MDS Working Groups Alliance for Microbicide Development. 2006.

18. Owen DH, Peters JJ, Kieweg SL, Geonnotti AR, Schnaare RL, Katz DF. Biophysical analysis of prototype microbicidal gels. Journal of Pharmaceutical Sciences. 2007;96(3):661-9.

19. Kieweg SL, Katz DF. Squeezing Flows of Vaginal Gel Formulations Relevant to Microbicide Drug Delivery. Journal of Biomechanical Engineering. 2006;128(4):540-53.

20. Katz D, Gao Y, Kang M. Using modeling to help understand vaginal microbicide functionality and create better products. Drug Delivery and Translational Research. 2011;1(3):256-76.

21. Kieweg SL. Mechanical analysis of vaginal gels intended for microbicide application [Ph.D]. Durham: Duke University; 2005.

22. Kundu PK, Cohen,I.M. . Fluid Mechanics. 4th ed. Oxford: Elsevier Inc. ; 2008.

23. Bird RB, Armstrong RC, Hassager O. Dynamics of Polymeric Liquids. New York: Wiley; 1987.

24. Barnhart KT, Izquierdo A, Pretorius ES, Shera DM, Shabbout M, Shaunik A. Baseline dimensions of the human vagina. Hum Reprod. 2006;21(6):1618-22.

25. Panayi DC, Digesu GA, Tekkis P, Fernando R, Khullar V. Ultrasound measurement of vaginal wall thickness: a novel and reliable technique. Int Urogynecol J Pelvic Floor Dysfunct. 2010;21(10):1265-70.

26. Hsu Y, Chen L, Delancey JO, Ashton-Miller JA. Vaginal thickness, cross-sectional area, and perimeter in women with and those without prolapse. Obstet Gynecol. 2005;105(5 Pt 1):1012-7. PMCID: 1226711.

27. Alperin M, Moalli PA. Remodeling of vaginal connective tissue in patients with prolapse. Curr Opin Obstet Gynecol. 2006;18(5):544-50.

28. Szeri AJ, Park SC, Verguet S, Weiss A, Katz DF. A model of transluminal flow of an anti-HIV microbicide vehicle: Combined elastic squeezing and gravitational sliding. Phys Fluids (1994). 2008;20(8):83101. PMCID: 2698280.

29. Martins P, Peña E, Calvo B, Doblaré M, Mascarenhas T, Natal Jorge R, et al. Prediction of nonlinear elastic behaviour of vaginal tissue: experimental results and model formulation. Computer Methods in Biomechanics and Biomedical Engineering. 2010;13(3):327-37.

30. Goh JTW. Biomechanical Properties of Prolapsed Vaginal Tissue in Pre- and Postmenopausal Women. International Urogynecology Journal. 2002;13(2):76-9.

31. Cosson M, Lambaudie E, Boukerrou M, Lobry P, Crépin G, Ego A. A biomechanical study of the strength of vaginal tissues: Results on 16 post-menopausal patients presenting with genital prolapse. European journal of obstetrics, gynecology, and reproductive biology. 2004;112(2):201-5.

32. Lei L, Song Y, Chen R. Biomechanical properties of prolapsed vaginal tissue in pre- and postmenopausal women. Int Urogynecol J Pelvic Floor Dysfunct. 2007;18(6):603-7.

33. Rubod C, Boukerrou M, Brieu M, Dubois P, Cosson M. Biomechanical properties of vaginal tissue. Part 1: new experimental protocol. J Urol. 2007;178(1):320-5; discussion 5.

34. Rubod C, Boukerrou M, Brieu M, Jean-Charles C, Dubois P, Cosson M. Biomechanical properties of vaginal tissue: preliminary results. International Urogynecology Journal. 2008;19(6):811-6.

35. Peña E, Calvo B, Martínez M, Martins P, Mascarenhas T, Jorge R, et al. Experimental study and constitutive modeling of the viscoelastic mechanical properties of the human prolapsed vaginal tissue. Biomechanics and Modeling in Mechanobiology. 2010;9(1):35-44.

36. Feola AJ, K. Jones, M. Alperin, R. Duerr, P.A. Moalli, and S.D. Abramowitch. Establishing an animal model for the evaluation of vaginal meshes. ASME Summer Bioengineering Conference; Lake Tahoe, CA2009.

37. Alperin M, Feola A, Duerr R, Moalli P, Abramowitch S. Pregnancy- and delivery-induced biomechanical changes in rat vagina persist postpartum. International Urogynecology Journal. 2010;21(9):1169-74.

38. Egorov V, Sarvazyan, A.P.,, inventor ARTANN LABORATORIES, INC, assignee. Methods for characterizing vaginal tissue elasticity. USA. 2011.

39. Carvalho MS, Scriven LE. Capillary and Viscoelastic Effects on Elastohydrodynamic Lubrication in Roller Nips. Journal of Tribology. 1996;118(4):872-9.

40. Fung YC. Elasticity of soft tissues in simple elongation. Am J Physiol. 1967;213(6):1532-44.

41. Haslach HW, Humphrey JD. Dynamics of biological soft tissue and rubber: internally pressurized spherical membranes surrounded by a fluid. International Journal of Non-Linear Mechanics. 2004;39(3):399-420.

42. Carter FJ, Frank TG, Davies PJ, McLean D, Cuschieri A. Measurements and modelling of the compliance of human and porcine organs. Medical Image Analysis. 2001;5(4):231-6.

43. Nicolle S, Vezin P, Palierne JF. A strain-hardening bi-power law for the nonlinear behaviour of biological soft tissues. Journal of biomechanics. 2010;43(5):927-32.

44. Jin ZM, Dowson D. Elastohydrodynamic Lubrication in Biological Systems. Proceedings of the Institution of Mechanical Engineers, Part J: Journal of Engineering Tribology. 2005;219(5):367-80.

45. Jones M, Fulford G, Please C, McElwain D, Collins M. Elastohydrodynamics of the Eyelid Wiper. Bulletin of Mathematical Biology. 2008;70(2):323-43.

46. Kieweg SL, Witelski, T.P., Katz, D.F. Free-surface coating flows of non-Newtonian vaginal gels: Numerical and experimental simulations of gravity-induced flow. Summer bioengineering conference; Amelia Island, Florida, USA2006.

47. Kheyfets VO, Kieweg, S.L. Free-surface coating flows of non-Newtonian gels: 3-D numerical simulation of gravity-induced flow. ASME Summer bioengineering conference; Keystone, Colorado, USA2007.

48. Hu B, and Kieweg, S.L. The effect of surface tension on the epithelial spreading of non-Newtonian drug delivery vehicles: Numerical simulations. ASME Summer bioengineering conference; Lake Tahoe, CA, USA2009.

49. Acheson DJ. Elementary Fluid Dynamics. Oxford: Clarendon Press; 2000.

50. Betelu SI, Fontelos MA. Capillarity driven spreading of power-law fluids. Applied Mathematics Letters. 2003;16(8):1315-20.

51. Kheyfets VO. Mathematical and Experimental Analysis of Microbicide Vaginal Gels [Ph.D]. Lawrence: University of Kansas; 2011.